Probabilistic Labeling in Radar Track-before-Detect Processing
Algorithms for tracking closely-spaced and/or interacting targets

Moreno León, C.

DOI
10.4233/uuid:039445ea-ce0e-445d-b07c-5e369fe7e708

Publication date
2023

Document Version
Final published version

Citation (APA)
Moreno León, C. (2023). *Probabilistic Labeling in Radar Track-before-Detect Processing: Algorithms for tracking closely-spaced and/or interacting targets*. [Dissertation (TU Delft), Delft University of Technology]. https://doi.org/10.4233/uuid:039445ea-ce0e-445d-b07c-5e369fe7e708

Important note
To cite this publication, please use the final published version (if applicable).
Please check the document version above.

Probabilistic Labeling in Radar Track-before-Detect Processing:

algorithms for tracking closely-spaced and/or interacting targets

Probabilistic Labeling in Radar Track-before-Detect Processing:

algorithms for tracking closely-spaced and/or interacting targets

Dissertation

for the purpose of obtaining the degree of doctor,
at Delft University of Technology,
by the authority of the Rector Magnificus, prof. dr. ir. T.H.J.J. van der Hagen,
chair of the Board for Doctorates,
to be defended publicly on
Monday 27th of November 2023 at 12:30 hours

by

Carlos MORENO LEÓN

Ingeniero de Telecomunicación,
Universidad de Alcalá, Spain,
born in Madrid, Spain.

This dissertation has been approved by the promoters:

promoter: Prof. dr. A. Yarovoy
copromoter: Dr. ir. J.N. Driessen

Composition of the doctoral committee:

Chairman: Rector Magnificus	Technische Universiteit Delft
Promoter: Prof. dr. A. Yarovoy	Technische Universiteit Delft (EEMCS)
Copromoter: Dr.ir. J.N. Driessen	Technische Universiteit Delft (EEMCS)

Independent members:

Dr. ir. S. Brüggenwirth	Fraunhofer FHR, Germany
Dr. G. Hendeby	Linköping University, Sweden
Prof. dr. D.M. Gavrila	Technische Universiteit Delft (3mE)
Prof. dr. ir. H.A.P. Blom	Technische Universiteit Delft (AE)
Prof. dr. ir. G.J.T. Leus	Technische Universiteit Delft (EEMCS)

The work in this thesis has been carried out under an external PhD enrollment at Delft University of Technology. The initial part of the research work was undertaken at Thales Nederland B.V., while the PhD candidate held a researcher position in the EC funded Marie Curie ITN FP7 project TRAX (Tracking in Complex Sensor Systems), grant agreement 607400. The major part of the research work was later undertaken aside from a full-time Radar Engineer position that the PhD candidate held at Fraunhofer FHR in Germany.

Keywords: Multiple Target Tracking, Radar Track-before-detect, Bayesian inference, Tracking of interacting/closely-spaced/unresolved targets, detection of target anomalous behavior, non-linear filtering, data-association free tracking, Sequential Monte Carlo methods, particle filtering

Printed by: IPSKAMP printing, Enschede, The Netherlands

Cover image: "Army RCCTO pursues drone swarming capability after first contract award" by Pvt James Newsome (11th Armored Cavalry Regiment) is in the Public Domain, CC0

Style: The author set this thesis in LaTeX using TU Delft House Style, with modifications by Moritz Beller
`https://github.com/Inventitech/phd-thesis-template`

ISBN 978-94-6384-512-0
An electronic version of this dissertation is available at
`http://repository.tudelft.nl/`

Contents

Summary

Radar-tracking of low-observable targets such as drones suffers from low detection performance. In these type of applications, it is desirable to avoid data thresholding in order to preserve the weak target signal in the raw sensor data. This thesis considers the Multiple Object Tracking (MOT) problem in the context of radar Track-before-Detect (TrBD) processing, where the raw radar data is fed into the filtering process without previous compression into a finite set of detection/plots.

Despite its inherent advantages, TrBD processing is in slow development. This is because most mathematical machinery developed over many decades for traditional Detect-before-track (DBT) processing cannot be transferred. Some approaches to the TrBD MOT problem manage to formulate rigorously the Bayesian state estimation problem for unknown and time varying number of targets. However, these solutions suffer from degraded estimation performance when considering the closely-spaced target scenarios targeted by this thesis. This type of degradation is showcased in chapter 2 and can be traced back to the lack of solutions for characterizing labeling uncertainty in the context of TrBD.

In traditional DBT context, Data Association (DA) techniques solve the pair-matching problem between plots and labels, which is a problem of probabilistic nature tackled in a pre-filtering stage. As plots do not even exist in TrBD, the problem of characterizing labeling uncertainty considered in this thesis can be described as the TrBD counterpart of the DA problem.

The labeling problem is tackled in this thesis at different levels. Chapter 3 derives a method to reduce labeling uncertainty by exploiting interacting target dynamics, which are commonly observed in closely-spaced target scenarios. In the same chapter, a contribution to the situational-awareness abstraction level is also provided. In particular, a Bayesian algorithm capable of inferring anomalous target-interacting behavior in the surveillance area is provided.

The remainder of the thesis places the focal point on DA-free characterization of labeling uncertainty. This problem is considered by assuming the worst-case scenario where the TrBD measurements do not carry any labeling information. This assumption does not preclude the incorporation of methods for reduction of labeling uncertainty in practical applications. For instance, micro-Doppler signature-based classification methods, other methods such as the one provided in chapter 3, or labeling solutions based on third party systems such as interrogators can be integrated with the proposed solutions in a Bayesian model-based manner.

Chapter 4 provides a sensible performance evaluation method suited for assessing the quality of track-formation by an arbitrary DA-free tracking solution. Examples of these solutions will be proposed in chapters 5, 6 and 7. It is a recurrent focus along these chapters to deal with the underlying problem of decomposing the Bayes posterior, as it is in this decomposition where the information about labeling resides. In order to evaluate the quality of the proposed DA-free decompositions, chapter 4 provides a particle filtering

algorithm able to calculate analytical references for evaluation of labeled tracks and labeling certainty estimates.

Chapters 5, 6 and 7 aim at inferring DA-free decompositions relevant for labeling uncertainty characterization. The method presented in chapter 5 derives an implementation of the Unique Decomposition (UD) theory by Blom and Bloem for non-linear and/or non-Gaussian (non-LG) systems. This implementation is used to tackle the labeling problem in TrBD by considering label-permutation-invariance characteristics of the posterior multitarget density.

The method developed in chapters 6 and 7 uses a novel approach coined as the Cross Modeling Tracker (CMT). Its novelty lies in decomposing the joint multi-object posterior density by means of hypothesizing crosses between objects. The notion of cross-between-objects is firstly defined in the low dimensional case based on physical interpretation, then an analytical generalization is derived for arbitrarily high dimensional spaces, were the definition of cross-between-objects has no physical interpretation.

Chapter 7 starts by providing numerical results on the estimation performance of the UD-based vs. the CMT algorithms. Both approaches provide comparable results in terms of track estimation and labeling uncertainty characterization when the targets are not extremely close to each other. The advantage of applying the UD-based solution is that approximation artifacts are prevented by design, allowing stable estimation with less amount of particles than the CMT.

The CMT outperforms the UD-based algorithm when tracking extremely closely-spaced targets, especially in cases where the multitarget density becomes unimodal. In spite of the CMT performing better, chapter 7 proves analytically that the CMT does not provide exact statistics of interest for track-formation, and illustrates how the CMT approximations degrade estimation performance for unresolved targets. Chapter 7 provides an optimized CMT algorithm based on analytically founded observations, which manages to mitigate the degradation due to the approximations compared to the original CMT algorithm.

The main advantage of the CMT is its wider applicability in arbitrarily high dimensional cases. This is a current limitation for the UD theory, which has no existent generalization for joint densities with more than two targets. The CMT can be considered as the first step towards the TrBD counterpart of DBT Multiple Hypotheses Tracking (MHT).

Samenvatting

Het door middel van radar volgen van slecht observeerbare doelen zoals drones wordt gehinderd door verminderde kwaliteit van detectie. Ten einde het zwakke signaal in de ruwe sensor data te behouden, is het in dit soort toepassingen wenselijk om het drempelen van data te voorkomen. Dit proefschrift behandelt Multiple Object Tracking (MOT) in de context van radar Track-before-Detect (TrBD), waarbij het filter proces gevoed wordt met de ruwe radar data, zonder voorafgaande compressie tot een eindige verzameling van detecties/plots.

Ondanks alle inherente voordelen, gaat de ontwikkeling van TrBD processing langzaam. Dat komt, omdat de meeste wiskundige technieken die ontwikkeld zijn gedurende vele tientallen jaren voor traditionele Detect-before-track (DBT) processing, niet overgenomen kunnen worden. Voor sommige oplossingsrichtingen voor het TrBD MOT probleem lukt het om het Bayesiaanse toestandsschattingsprobleem strikt te formuleren voor een onbekend en variabel aantal doelen. Echter, de schattingskwaliteit van deze oplossingen vermindert wanneer closely-spaced target scenarios; waar dit proefschrift zich op richt, in beschouwing worden genomen. Dit soort degradatie wordt geillustreerd in hoofdstuk 2 en kan herleid worden naar het ontbreken van oplossingen voor het karakteriseren van de onzekerheid in de labeling in de TrBD context.

In de traditionele DBT context lossen Data Associatie (DA) technieken het probleem van het bij elkaar passen van plots met labels op, hetgeen een probleem van kansrekeningstechnische aard is dat afgehandeld wordt in een pre-filtering stap. Omdat plots niet bestaan in TrBD, kan het probleem van het karakteriseren van de onzekerheid dat beschouwd wordt in dit proefschrift, beschreven worden als de TrBD tegenhanger van het DA probleem.

In dit proefschrift wordt het probleem van labeling op meerdere niveaus aangepakt. Hoofdstuk 3 leidt een methode voor het reduceren van labelingonzekerheid af, door gebruik te maken van onderling samenhangende doelsdynamica, hetgeen vaak voorkomt in closely-spaced scenarios: In hetzelfde hoofdstuk wordt een bijdrage geleverd aan het abstractieniveau van situational awareness. In het bijzonder wordt een Bayesiaans algoritme gepresenteerd dat in staat is om abnormaal onderling doelsgedrag te onderkennen.

Het vervolg van het proefschrift focusseert op de DA-vrije karakterisering van labelingonzekerheid. Dit probleem wordt beschouwd onder de aanname van het worst-case scenario, waarbij de TrBD metingen geen enkele informatie ten aanzien van de labeling bevatten. Deze aanname sluit het gebruik van methoden voor het reduceren van labeling uncertainty in praktische gevallen niet uit. Zo kunnen bijvoorbeeld op micro-Doppler signatuur gebaseerde classificatie methoden, zoals die gegeven in hoofdstuk 3, of labeling oplossingen gebaseerd op third party systemen, waaronder zogeheten interrogators, op een Bayesiaanse model gebaseerde wijze geintegreerd worden.

Hoofdstuk 4 verschaft een verstandige evaluatiemethode die geschikt is voor het beoordelen van de kwaliteit van track formatie van een willekeurige DA-vrije tracking oplossing. Voorbeelden van dergelijke oplossingen worden voorgesteld in de hoofdstukken 5, 6 en

7. De terugkerende focus in deze hoofdstukken is hoe om te gaan met het onderliggende probleem van de decompositie van de Bayesiaanse a posteriori kansdichtheid, omdat in deze kansdichtheid de informatie over de labeling aanwezig is. Om de kwaliteit van de voorgestelde DA-vrije decomposities te beoordelen, verschaft hoofdstuk 4 een particle filtering algoritme dat is staat is om analytische referentie getallen te berekenen ten behoeve van de evaluatie van de gelabelde tracks en de schattingen van de labelingonzekerheid.

Hofdstukken 5, 6 en 7 richten zich op DA-vrije decomposities die relevant zijn voor het karakteriseren van labelingonzekerheid. De methode in hoofdstuk 5 leidt een implementatie af van de Unique Decomposition (UD) theorie van Blom en Bloem voor niet lineaire en/of niet-Gaussische (non-LG) systemen. Deze implementatie wordt gebruikt om labelling in TrBD aan te pakken door middel van het beschouwen van label-permutatie-invariante karakteristieken van de a posteriori multitarget kansdichtheid.

De methode die ontwikkeld wordt in hoofdstukken 6 en 7, gebruikt een nieuwe methode die de naam Cross Modeling Tracker (CMT) gekregen heeft. De nieuwheidswaarde zit in de decompositie van de gezamenlijke multi-object a posteriori kansdichtheid door middel van het veronderstellen van het kruisen van objecten. Het begrip van een kruising tussen objecten wordt eerst gedefinieerd in een laag dimensionale situatie die gebaseerd is op een fysische interpretatie, waarna een analytische generalisatie wordt afgeleid voor arbitrair hoog dimensionale ruimtes, waarbij de definitie van een kruising tussen objecten geen fysische betekenis heeft.

Hoofdstuk 7 begint met het verschaffen van numerieke resultaten van de schattingsprestatie van het UD-gebaseerde algoritme tegenover het CMT-algoritme. Zolang de doelen niet extreem dicht bij elkaar zijn, leveren beide oplossingen vergelijkbare resultaten op in termen van onzekerheden in de doelsschatting en de labeling. Het voordeel van het gebruik van de UD-gebaseerde oplossing is dat benaderingsfouten door het ontwerp voorkomen worden, hetgeen een stabiele schatting mogelijk maakt met minder particles dan met CMT.

In het geval van doelen die extreem dicht bij elkaar zitten, presteert de CMT-methode beter dan het UD-gebaseerde algoritme, vooral in die gevallen waarbij de multitarget kansdichtheid unimodaal wordt. Desondanks bewijst hoofdstuk 7 analytisch dat de CMT geen exacte statistieken levert ten aanzien van het formeren van tracks en illustreert hoe de benaderingen in de CMT de schattingsprestatie voor niet geresolveerde doelen verminderen. Hoofdstuk 7 verschaft een geoptimaliseerd CMT algoritme, dat is gebaseerd op analytisch gefundeerde bevindingen, dat er in slaagt om het effect van de benaderingen te verminderen vergeleken met het originele CMT algoritme.

Het belangrijkste voordeel van de CMT is zijn bredere toepassing in willekeurig hoog dimensionale situaties. Dit is een huidige beperking van de UD-theorie, waarvoor nog geen generalisatie voor gezamenlijke kansdichtheden voor meer dan twee doelen beschikbaar is. De CMT kan beschouwd worden als de eerste stap naar de TrDB tegenhanger van de DBT Multiple Hypotheses Tracking (MHT).

Acknowledgements

My first acknowledgement goes to Dr.ir. Hans Driessen, for accepting the challenge. Having him as a manager at Thales and as a daily supervisor at TU-Delft has been an absolute honor, both at professional and personal levels. His encouragement, enthusiasm, empathy and constant availability have been crucial throughout the entire process.

I would like to thank Prof.dr. Alexander Yarovoy, my PhD promoter, for driving my PhD project in a tricky set of circumstances. His experience and commitment have been essential for my external PhD enrollment to result in a thesis book.

Aside from my formal supervisors, I would like to thank Dr. Pranab Mandal and Dr. Martin Podt for the fruitful discussions and collaborations over my time in The Netherlands. I am grateful to Prof.dr. Lyudmila Mihaylova, for hosting my research secondment in England. My experience working in her department at the University of Sheffield could not have been better. I would also like to thank Dr. Maria A. Gonzalez-Huici, my manager in Fraunhofer FHR, for her support during my time in Germany.

I would like to thank the members of my defense committee, Prof.dr.ir. Henk A.P. Blom, Dr.ir. Stefan Brüggenwirth, Dr. Gustaf Hendeby, Prof.dr. Dariu M. Gavrila and Prof.dr.ir. Geert J.T. Leus for their reviews, comments and suggestions for improving my dissertation.

At the beginning of my PhD, I had the genuine pleasure to meet Fernando and Paolo in the context of the TRAX project. The shared time in and out of the office was fantastic. Part of the nice experience was also thanks to the Hertong family, for putting us under the same roof and sharing an authentic Dutch culture. Thank you, Sonja and Han, for the always welcoming atmosphere.

Furthermore, I would like to thank the amazing people I have met in Germany and Denmark. Fernando, Aitor, David and Avinash, colleagues in the Cognitive Radar department, who made the working experience a real pleasure and became friends before or during the COVID-19 pandemic. I would also like to thank my good friend Jorge for providing writing advice on the last drafts of this manuscript and for the many hours we shared, helping each other and learning together. On the Danish side of the border, I am truly glad to have my good old friend Lea closer again in wonderful Copenhagen.

I am grateful to my friends in Spain, for making me feel like I never left Madrid whenever I am back in my beautiful country, even after ten years living abroad. Thanks to the friends I have from my "serious" cycling days and from my university time. I did not want not mention any name so as not to forget anyone, but I owe Ana a great debt of gratitude. Finally, I thank my friends from the neighborhood where I was born and raised, and other members from "La Taja del Cordero" gang, for not moving around too much, making it easy for me to find them whenever I am back. Special mention to Guille, for leaving a trail of fantastic memories that makes him more present than ever.

On a personal note, my deepest gratitude is to Larissa, for giving me all the love and caring, and for being my unconditional support through thick and thin. Last but definitely not least, I am grateful to my family in Madrid and La Rioja, especially to my parents

Guillermo and Rosa for being the best team ever, and to my sisters Cristina and Elena, who are looking down from heaven sending us all their love and energy.

Carlos
Copenhagen, November 2023

Acronyms

ACC: Adaptive Cruise Control.

AoA: Angle of Arrival.

CFAR: Constant False Alarm Rate.

CMT: Cross Modeling Tracker.

DA: Data Association.

DBT: Detect-before-Track.

EDM: Extrapolation-Decomposition-Merging.

FFT: Fast Fourier Transform.

FISST: Finite-Set Statistics.

FMCW: Frequency Modulated Continuous Wave.

GNN: Global Nearest Neighbor.

GOSPA: Generalized OSPA.

I/Q: in-phase and quadrature-phase.

ICAO: International Civil Aviation Organization.

IFF: Identification Friend or Foe.

JPDA: Joint Probabilistic Data Association.

LMB: Labeled Multi-Bernoulli.

LPE: Labeled Point Estimates.

MAP: Maximum a Posteriori.

MD: M-dimensional.

MCMC: Markov Chain Monte Carlo.

MFSR: Multi Function Surveillance Radar.

MHT: Multiple Hypothesis Tracking.

MM: Multiple Model.

MMOSPA: Minimum MOSPA.

MMSE: Minimum Mean Square Error.

MOSPA: Mean OSPA.

MOT: Multiple Object Tracking.

non-LG: non-linear and/or non-Gaussian.

OSPA: Optimal Subpattern Assignment.

PDF: Probability Density Function.

PF: Particle Filter.

PHD: Probability Hypothesis Density.

PI: Permutation Invariant.

PSV: Permutation Strictly Variant.

RCS: Radar Cross Section.

RFS: Random Finite Sets.

RPAS: Remotely Piloted Aircraft Systems.

SIR: Sequential Importance Resampling.

SNR: Signal to Noise Ratio.

TrBD: Track-before-Detect.

UAV: Unmanned Aerial Vehicle.

UD: Unique Decomposition.

WSN: Wirelesses Sensor Networks.

List of Figures

List of Tables

1

Introduction

1

The recent rise of Unmanned Aerial Vehicle (UAV) development has enabled new military strategies. Traditional plot-based tracking algorithms are not optimal for tracking these low-observable targets. This is because low-observable target signals often do not exceed the detection threshold and do not produce plots. In these cases, it is desirable to avoid thresholding so as to preserve the weak signal information in the raw sensor data [2]. Nevertheless, the consideration of point measurements commonly referred to as "plots", is still imperative nowadays for the large majority of state-of-art tracking algorithms. This also applies for the approaches based on the relatively recent application of Finite-Set Statistics (FISST) to Multiple Object Tracking (MOT) [3].

Track-before-Detect (TrBD) processing tackles the MOT problem by incorporating non-thresholded data (also called radar video), rather than plots, into the tracking algorithm. Therefore, TrBD processing of radar data has the potential to enhance the performance of counter-UAV defense systems when tracking low-observable targets. In the context of radar systems, non-thresholded data sets are for instance range-Doppler or range-azimuth maps. Some solutions exist for the specific TrBD MOT problem, such as the ones presented in [4], [5], [6] and more recently in [7]. However, these solutions lack labeling uncertainty characterization, resulting in degraded performance when tackling closely-spaced targets.

1.1 Motivation

Labeling uncertainty characterization, which is traditionally realized by Data Association (DA) techniques in Detect-before-track (DBT) approaches, is not trivial in TrBD due to the absence of detection/plots. The inherent advantages of TrBD tracking for tackling low-observable target scenarios, motivate this thesis to address DA-free characterization of labeling uncertainty. This is the major motivation of this thesis and the one producing most thesis results.

Closely-spaced targets are required to perform coordinated maneuvering in order to become and remain closely spaced. Most existing techniques for tracking in scenarios involving closely-spaced targets assume independent motion of the various targets. This is an additional motivation which triggers the study on interacting motion modeling and its advantages when incorporated in the tracking algorithms.

In complex surveillance scenarios, the transformation of tracking results into relevant situational awareness is not trivial for a human operator. For this reason, an additional level of abstraction is incorporated in advanced software radar architectures. This layer of abstraction operates at semantic level, providing meaningful interpretation of situational awareness. Anomaly detection is one example relevant in coastal surveillance, where for instance, the smuggling of goods is a major concern. This motivates the thesis to study how estimation of target interactions may aid at detecting such type of malicious target behavior. The interpretation of situational awareness has the potential to provide early warnings, which would otherwise escape from visual inspection of the tracks.

1.2 Historical MOT interest VS relevance of new MOT problems

MOT is one of the major problems addressed in the Information Fusion community. MOT refers to the problem of jointly estimating the presence and states or trajectories of objects based on noisy measurements from sensors such as radar or camera. MOT finds its applications in both military and civilian contexts. To name a few societal applications, MOT solutions are an essential component in radar area surveillance and play a key role in autonomous navigation.

In the context of MOT for autonomous navigation, optical systems such as LIDAR and camera have been used due to their ability to produce high quality data under favorable weather and lighting conditions. However, safety demands in self-driving industry point to MOT solutions based on radar as a non-replaceable technology due to its robustness against non-favorable conditions [8]. Self-driving demands encourage the development of radar-based MOT solutions not only for tracking but also for radar platform self-localization [9]. Lower levels of automation based on radar MOT solutions are present in standard commercial-off-the-shelf products. For instance, radar-based Adaptive Cruise Control (ACC) for assistance to navigation [10] has become increasingly popular in mass-produced cars over the last decade.

The long lasting interest in radar-based MOT has driven the development of many MOT Bayesian solutions, most of the solutions model sensor measurements as radar plots. This modeling already constraints the processing capabilities of the radar system from a very early stage. Indeed, discarding part of the data-set via thresholding is opposed to the idea of inferring as much information as possible from the measurement set. One reason for modeling measurements after thresholding is that traditional computational resources would not run tracking algorithms in real-time, unless data complexity is reduced to detection plots.

Aside of plot-based MOT being pushed by high interest in radar applications, the development of plot-based MOT algorithms is an attractive mathematical problem in its own right. This dual interest has set a favorable context for engineering successful plot-based trackers for many decades.

The increasing interest in new tracking problems where sensors do not provide point measurements, but rather intensity maps type of measurements, requires the consideration of more complex observation models. An important consequence of not modeling point-measurements is that none of the traditionally accepted tracking algorithms, such as for instance Multiple Hypothesis Tracking (MHT) [11], can be utilized.

The relevance of new MOT problems based on intensity map measurements can be easily justified. For instance, MOT relying on Wireless Sensor Networks (WSN) becomes relevant for the tracking of objects in mountainous regions, where radar performance is severely degraded by extensive shadow regions. Ito and Godsill recently studied this MOT problem using intensity maps data given by Received Strength Signal Indicator (RSSI) readings [7]. An extensive study of a similar MOT problem can be found in [12].

One does not need to depart from the radar sensor to find out that range-Doppler maps (see Fig. 1.1) or range-azimuth maps are certainly richer measurement sets than the detections extracted semi-heuristically from these maps (e.g. via Constant False Alarm

1

Rate (CFAR) detection). In fact, incorporation of such radar intensity maps inside the tracker is essential, for instance, in radar MOT problems involving low-observable objects. Low-observable objects are those delivering measurements for which the sensor responses have an SNR value lower than 10dB (see Fig. 1.1 b). In these cases, it is desirable to avoid thresholding so as to preserve the weak signal information in the raw sensor data [2].

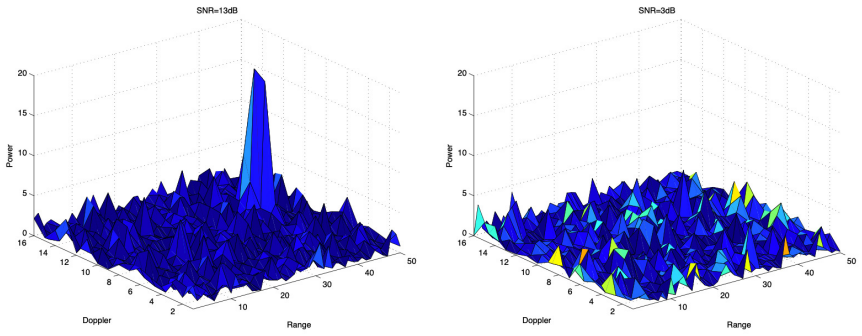

(a) (b)

Figure 1.1: Range-Doppler maps from two scenarios involving high and low SNR targets. In a) the SNR is high and it is easy to discern the target as a high peak. In b) the SNR is low and it is not possible to distinguish the target from the noise.

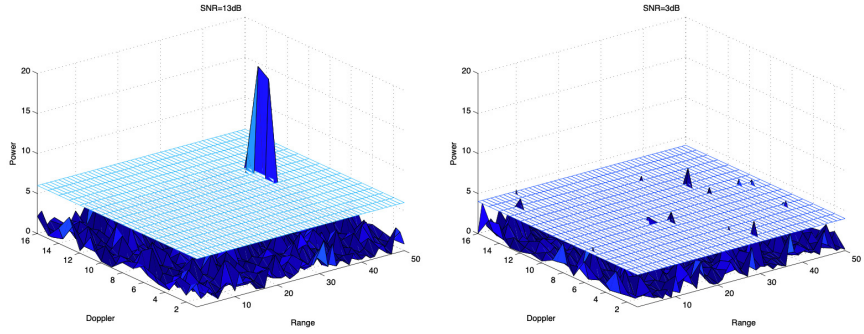

(a) (b)

Figure 1.2: In low SNR target scenarios, the target may not lead to a detection.

1.2.1 Track-before-detect (TrBD) radar tracking

TrBD algorithms provide solutions to the problem of tracking targets avoiding undesired data thresholding. This is done by means of using multiple frames of the raw sensor data. Consequently, TrBD algorithms jointly estimate the existence of the target (detection) as well as track its kinematic state (filtering). In fact, it is the existence of a track that implicitly

reports the detection of a target as opposed to what happens in the traditional processing chain, where the existence of detections may trigger the initiation of tracks (according to track management system heuristics).

Among all sensor systems (both in centralized and distributed architectures) providing intensity maps type of measurements, this thesis focuses on the development of tracking algorithms for radar intensity maps, e.g. the ones in Fig. 1.1. TrBD MOT does not only prevent loss of potentially relevant information in these maps. Additionally, TrBD MOT copes with closely-spaced objects tracking in cases where a DBT approach would have to deal with merged measurements. Therefore, TrBD MOT provides an inherently increased resolution capability over DBT MOT, which makes it all the more important to address the characterization of labeling uncertainty in the absence of detections.

1.3 Situational awareness

The level of situational awareness offered by radar-based solutions is directly linked to the operational performance of the radar system. The boundaries of operational performance are strictly dependent on two main aspects: the quality or the radar measurements and the quality of the processing algorithms turning radar measurements into user-level data. Drawing a line between the analog and digital parts in the radar receiving path provides a reasonable split between these aspects in most radar systems.

A Frequency Modulated Continuous Wave (FMCW) radar can be taken as an example to introduce the scope of this thesis in the context of a radar system. Firstly, every hardware design choice along the signal path, from signal generation to sampling of the beat frequency signal, conditions the quality of the radar measurements. These measurements are the "in-phase and quadrature-phase" (I/Q) samples in the so-called “data cube”. This is the first input to the processing algorithms. For a particular “data cube”, software design involving signal and data processing choices, conditions the quality of the user-level data. A higher level governing the quality of both measurements and user-level data involves the online tuning of hardware and software parameters. This tuning task has been traditionally performed by a radar operator to a very limited extend, e.g. by means of switching between operational profiles or modes.

Over the last decades, most advanced multi-function radar systems are increasingly incorporating a level of abstraction referred to as cognitive control [13], [14], [15]. These cognitive radars assist the (human) operator in the tuning of hundreds of parameters in real time according to some definition of optimality. It can be argued that cognitive radars introduce a remarkable control processing-load even before the generation of the transmitted signal based on various sensing-control loop closure concepts [16], [17], [18], [19], [20] and [21]. Ultimately, these concepts contribute to optimize the quality/usability of expected I/Q samples as well as the tuning of processing parameters so as to enhance overall operational performance and situational awareness.

1.4 Scope of the thesis

Based on previous definitions, the processing software in a generic radar can be separated in sensing software and control software. A minimalistic decomposition of the sensing software can be made based on three levels: i) digital signal processing, ii) statistical

data processing and iii) analysis of situational awareness. Common submodules in i) are: extraction of range Doppler maps (via double FFT processing), CFAR detection, Angle of Arrival (AoA) estimation, clustering, plot extraction, clutter removal, ambiguity unfolding, signature-based classification etc. The major module in level ii) is the MOT algorithm. The level iii) may vary significantly from one system to another depending on the application. In the general case, it will be built as a set of post-processing analyzing algorithms.

The scientific content in this thesis is inherently within the statistical data processing level ii). Furthermore, key functionalities in traditional DBT MOT such as detection, clustering and plot extraction are implicitly tackled given the TrBD approach to the MOT problem adopted in this thesis. Therefore, a remarkable portion of the functionalities in i) is covered as well. Finally, a minor part of the results fall under level iii). In particular, by means of modeling target interactions, a Bayesian method for detecting abnormal target behavior will be provided. Overall, this thesis provides various contributions on algorithm design to tackle MOT problems in complicated surveillance scenarios. The type of scenario complexity considered in this thesis involves low-observable, closely-spaced and potentially interacting targets.

1.5 Related open problems

The thesis investigates problems associated to the tracking of low-observable, closely-spaced and/or interacting targets in TrBD context.

1.5.1 The problem of tracking interacting targets

Interacting and even coordinated motion can for instance be found in groups of drones that intentionally move together in formation (see Fig. 1.3). Coordinated maneuvering is required for these objects to become and remain closely spaced, coordinated maneuvering is also required for instance when well-separated objects are executing a joint plan. Monitoring some of these scenarios may be the purpose of, for instance, a ground-based counter UAV radar or a radar-based coastal surveillance system. In both scenarios, targets become low-observable either due to low RCS in the case of the drones or due to high intensity sea clutter in the case of the coastal surveillance system (see Fig. 1.4).

Detection of anomalous target behavior

Inference of situational awareness is the most relevant high level application of area surveillance systems. In particular, one important societal application is detecting suspicious target behavior. In most of such anomalous scenarios, high degree of interaction can be observed between the targets. For instance, coordinated motion of the targets is inherent in attack missions involving formations of air-targets or drone swarms. Also, goods smuggling in coastal areas commonly involves at least two well-separated objects performing coupled maneuvering way before gathering close to each other.

Discriminating suspicious target behavior from the ones involving regular activities is vital in safety assessment. By means of detecting spikes in the level of target interaction, one may detect irregular activities in early stages.

Figure 1.3: Drones are low-observable. Therefore, TrBD filters have the potential to outperform traditional detection-based tracking algorithms when tracking these types of objects. Additionally, drones dynamic behavior is specially constrained by interactive motion when flying in formation. Image from"Army RCCTO pursues drone swarming capability after first contract award" by Pvt James Newsome (11th Armored Cavalry Regiment) is in the Public Domain, CC0

Degraded tracking performance due to underestimation of coordinated motion modeling

Sensor resolution is a physical limitation affecting the quality of labeling decisions in closely-spaced targets scenarios. Additionally, even when the targets can be resolved in the measurements; scan update rate limitations may also preclude easy labeling decisions. Slow measurement update rates in the other of two to six seconds can for instance be found in mechanically rotating surveillance radars. When targets are too maneuverable for a particular measurement update rate, the present state of one target may not only correlate with its own previous state but also with the previous state of another target. This may introduce uncertainty in the solution of the so-called target labeling problem [22].

Mentioned effect due to limited update rate can be mitigated when accounting for realistic target maneuverability in the dynamic models. Sometimes, target maneuverability is complex to model, for instance due to interacting motion between targets. It is then a common practice to use standard independent motion models such as the "Continuous White Acceleration" model [23]. When the realistic motion of targets is captured very poorly, labeling ambiguity (DA ambiguity in traditional DBT MOT) may get even overlooked. Not considering labeling ambiguity results in severe estimation under-performance as the MOT method may provide a single (potentially faulty) labeling solution [24]. Disregarding whether DBT or TrBD techniques are considered, incorporation of interactive motion modeling in the estimation algorithms is expected to improve tracking performance.

1

Figure 1.4: Crowded harbor where objects dynamics are affected by the existence and dynamics of other objects.

1.5.2 The labeling problem when tracking closely-spaced objects in TrBD

The problem of deciding which track state estimate belongs to which physical object over time is known as the labeling problem. Labels are considered as unique identifiers assigned to each physical object in the track initiation stage. In closely-spaced objects tracking, sensor systems may not provide enough information to uniquely match objects labels and track-state estimates consistently over time, leading to uncertainty in the labeling [22].

The terms labeling problem and labeling uncertainty might be misleading, hence it is important to remark that there is no uncertainty in the labels as they have been assigned (and are therefore fully known) within the tracker. The uncertainty is about the assignment of tracks to the fully known set of labels [24]. However, due to historical reasons we will continue referring to this problem and the uncertainty as labeling problem and labeling uncertainty. As mentioned before, labeling uncertainty can play a role already in sensor systems even if the objects can be resolved by the sensor. This will occur if maneuverability of the objects and/or sensor update intervals get large.

Characterization of labeling uncertainty

DA is an essential component in DBT tracking which wraps the filtering process and turns it into a tracker by explicitly characterizing labeling uncertainty. This is done by solving the pair matching problem. In words of Peter Willett regarding one of his recent talks on Data Association and Target Tracking: “To thread measurements (well, many call them “hits” or “plots”) of radar, sonar or imaging observations to a credible, smooth and reportable trajectory requires a filter. We will discuss those - Kalman, Unscented, particle, etc. - very briefly. But one cannot even begin to filter without knowing which hits come from which targets, and which hits are complete nonsense (clutter). When wrapped inside some scheme for such data-association, a filter becomes a tracker.”

DA is imperative in DBT, but impossible in TrBD. In other words, due to the absence of detection points, no kind of DA solution can be formulated in TrBD. However, this does not mean that labeling uncertainty does not exist or can be overlooked in TrBD context.

Assumptions

The specific problem formulations in this thesis will consider two assumptions that will hold throughout the chapters. Firstly, regarding characterization of labeling uncertainty, this thesis considers the worst case scenario by assuming that intensity map measurements do not provide any labeling information. In other words, it is assumed that the likelihood model for the measurements given the state is invariant under label permutations. Despite this assumption, and although techniques based on identification through measurements fall out of the scope of this thesis, the solutions that will be presented allow seamless integration of classification techniques in order to reduce labeling uncertainty when tracking objects of different radar signatures. Secondly, this thesis considers the TrBD MOT problem assuming the number of targets is fixed and known. This assumption aids at isolating the problem of characterizing labeling uncertainty by disregarding the problem of cardinality estimation. On the topic of cardinality estimation, some solutions already exits for the TrBD MOT problem, see [4].

1.6 Selected Challenges for PhD research

The first challenge in this thesis is showcasing how tracking performance becomes degraded as a consequence of overlooking labeling uncertainty estimation, in the context of TrBD. This will be presented in Chapter 2. The second challenge is studying methods for labeling uncertainty reduction. In particular, due to the first assumption, these methods should not rely on radar-signature-dependent classification algorithms or third party systems such as interrogators etc. Instead, labeling uncertainty reduction should be tackled inside the filtering process by formulating the challenge from the target dynamics point of view.

The third challenge of this thesis is automatically detecting anomalous target behavior in the surveillance area. In particular, this thesis focuses on the type of anomalous behaviors involving some level of coordinated target-maneuvering. Second and third challenges will be tackled in Chapter 3.

TrBD processing poses difficulties for root-cause identification of underperformance due to its early stage of development and adoption. However, mentioned first challenge-showcase will illustrate analogies with identified concerns in traditional DBT context. In particular, the problems of "labeling-confusion" and "track-coalescence" in TrBD processing will be mapped to well identified problems in the Information Fusion community. In fact, TrBD "labeling confusion" has the same effect as DBT Global Nearest Neighbor (GNN) "wrong DA". Additionally, TrBD "track-coalescence" has the same effect as DBT Joint Probabilistic Data Association (JPDA) "track-coalescence". Identification of the root-causes producing "labeling confusion" and "track-coalescence" in TrBD will also be part of the first challenge.

Following with analogies in well-developed DBT algorithms, the main challenge in this thesis is to pave the way for the development of the "MHT counterpart" algorithm for TrBD trackers. This defines the ambitious goal of preventing described estimation underperformance by extending existent TrBD developments in a similar way as DBT

MHT was created to overcome the underperformance of DBT GNN and JPDA. To realize this extension, the TrBD MOT problem (including the subproblem of DA-free labeling characterization) for known and constant number of closely-spaced objects, is considered from chapter 4 to the end of the thesis.

1.7 Proposed solutions

This thesis formulates the TrBD MOT problem in the Bayesian framework to tackle the first challenge. Based on such formulation, this thesis proposes the incorporation of interacting target motion models in order to tackle the second and third challenges. By means of modeling such interactions, Chapter 3 provides an automatic parameter tuning method to do on-line learning and exploitation of coupled accelerations between targets. For the first time in literature, the presented method exploits such information to close the sensing-tuning loop inside the tracker. This automatic tunning method will result in enhanced tracking performance, including reduction of labeling uncertainty. To solve the third challenge, this thesis proposes the incorporation of interacting behavior modeling in a Multiple Model (MM) Bayesian filter implementation.

Tackling the challenge of DA-free characterization of labeling uncertainty is instrumental to prevent degraded tracking performance in TrBD MOT of closely-spaced objects. In order to tackle this challenge, the thesis presents two methods to infer label-dependent decompositions of the joint multiobject posterior density. The first method derives an implementation of the Unique Decomposition (UD) by Blom and Bloem [25] for non-linear Gaussian systems. This implementation is used to tackle the labeling problem by looking at the label-permutation-invariance characteristics of the posterior density. The second method is coined as the Cross Modeling Tracker (CMT), its novelty lies in decomposing the joint multiobject posterior density by means of hypothesizing crosses between objects.

1.8 Structure of the thesis and publication status

Chapter 2 formulates the TrBD MOT problem in the Bayesian framework and showcases the labeling problem for closely-spaced objects tracking. An extensive literature review on this problem is provided as well. Chapter 3 looks at the labeling problem from the dynamics point of view, providing an algorithm able to learn and exploit interacting target motion. In the same chapter, an application of the algorithm to detect anomalous target behavior is also illustrated. These results have been published in [26]. Chapter 4 introduces an evaluation criterion especially suitable for comparison of estimation performance between different DA-free trackers. This result has been published in [22]. Chapter 5 generalizes existent implementations of the UD to non linear-Gaussian problems, resulting in a DA-free Particle Filter (PF) algorithm to solve the TrBD MOT problem. This result has been submitted for publication in IEEE *Transactions on Aerospace and Electronic Systems* as "Implementation of the Unique PDF Decomposition for tracking closely-spaced objects with Track-Before-Detect radar systems". Chapter 6 derives the so-called CMT, a new DA-free Bayesian solution resulting from physical interpretation of the labeling problem in the low dimensional case. This result has been published in [27]. Chapter 7 compares the PF solutions presented in chapters 5 and 6 based on the performance evaluation method in chapter 4. Additionally, the CMT solution is optimized in order to account for the tracking

of unresolved targets. The manuscript for submitting these contents to the *Journal of Advances in Information Fusion* is under preparation.

2

Track-before-detect MOT problem and Labeling subproblem

2.1 Introduction

The TrBD MOT problem introduced in previous chapter encapsulates the labeling subproblem. This subproblem is inherent in the estimation of joint multi-target position uncertainties. In TrBD, the labeling problem should be tackled by probabilistically characterizing the pair-matching mapping between two sets: labels and tracks. Note that this differs from the pair-matching problem formulated to associate the set of detections and the set of labels in DBT. In fact, the labeling problem in DBT is solved in a pre-filtering stage via DA, while the same problem in TrBD needs to be solved in a post-filtering stage.

Solving the labeling problem is not always required by the radar system. Examples can be found in autonomous-driving applications based on automotive radar. For instance, in radar-aided Adaptive Cruise Control (ACC), the relevant information is only extracted from the track in front of the vehicle. In this case, it is not even relevant whether track labels have been swapped, for instance due to vehicles in track being temporally closely-spaced. In fact, using a GNN-based tracking algorithm to process the plots will accomplish the task. Note that although GNN provides labeled point estimates, these come from hard DA decisions. Since DA uncertainties are not propagated over time, one cannot keep control over label confusion. It is in this particular sense that GNN does not solve the labeling problem, as for instance DBT MHT would do.

In many other radar applications however, solving the labeling problem without relying on signature-dependent classification is important. This is the case when for instance a Multi Function Surveillance Radar (MFSR) system attempts to keep "identities" of existent tracks. Solving the labeling problem becomes relevant in this cases because the use of classification modes imposes demanding time-on-target and heavy processing. As these demands need to be taken into account by the scheduler in the radar cognitive-processor, classification tasks may not monopolize the resources in order to preserve optimal over-

all functionality. In other words, classification time-budget may be limited in complex scenarios so as not to compromise tracking performance and searching of new threads. Additionally, even when used, classification methods may not aid at solving the labeling problem when tracking targets of similar radar signature as it happens to be case with drone swarms.

The labeling problem is specially challenging in closely-spaced objects scenarios, and lacks solutions in TrBD. Labels have been rigorously incorporated in MOT solutions by two different means. Firstly, by using random vector formulations. In this case, the order of partitions in the random vector implicitly determines the labels of the tracks. Secondly, by using Random Finite Sets (RFS) formulations [3] and explicitly introducing labels as additional components in the (unordered) state variable.

The scope of this thesis is limited to the case of known and constant number of objects in order to isolate the essence of the labeling problem. Inside this scope, one is not interested in the built-in cardinality estimation capabilities of RFS formulations. For this reason, vector formulations are considered sufficient to tackle the labeling problem along this thesis. Namely, the incorporation of labels in this thesis is given implicitly by the order of the partitions in the state vector.

2.2 DBT vs TrBD processing architecture

In a traditional MOT setting, the raw radar data is preprocessed through detection, clustering and extraction stages (see Fig. 2.1 a). Finally, the tracker is fed with the preprocessed radar data. Unlike traditional MOT settings, integrated processing settings allow the tracker to make use of the raw radar data with no prior processing nor associated information losses (see Fig. 2.1 b). The term TrBD is more extended in literature than the term integrated processing, so TrBD will be used along the rest of the thesis.

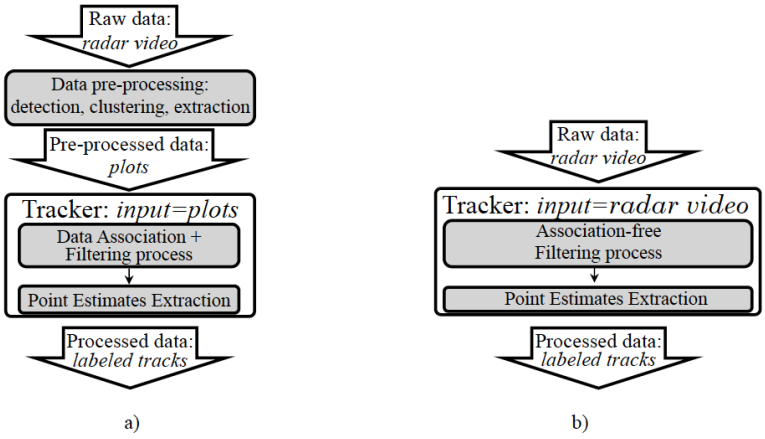

Figure 2.1: Block diagrams of traditional (detect-before-track) and integrated (track-before-detect) approaches to the Multiple Object Tracking problem in figures a) and b) respectively.

Both traditional and TrBD approaches provide a solution to the MOT problem including extraction of labeled point estimates (note that several point estimates with the same label

define a track). However, this does not mean that both tracking approaches provide a legitimate solution to the labeling problem. While in a DBT tracker, preprocessing raw data before filtering allows to explicitly characterize labeling uncertainty (e.g. MHT does this), current TrBD trackers do not have control over label confusion in the reported tracks. Therefore, in vanilla TrBD trackers, labeling confusion may get unnoticed unless captured by heuristic ad-hoc mechanisms. In this particular sense, this is similar to what happens in DBT GNN-based trackers. The main difference being that GNN does not propagate DA uncertainties over time deliberately, in TrBD trackers DA does not even take place (see Fig. 2.1 b)) as the radar image is fed into the filtering process without previous compression into a finite set of points. Examples of this type of data incorporation can be found, for instance, in Ch. 11 in [28].

2.2.1 Implications of TrBD tracking in processing architecture

Performing MOT based on map data does not only involve the replacement of observation models in the Bayes recursion. From the processing architecture point of view, structural changes are also required, leading to the removal of the detector and integration of the tracker inside the radar processing chain, so that detection and track-confirmation occur simultaneously. In practice, the detection algorithm and additional pre-processing is replaced by a single TrBD algorithm, which also implements the tracking functionality. For this reason the term TrBD is also known as "integrated processing" in some references.

When shifting from DBT to TrBD systems, changes in the algorithm design should follow from mentioned changes on architecture and data flows. In principle, it should be sufficient with replacing the DBT observation likelihood model by the TrBD one. In fact, as Bayesian inference provides a generic framework for incorporating data, the generation of the posterior density of interest should follow from mentioned likelihood model replacement. However, the mere replacement of the observation likelihoods does not produce TrBD posterior densities with the labeling structure offered by algorithms such as DBT MHT. The ability to generate this structure is ruled out in vanilla TrBD as pre-filtering DA cannot be formulated due the absence of detections.

Common practice in TrBD tracking and associated drawbacks

Existent TrBD tracking solutions do Bayesian filtering using raw measurement observation likelihoods and manage to formulate rigorously the Bayesian state estimation problem for unknown and time varying number of targets, for instance see [4]. In connection to the discussion in previous subsection, these solutions overlook that the mere replacement of likelihood models in the Bayes update cannot make up for the pre-filtering labeling uncertainty characterization offered by, for instance, DBT MHT. Nevertheless, this does not degrade estimation performance in non-closely-spaced target scenarios. In cases where the objects move far apart from each other, labeling uncertainty is negligible and a TrBD tracker such as the one in [4] suffices to infer the correct pair-matching between labels and point estimates, leading to proper track estimation. However, when the t objects move closely-spaced, labeling uncertainty degrades tracking performance and even the optimal MOT solution is prevented from stating the correct pair-matching (label/point-estimate) free of uncertainty. Under these complicated conditions, regular TrBD trackers result either

on overconfidence of labeling decisions or "track-coalescence". The former issue raises the probability of labeling confusion, the later severely degrades the performance of estimation on target dynamics.

2.3 Problem description

Consider an MOT problem based on raw (TrBD) measurements and a scenario containing t objects moving in a M-dimensional space ($t-MD$ setting). Additionally, consider that t is constant and known by the tracker.

According to commented drawbacks in previous subsection, it is precisely due to the physical limitations for providing uncertainty-free labeling in complicated scenarios, that estimation of certainty regarding all potential labeling possibilities is a topic of major importance. For this reason, the labeling problem considered in this thesis is described by the following two questions:

- What is the list of $t!$ labeled point estimates for the current dynamic state of the objects? Here each labeled point estimate hypothesizes the state of the t targets with indication of the labels.

- What is the certainty corresponding to each labeled point estimate in the list?

2.3.1 Problems with current TrBD MOT solutions

Regular TrBD trackers are known to fail at answering the questions due to the drawbacks highlighted in previous section. This subsection digs deeper into the root-cause of these drawbacks by showcasing the degraded tracking performance of regular TrBD algorithms. Both "labeling overconfidence" and "track coalescence" will be exemplified with numerical simulations. Firstly, "labeling overconfidence" is due to the fact that particle-based approximations (required due to the highly non-linear nature of the TrBD measurement models) cannot approximate multimodal densities for long periods of time [1], leading to the so-called particle "self-resolving" artifact. Secondly, "track-coalescence" underperformance [29] is due to extraction of Minimum Mean Square Error (MMSE) point estimates from a TrBD multimodal posterior density. In regular TrBD implementations, both errors get unnoticed without heuristic built-in mechanisms.

The particle "self-resolving" artifact is linked to the "particle mixing" phenomenon observed in [1] and illustrated by particles of different colors being mixed in similar regions of the state space in Fig. 2.2

When "particle mixing" happens, different particles are represented with permuted order of partitions in the state vector. This phenomenon is natural and expected when approximating multimodal densities, which are characteristic in the tracking of closely-spaced objects. In fact, it is in the multimodality of the multi-object Bayes posterior where the information about labeling resides [1][30].

The root cause of cloud "self-resolving" is the impoverishment of the particle cloud [31] observed in implementations with resampling stage such as the Sequential Importance Resampling (SIR) filter. Therefore, particle "self-resolving" is an artifact as it destroys the natural mixing in the particle cloud, concentrating all the particles in one of the modes and overlooking other areas of high probability mass such as the ones supporting

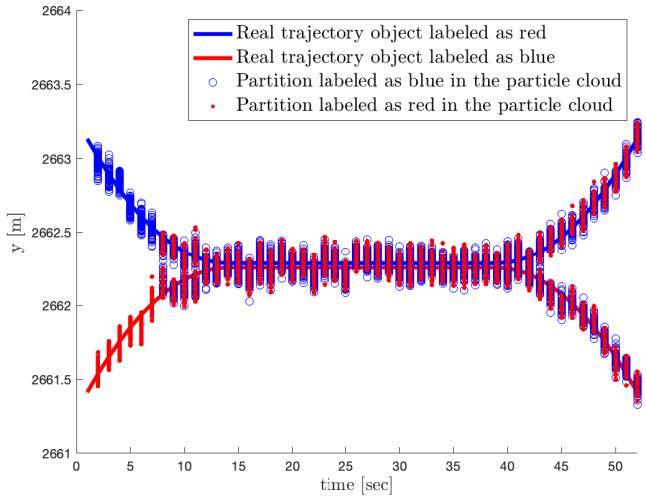

Figure 2.2: Illustration of expected "particle mixing" phenomenon when targets are closely-spaced and after separation. The particle filter is not "self-resolved" when "particle mixing" can be preserved.

alternative labeling hypotheses. This is the reason why particle "self-resolving" may lead to unnoticeable labeling confusion as illustrated in Figs. 2.3, 2.4 and 2.5.

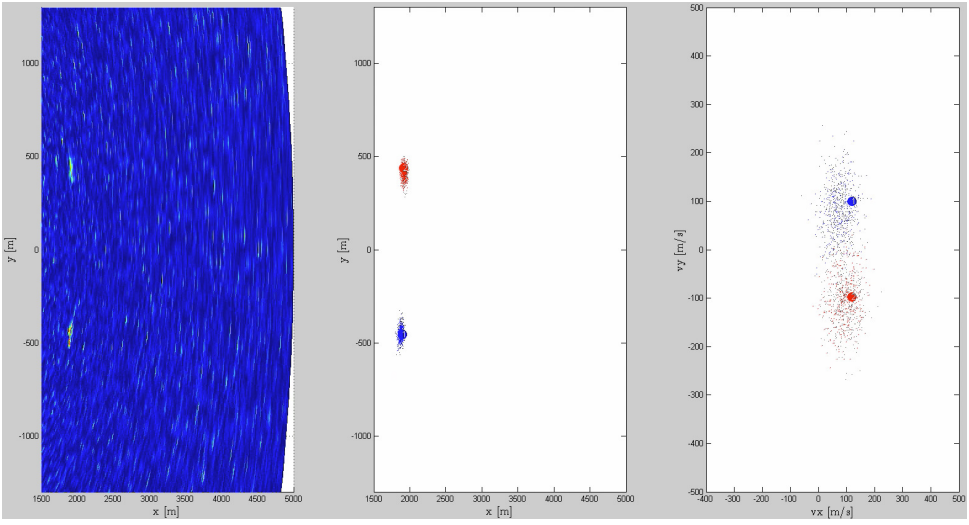

Figure 2.3: Results from a TrBD tracking implementation: raw-data on the left hand side, labeled ground truths and labeled particles for position and velocity dimensions in the center and in the right hand side respectively. Before the two targets become closely-spaced, the particle filter assigns labels correctly.

There are some generic solutions to tackle "self-resolving". In fact, any attempt to

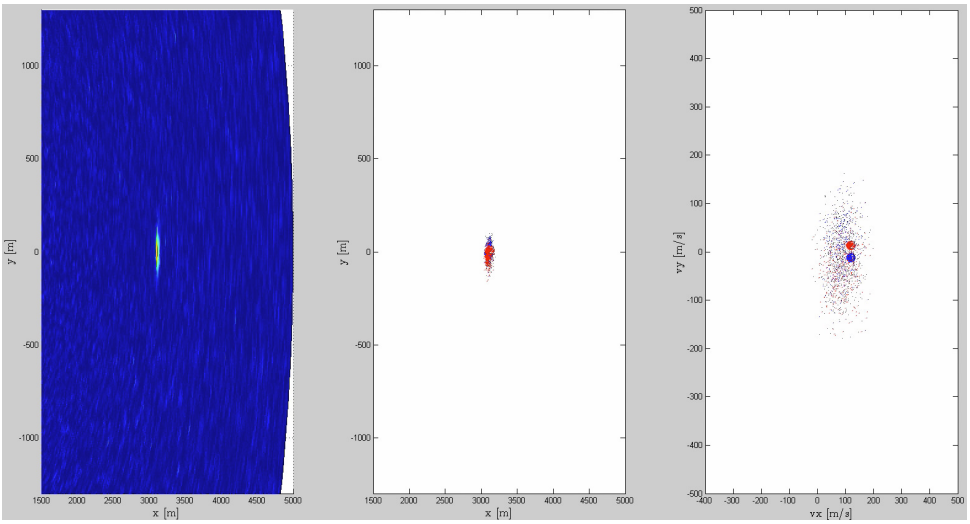

Figure 2.4: When the targets become closely-spaced "particle mixing" occurs, representing high labeling uncertainty.

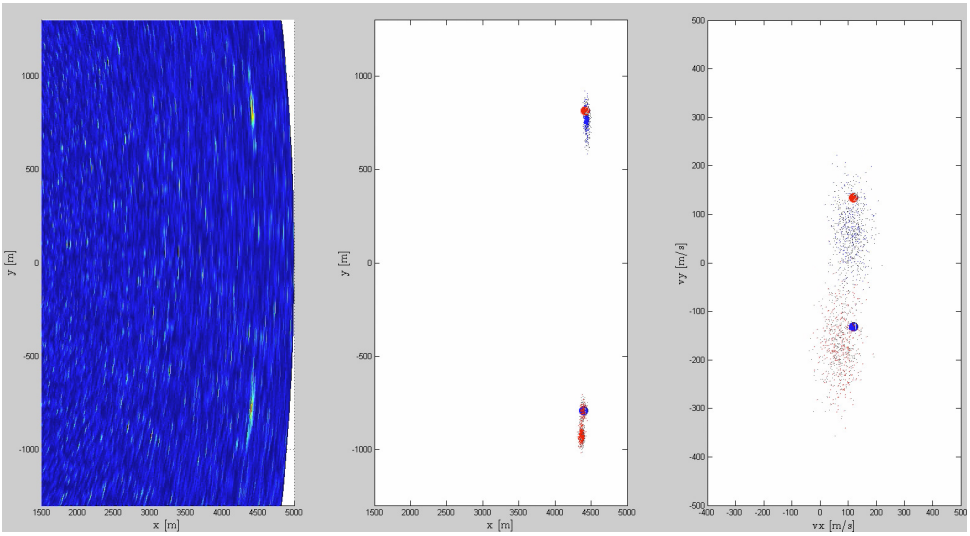

Figure 2.5: After the targets split, the PF "self-resolves" eventually due to its inability to approximate multimodal densities over long periods of time [1], leading to labeling confusion approximately 50% of the time.

mitigate impoverishment of the particle cloud, will reduce "self-resolving". These attempts can for instance be found in the Markov Chain Monte Carlo (MCMC) filters and the particle-flow filters [32]. A specific approach for mitigating particle "self-resolving", relevant in the context of our problem, is the one by García-Fernández et al in [33] based on a PF implementation with "mirror" particles.

Later in this thesis, a new alternative method to keep the multimodal character of the TrBD posterior density will be provided. This will be achieved by means of propagating the invariant component of the Unique density Decomposition (UD) [25] on isolation from the rest of the TrBD posterior density. Another way to illustrate successful operation of the filter after target separation is by representing the distribution of probability mass in the joint space as in the right hand side of Fig. 2.6.

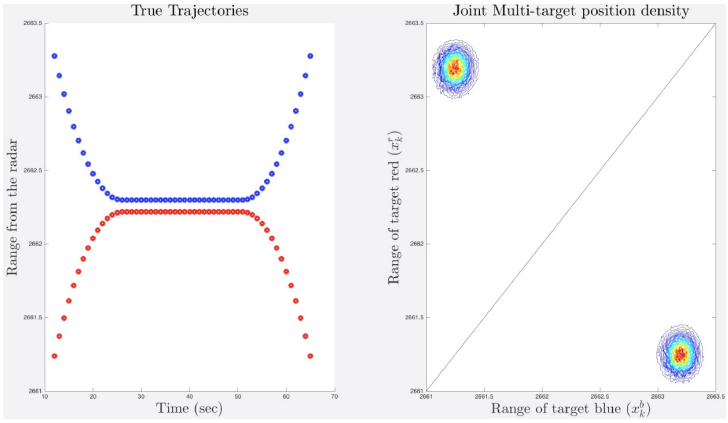

Figure 2.6: Symmetric bi-modal approximation of the position density associated to the last scan of the trajectories. This spread of probability mass represents that "particle mixing" has been preserved after target separation.

This type of symmetric spread of probability mass also represents that the PF implementation does not suffer "self-resolving". As opposed to the "self-resolved" particle cloud in Fig. 2.5, this particle-based approximation constitutes a reliable base-line for the tracker to take informed track-formation decisions. In fact, the multi-modal character of the density represents that the filter "remembers" a previous closely-spaced target situation leading to strong labeling uncertainty. In this particular case, the two modes hypothesize the existence of two objects in the same two specific locations, but disagree on the assignment of labels.

Even under the assumption that the filtering method captures the multimodal character of the Bayes posterior, naive track extraction leads to tracks nowhere close to the real trajectories after targets split. This "track-coalescence" undesired effect is illustrated in Fig. 2.7, where tracks are extracted via optimization over the common MSE metric by partitions in the particle cloud from Fig. 2.2.

Mentioned undesirable effects happening in TrBD context can be related to recognized underperformance in DBT context. In particular "track-coalescence" occurs when DBT JPDA-based methods operate in scenarios with high DA uncertainties. In DBT, this problem can be tackled with JPDA* [34], which inserts a simple heuristic in the JPDA algorithm. The "track-coalescence" problem has been also tackled in literature by extracting tracks based on Maximum a Posteriori (MAP) or Mean Optimal Subpattern Assignment (MOSPA) optimization. In both cases, preventing track-coalescence is achieved at the cost of disregarding labeling uncertainty, and therefore losing control over labeling confusion. As this is undesirable in applications where labeling of the objects matters, this thesis

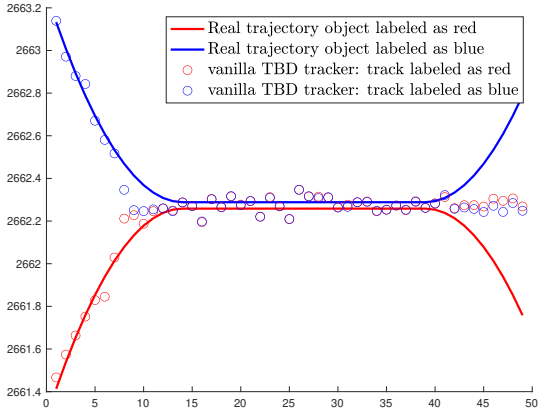

Figure 2.7: Illustration of degraded track estimation performance known as track-coalescence.

develops the TrBD methods presented in chapters 5, 6 and 7 to provide track extraction based on the labeled metric MMSE, while preventing "track-coalescence" and keeping control of labeling uncertainties. This will be done by inferring a particular decomposition of the Bayes posterior density. This desired decomposition of the Bayes posterior should be relevant for labeling uncertainty characterization [24], but should not rely on any DA technique so as to be usable in TrBD. In another analogy to the better understood DBT context, the desired decomposition could be considered as the TrBD counterpart of the DBT MHT decomposition for known and constant number of targets.

2.4 Formulation of the labeling problem in TrBD

The formulation of the labeling problem in TrBD, and the link between the DA problem and the labeling problem in DBT is formulated mathematically in this section based on the following definitions:

- DA defines hypotheses matching plots and labels.
- Labeling association defines hypotheses matching updated point estimates and labels.

Ambit:

- DA applies before update.
- Labeling association applies after update and point estimates extraction.

Applicability:

- DA is used to generate updated DA-dependent densities, these are the ones resulting from taking the prior densities and updating them according to the DA hypotheses.

- Labeling association is used to extend existing tracks, this is done by association of extracted point estimates to existent tracks. Note that this is equivalent to consider the "pair matching" problem between extracted point estimates and labels.

The relevant problem from the application point of view is the labeling problem. The link between the DA and labeling problems can be described in the context of traditional DBT trackers. In fact, DBT filters only tackle the DA problem but, once the DA problem is solved, the solution of the labeling problem follows right away: one only needs to perform DA-dependent updates and extract (labeled) point estimates, from each DA-dependent posterior density.

To support the claim that once DA is solved in DBT, the solution of the labeling problem follows right away, let us take the following assumptions without loss of generality.

- Perfect detectability, no false detections.
- No merged measurements.
- The measurements do not provide any info about label.

Let us define $\boldsymbol{\varkappa}_k$ as the vector of plots at time step k with explicit indication of correct DA: $\boldsymbol{\varkappa}_k = [\boldsymbol{p_1}, \boldsymbol{p_2}, ..., \boldsymbol{p_t}]^T$. In other words, the information in $\boldsymbol{\varkappa}_k$ is based on "known DA" as the subscripts are not only used to differentiate one plot from another, but they also link the plots to the labels of the targets which generated the plots, e.g. the plot in the first position of $\boldsymbol{\varkappa}_k$ has been generated by target 1, being this statement not a hypothesis but a fact.

In practice, the tracker cannot access $\boldsymbol{\varkappa}_k$ but a version of it with unknown DA, which we denote as $\boldsymbol{z}_k = [\boldsymbol{d_1}, \boldsymbol{d_2}, ..., \boldsymbol{d_t}]^T$. Note that the subscripts here are merely differentiating one plot from another, but they do not represent correct DAs. Let us define the vector $\boldsymbol{\omega} = [\pi_1, \pi_2, ..., \pi_{t!}]^T$, which contains the functions to perform all possible permutations of t elements in a vector. For instance, $\boldsymbol{\omega} = [\pi_1(\boldsymbol{z}_k), \pi_2(\boldsymbol{z}_k), ..., \pi_{t!}(\boldsymbol{z}_k)]^T$ represents all possible permutations of the plot vector $\boldsymbol{z}_k$.

In short, the subscripts in $\boldsymbol{\varkappa}_k$ provide correct DA while the subscripts in $\boldsymbol{z}_k$ provide differentiation between the elements. Although the subscripts in $\boldsymbol{z}_k$ happen to coincide with the particular order in which plots are collocated in the vector, this could have been different. In fact, as the order is random:

$$P(\boldsymbol{z}_k = \pi_m(\boldsymbol{\varkappa}_k)) = P(\boldsymbol{z}_k = \pi_n(\boldsymbol{\varkappa}_k)) \qquad \forall\{m,n\} : \{\pi_m, \pi_n\} \in \boldsymbol{\omega} \tag{2.1}$$

Let us consider the state vector $\boldsymbol{s}_k$, where the individual states of t objects are stacked with explicit indication of labels: $\boldsymbol{s}_k = [\boldsymbol{s}_k^1, \boldsymbol{s}_k^2, ..., \boldsymbol{s}_k^t]^T$. Solving the DA problem requires: generation of DA hypotheses and evaluation of the DA hypotheses.

Let us use $\boldsymbol{h}_k$ to note the set of generated DA hypotheses: $\boldsymbol{h}_k = \{(\boldsymbol{a_1}, \boldsymbol{a_2}, ..., \boldsymbol{a_{t!}})\}$, where $\boldsymbol{a_m} = \pi_m(\boldsymbol{z}_k)$. Note that the subscripts in the vector $\boldsymbol{a_m}$ are not labels, the labels are implicit in the order of the elements represented by $\boldsymbol{a_m}$. Note that in any case, these labels represent hypotheses of association not correct associations. $\boldsymbol{a_m}$. For illustrative purposes, consider a simple two objects case and the association hypothesis $\boldsymbol{a_1} = [\boldsymbol{d^2}, \boldsymbol{d^1}]^T$. According to the notation, $\boldsymbol{a_1}$ hypothesizes that the detection which came in second position in $\boldsymbol{z}_k$ was produced by target labeled as 1 and the one which came in first position was produced by the target labeled as 2.

Given the model for the likelihood of the measurements conditioned on the state $l(z_k|s_k)$, a DA dependent decomposition of $p(s_k|Z_k)$ can be formulated as:

$$p(s_k|Z_k) \approx \sum_{m=1}^{t!} l(\pi_m(z_k)|s_k)p(s_k|Z_{k-1}) \tag{2.2}$$

From Equation (2.2), one can conclude that in DBT an analytical decomposition relevant for labeling characterization follows from solving the DA problem. In fact, each component in the sum directly relates one DA hypotheses $\pi_m(z_k)$ with its association-dependent posterior density $l(\pi_m(z_k)|s_k)p(s_k|Z_{k-1})$. Furthermore, extraction of sufficient statistics from each component in the sum, by minimizing the MMSE, provides a labeled point estimate. Note that a labeled point estimate explicitly hypothesizes one particular association between point estimates and labels. According to this labeling association, the tracks can be extended. This trivial derivation demonstrated in DBT context that, once DA is solved, the solution of the labeling problem follows right away.

- Remarks:
  - The analytical evaluation of labeling association hypotheses has a one-to-one relation to the evaluation of DA hypotheses. In particular, the certainty associated to the labeled point estimate extracted from $l(\pi_m(z_k)|s_k)p(s_k|Z_{k-1})$ is:
$$p(\pi_m(z_k)|Z_k) = \frac{\int l(\pi_m(z_k)|s_k)p(s_k|Z_{k-1})ds_k}{\sum_{m=1}^{t!}\int l(\pi_m(z_k)|s_k)p(s_k|Z_{k-1})ds_k} \tag{2.3}$$
  - Under the assumption that $p(s_k|Z_{k-1})$ can be formulated as one single density $\forall k$, Equation (2.2) does not run into "combinatorial explosion" over time. As will be explained in chapter 4, this assumption only holds in implementations using particle-based approximation of the various DA-dependent updated densities.
  - This analytical derivation is the base of the optimal reference derived in chapter 4 and that will be used to evaluate the proposed DA-free methods proposed in the last chapters of the thesis.

As a conclusion, it is trivial to solve the labeling problem in DBT by tackling the DA problem. Unfortunately, the same analytic method cannot be applied in TrBD filtering to solve the labeling problem due to the absence of detections.

In TrBD context, the raw data noted by $\mathbf{z}_k$ is defined as the power reflected from the tracking scenario for each radar cell at time step k. For instance, a 2D range-bearing raw data-set $\mathbf{z}_k$ can be modeled as in [4] by $N_r \times N_b$ power measurements z_k^{ij}, where $i = 1, 2, ..., N_r$ and $j = 1, 2, ..., N_b$. The same TrBD measurement model has been used to generate the raw measurements illustrated in the left hand side of Figs. 2.3, 2.4 and 2.5. The detailed formulation of this TrBD measurement model will be provided in chapter 3.

The permutation of measurement z_k by using the functions in $\boldsymbol{\omega}$ cannot be replicated for the TrBD measurements $\mathbf{z}_k$. In fact, $\pi_m(\mathbf{z}_k)$ has no physical interpretation, so it cannot be used to decompose the TrBD posterior density. However, note that the evaluation of

$l(\pi_m(\boldsymbol{z}_k)|\boldsymbol{s}_k)$ and $l(\boldsymbol{z}_k|\pi_m(\boldsymbol{s}_k))$ are equivalent for a given prior density $p(\boldsymbol{s}_k|\boldsymbol{Z}_{k-1})$. Therefore, one could interpret that Equation (2.2) does have a TrBD counterpart:

$$p(s_k|\mathbf{Z}_k) \propto \sum_{m=1}^{t!} l_{TrBD}(\mathbf{z}_k|\pi_m(s_k))p(s_k|\mathbf{Z}_{k-1}) \tag{2.4}$$

where we use $p(s_k|\mathbf{Z}_k)$ to denote the posterior density, $l_{TrBD}(\mathbf{z}_k|\boldsymbol{s}_k)$ to denote the likelihood model for the raw measurements conditioned on the state and $p(s_k|\mathbf{Z}_{k-1})$ to denote the predicted density. We consider the worst case scenario, where TrBD measurements do not incorporate information about objects' labels (as described by the first assumption in the introductory chapter). Under this assumption, $l(\mathbf{z}_k|\boldsymbol{s}_k)$ is invariant with respect to permutation of partitions in the state vector:

$$l(\mathbf{z}_k|\pi_m(s_k)) = l(\mathbf{z}_k|\pi_n(s_k)) \quad \forall\{m,n\} : \{\pi_m,\pi_n\} \in \omega \tag{2.5}$$

This is a remarkable difference with respect to DBT, where $l(\boldsymbol{z}_k|s_k)$ is permutation variant (even when the measurements do not provide any information about the labels). Due to (2.5), Equation (2.4) provides a decomposition in which all components end up being identical disregarding whether the objects are closely-spaced or not. As this does not make sense, Equation (2.4) cannot be relevant for labeling characterization in TrBD. In fact, Equation (2.4) can be simplified as:

$$p(s_k|\mathbf{Z}_k) \propto \sum_{m=1}^{t!} l(\mathbf{z}_k|\pi_m(s_k))p(s_k|\mathbf{Z}_{k-1}) \propto l(\mathbf{z}_k|s_k)p(s_k|\mathbf{Z}_{k-1}) \tag{2.6}$$

The simplification in Equation (2.6) illustrates that, although $p(s_k|\mathbf{Z}_k)$ can be calculated, an analytical decomposition of $p(s_k|\mathbf{Z}_k)$ relevant for labeling characterization cannot be accessed by the TrBD filter. The inference of relevant label-dependent decompositions of $p(s_k|\mathbf{Z}_k)$ in TrBD defines the specific problem which needs to be tackled to answer the two questions of interest formulated by the problem description in section 2.3.

2.5 Related literature

A plethora of MOT techniques have been developed over recent decades including Joint Probabilistic Data Association (JPDA) [35], MHT [11] and Probability Hypothesis Density (PHD) [36]. These algorithms are designed to work with detections. As the scope of this thesis is within TrBD MOT, none of these methods are suitable.

Some RFS-based trackers use multitrajectory densities instead of multiobject densities [37]. A multitrajectory random variable incorporates the states of the entire history for each trajectory in the set. With this information, track formation is enabled without any type of label incorporation. [38] describes multitrajectory RFS methods accommodating standard (point based) measurements. Interestingly, it also mentions that the method can be applied to TrBD measurement. However, the guideline in [38] regarding TrBD measurement update is to proceed as in [39], where a multiobejct RFS filter is used instead of a multitrajectory RFS. In particular, the method in [39] tackles TrBD measurements by means of fitting a particle-based multiobject density approximation as a Labeled Multi-Bernoulli (LMB) RFS density after each filtering iteration. Nonetheless, this would not

allow propagation of labeling uncertainty as one would need to use a LMB mixture to do so.

In [40], a backward simulation method is proposed to recover full trajectory (labeling) information from unlabeled filtering mutiobject densities. However, the process (generating unlabeled filtering posteriors, recovering trajectory information and marginalizing to obtain the filtering density of interest) involves a complexity overhead unfordable by practical implementations targeted in this thesis. More specifically, this complexity is prohibitive when implementing this solution in TrBD context, where RFS prior conjugacy cannot be exploited as particle-based approximations are required to accommodate highly nonlinear TrBD observation models. Additionally, the problem in the scope of this thesis does not even need to be formulated with RFS as the number of objects is assumed known and constant.

Aoki et al. provided a mathematical characterization of the labeling uncertainties with clear physical interpretation in [41]. However, the proposed Multitarget Sequential Monte Carlo filter algorithm involves computational complexity of $O(N_p^2 t!^2)$, being N_p the number of particles. This computational bottleneck is prohibitive for tracking in scenarios with more than two objects.

Blom and Bloem [25] introduced a decomposition of the exact Bayes posterior density into the weighted sum of permutation invariant and permutation strictly variant components. The so-called Unique Decomposition (UD) was used by García-Fernández in [33] to provide a particle filtering solution relevant for our problem description. The main focus in [33] is on calculating the probability of successful labeling after object separation, assuming the posterior multiobject density has symmetric nature [42][30]. In particular, the contribution of García-Fernández to the labeling problem is based on linking the so-called probability of successful labeling to the particular metric and point estimate considered [33]. These contributions were exemplified for the tracking of two objects with a Wireless Sensor Network (WSN).

A generalization of the UD [25] was provided by Croise et al. in [43], where the main focus is on demonstrating how the UD can be used to approximate MMOSPA estimates. Although MMOSPA estimates do not provide answers to the questions in the Problem Description section due to its unlabeled nature, it is important to remark that the consideration of OSPA metric (or its generalization GOSPA) has been reported successful at preventing track-coalescence. Nevertheless, MMOSPA estimates are very computationally demanding to calculate and therefore its implementation in dynamic systems has only been reported under some approximations [44] [45].

The use of MMOSPA estimates has been encouraged by the majority of reviewed solutions. Only [33] has reported successful results at avoiding track-coalescence using MMSE estimates. This becomes possible as the specific problem formulated in the Problem Description section is tackled by incorporating characterization of labeling uncertainty in the filtering process. Interestingly, this characterization does not rely on DA techniques and therefore it is usable in TrBD. Unfortunately, although proposed as future work in [33], the generalization of this solution for more than two objects has not been addressed.

2.6 Conclusions and connections to upcoming chapters

Does the fact that DA cannot be formulated in TrBD mean that the labeling problem is inherently solved through Bayesian filtering? To answer this question, it is important to note that it is in the multimodality of the Bayes posterior where the information about labeling resides. In fact, when the multitarget density becomes multimodal, the modes tend to show up in symmetric regions of the joint state space (when the objects get sufficiently separated after being closely-spaced) [1][30].

The answer to the question is no, vanilla TrBD tracking algorithms, such as the one in [4] provide a non-decomposed posterior density, which happens to be multimodal in scenarios where closely-spaced targets are involved. Unlike in DBT tracking, where DA decomposes the multimodal posterior density based on labeling uncertainty, one cannot rely on any existent decomposition method for the TrBD problem. Therefore, the labeling problem is not solved inherently through plain TrBD Bayesian filtering.

Connections to the contributions in upcoming chapters can be made on the basis of the labeling problem. There is a clear distinction between chapter 3 and chapters 5, 6 and 7. In chapter 3, the focus is on labeling uncertainty reduction. Chapters 5, 6 and 7 focus on labeling uncertainty characterization. Chapter 4 provides a criterion to evaluate the algorithmic solutions provided in chapters 5, 6 and 7. Chapter 3 illustrates that proper estimation of targets interacting-dynamics aids at reducing labeling uncertainty so as to avoid label confusion even in scenarios with closely-spaced targets. Chapters 5, 6 and 7 provide the main contribution of this thesis by considering a more generic TrBD MOT problem, where labeling uncertainty reduction methods are not implemented or simply not sufficient to provide uncertainty-free point-estimate-to-label assignment. Resorting again to analogies with traditional DBT methods, chapters 5, 6 and 7 attempt to derive and implement the TrBD counterpart of DBT MHT for constant and known number of targets.

3

Tracking of Interacting targets

3.1 Introduction

Before delving into the main contribution of this thesis, namely generic TrBD labeling uncertainty characterization, this chapter illustrates how labeling confusion can be tackled in particular scenarios where interacting targets are involved. This chapter looks at the labeling confusion problem from the dynamics point of view, which is especially effective when some structure can be extracted from the coupled motion of the targets. Detection of anomalous target behaviors is a related higher level challenge, which is also considered in this chapter. Both challenges are tackled by means of modeling and estimating interacting targets motion.

Interacting and even coordinated motion can be found in objects that fly in formation, groups of objects that intentionally move closely together as a group such as drone swarms, and even well-separated objects that are executing a joint plan. There exist all sorts of other constraints on movements due to environmental limitations. These could come from circulation infrastructure or rules and the physical size of objects. Due to these types of limitations, target dynamics are also affected. For example, road vehicles may not be able overtake each other unless following some particular trajectories. For flying objects, some rules apply in controllable scenarios as defined in the International Civil Aviation Organization (ICAO) for Remotely Piloted Aircraft Systems (RPAS) regulation [46]. These rules determine remain-well-clear and collision-avoidance volumes for maneuvering of closely-spaced objects according to Fig. 3.1.

In hostile scenarios, regulations in [46] are obviously not taken into account. However, due to the physical dimensions of targets, closely-spaced trajectories are still constrained by the collision volumes as objects cannot simply keep on moving through each other.

Unlike in signature-based classification solutions, where labeling information is extracted via characterization of measurements, this chapter focuses on estimating labeling

The contents provided in this chapter have been published in "Tracking of interacting targets," C. M. Leon, L. S. Mihaylova and H. Driessen, in *proceedings of the 20th International Conference on Information Fusion*, Xi'an (China), 2017, pp. 1-8.

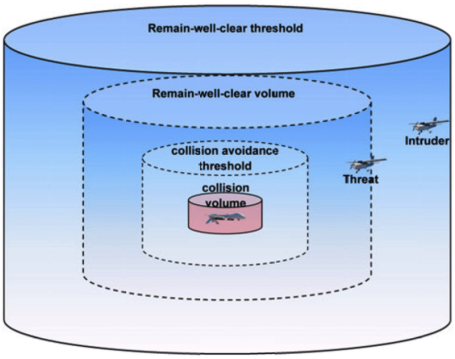

Figure 3.1: Thresholds and volumes affecting closely spaced object as defined by the ICAO RPAS.

information by characterizing coupled target dynamics. Given a previously labeled set of tracks, if prediction of exact dynamic states of the objects would be possible, there would not be uncertainty so as to which label corresponds to which track. Although exact prediction is not possible, this chapter illustrates how on-line learning of dynamic coupling-parameters aids at producing better prediction models. As a result, labeling confusion can be reduced even in closely-spaced target scenarios.

Some literature exists on group tracking, which is certainly a particular case of interacting targets tracking. In [47], a framework based on the so called "Evolving Networks" is proposed to perform targets state estimation and group structure discovery. The method relies on a graphical network-like representation where each node represents a different target. When the targets are considered in the same group, the evolution model becomes coupled along the coordinates of different objects. However, although it is fairly understandable that different objects traveling in a group are interacting with each other, the method does not cover any kind of interactions between targets which are not considered in the same group. Modeling this type of interactions between non-closely-spaced targets is relevant for detection of anomalous behavior of targets that are far away from each other.

In this chapter we present a method for tracking interacting targets disregarding whether or not the targets are close to each other. The method relies on parametric modeling of targets interactive motion. The presented filtering solution incorporates the parameters of the model in the state vector together with the targets dynamic state. Moreover, the parameters of these interactive motion models are auto-tunable as they are modified on-line, exploiting the (Bayes) posterior certainty of estimation results. The proposed method is applied in a simulated MOT application where target dynamics become coupled and independent alternatively along the simulation.

Numerical simulations will show that the presented approach results in estimation error reduction, allows detection of interactive target behaviors and reduces labeling confusion for closely-spaced targets in TrBD tracking. The benefits of modeling interacting target dynamics also apply in traditional DBT MOT, aiding at reducing DA uncertainties. However, simulations in this chapter are based on TrBD measurements to align with the research

direction of the thesis.

3.2 Proposed approach

The method presented in this chapter is motivated by the idea that all possible interacting behaviors can be modeled relying on two different sources of information. Firstly, the set of points that the targets get attracted to or repulsed from. Secondly, the models of interaction between the targets and these points of attraction/repulsion. By these means, any interacting behavior can be understood as variable accelerations of the targets in relation with the set of attraction/repulsion points. These unknown points can be variable in number, fixed, dynamic, or even be another target of interest.

A complete solution would estimate the attraction/repulsion points, the coupling parameters (modeling interactions between the targets and these points), and the dynamics of the targets, all together in the joint space. To this end, we model target interactions by using a very simplified version of the so-called Social Force models applied separately for each coordinate. Social Force models, introduced by Helbing [48], have been used extensively in pedestrian tracking. In these applications, social forces are proven to effectively reduce data association errors as in [49]. Several challenges as handling occlusions [50] or tracking with cameras with no overlapping fields of view [51] have been tackled by using these models.

The chapter is organized as follows. In Section 3, the assumptions of the interacting target motion model are formulated in continuous time and the associated discretized model is derived. In Section 4, the incorporation of the discretized model in a TrBD MOT application is discussed. First, the measurement model is defined and then, it is put together with the proposed interacting motion model in the context of recursive Bayesian estimation. In Section 5, simulation examples are presented. Firstly, preliminary results showing estimation error reduction are provided. Secondly, detection of suspicious target interacting-behavior is illustrated based simulation results using a Multiple Model (MM) filtering implementation. In the final part of section 5, it is shown that labeling confusion can be prevented by means of inferring coupled target-dynamics. Conclusions are provided in section 6.

3.3 Interacting Target Motion Modeling

Independent target motion models are oftentimes used for the tracking of any target disregarding its degree of interaction. This subsection formulates a generic dynamic system to set the base line. Interacting dynamics modeling will be incorporated to the base line in the following subsection. For sake of simplicity in the formulation, let us consider 2D objects. For each object, the state vector $s(t)$ comprises two coordinates (x and y) and for each coordinate we consider two dimensions: position ($x(t)$, $y(t)$) and velocity ($\dot{x}(t)$, $\dot{y}(t)$). Then $s(t) = [x(t)\ \dot{x}(t)\ y(t)\ \dot{y}(t)]^T$.

A generic continuous-time dynamic model can be represented by a first order linear differential stochastic system as in Fig. 3.2.

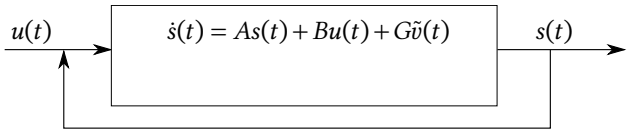

Figure 3.2: Generic first order linear dynamic system

where A is called the *system matrix*, B is the (continuous-time) *input gain*, G is the (continuous-time) *noise gain*. $s(t)$ is the state vector, $u(t)$ is the input vector and $\tilde{v}(t)$ is the (continuous-time) process noise. The Continuous White Noise Acceleration model [23] is a widely used independent target motion model. It is characterized by having zero input contribution and matrices,

$$A = diag(A_1, A_2, ..., A_N) \tag{3.1}$$

where N is the total number of coordinates,

$$A_n = \begin{pmatrix} 0 & 1 \\ 0 & 0 \end{pmatrix}; n = 1, ..., N \tag{3.2}$$

$$G = diag(G_1, G_2, ..., G_N) \tag{3.3}$$

$$G_n = \begin{pmatrix} 0 \\ 1 \end{pmatrix}; n = 1, ..., N \tag{3.4}$$

being $\tilde{v}(t)$ continuous-time Standard White Gaussian.

In some more elaborated models the input contribution is considered. When the input vector is fully known, it only causes an explicit time dependency in the deterministic part of the evolution model. However, in MOT applications, the control signals applied on each target are seldomly modeled (if ever) by the tracking system. Therefore, the control vector causes also a dependency in the random component $\tilde{v}(t)$. As we will see in Subsection 3.3.1, the unknown control vector will be considered part of the state vector to be estimated by the tracker.

3.3.1 Assumptions on targets interaction

Interacting targets perform accelerations depending on the dynamics of other objects and the environment. Therefore, independent target motion modeling is not optimal when tracking interacting targets as coupled accelerations get overlooked. In this subsection our parametric model of targets interaction is presented.

In this chapter we consider a toy scenario where two objects (labeled as "b" and "r") move in 2D, the state vector can be represented as $s(t) = [s^b(t)\ s^r(t)]^T$. Furthermore, we assume that the target labeled as "b" is the only point of attraction/repulsion.

When the motion along the same coordinates is assumed to be coupled for different targets, obtaining an explicit expression of the model in discrete time is not straightforward. Special considerations have to be taken into account as the calculation of the discrete transition matrix and the covariance of the discrete process noise cannot be decomposed

at coordinate level. Therefore, interacting assumptions need to be defined in continuous time and the discretization of the transition model needs to be worked out. The assumed structure of the interactive motion is formulated as,

$$\ddot{x}^r(t) = k_1(x^b(t) - x^r(t)) - k_2\dot{x}^r(t) \tag{3.5}$$

$$\ddot{y}^r(t) = k_1(y^b(t) - y^r(t)) - k_2\dot{y}^r(t) \tag{3.6}$$

with k_1 and k_2 assumed constants with units $[s^{-2}]$ and $[s^{-1}]$ respectively.

The model basically represents that the accelerations performed by the object labeled as "r" are the result of combining two aspects. These are: the intention of target labeled as "r" to interact with the target labeled as "b" and the maneuvering limitations of the target labeled as "r" due to inertia. The second aspect is especially dominant in fix wing air targets. In this particular case only two parameters are needed (k_1 and k_2). We consider the state vector ordered in the following manner, $s(t) = [s_x(t)\ s_y(t)]^T$ where,

$$s_x(t) = [x^b(t)\ \dot{x}^b(t)\ x^r(t)\ \dot{x}^r(t)]$$

$$s_y(t) = [y^b(t)\ \dot{y}^b(t)\ y^r(t)\ \dot{y}^r(t)]$$

Expresions in (3.5) and (3.6) can be directly incorporated as inputs in the generic model from Fig. 3.2. Choosing to do so allows us to consider the input as a good representation for the intention of the pilot controlling the "r" object. In this case, matrix B is given by,

$$B = diag(B_n, B_n), \tag{3.7}$$

$$B_n = (0\ 0\ 0\ 1)^T \tag{3.8}$$

and,

$$u(t) = Ks(t), \tag{3.9}$$

where,

$$K = diag(K_n, K_n), \tag{3.10}$$

and

$$K_n = (k_1\ 0\ -k_1\ -k_2) \tag{3.11}$$

By these means, we have modeled accelerations depending on unknown control decisions (which ultimately depend on the dynamics of other objects). Now, we can put this model for the accelerations together with a Continuous White Noise Acceleration model,

$$\dot{s}(t) = As(t) + BKs(t) + G\tilde{v}(t) = (A + BK)s(t) + G\tilde{v}(t) \tag{3.12}$$

resulting in the system,

$$\dot{s}(t) = A_c s(t) + G\tilde{v}(t) \tag{3.13}$$

where,

$$A_c = diag(A_p, A_p), \tag{3.14}$$

being A_p the matrix,

$$A_p = \begin{pmatrix} 0 & 1 & 0 & 0 \\ 0 & 0 & 0 & 0 \\ 0 & 0 & 0 & 1 \\ k_1 & 0 & -k_1 & -k_2 \end{pmatrix} \tag{3.15}$$

3.3.2 Discretization of the continuous time model

We can split the discretization of the system from (3.13) in two equal parts and associate the separate results (for "x" and "y" directions) with block chunks in the discrete transition matrix and the covariance matrix of the discrete process noise. The discretization will be derived for one of the two directions and duplicated for the other. If we select the direction "x" for discretization,

$$\dot{s}_x(t) = A_p s_x(t) + G\tilde{v}_x \tag{3.16}$$

where,

$$\tilde{v}_x = \begin{bmatrix} \tilde{v}_{x^b} \\ \tilde{v}_{x^r} \end{bmatrix} \tag{3.17}$$

its discrete version can be represented as,

$$s_{x,k+1} = A_b s_{x,k} + v_{x,k} \tag{3.18}$$

Moreover, the discretization of the entire system in (3.13) can be expressed as,

$$s_{k+1} = A_d s_k + v_k \tag{3.19}$$

where A_b can be replicated in the discrete system transition matrix A_d as,

$$A_d = \begin{pmatrix} A_b & 0 \\ 0 & A_b \end{pmatrix} \tag{3.20}$$

the derivation of A_b can be found in Appendix A.1, as well as the definition of $\lambda's$, resulting on:

$$A_b = \begin{pmatrix} 1 & \delta t & 0 & 0 \\ 0 & 1 & 0 & 0 \\ \frac{\lambda_2(1-e^{\delta t\lambda_3})-\lambda_3(1-e^{\delta t\lambda_2})}{\lambda_2-\lambda_3} & A_b(3,2) & \frac{\lambda_2 e^{\delta t\lambda_3}-\lambda_3 e^{\delta t\lambda_2}}{\lambda_2-\lambda_3} & \frac{e^{\delta t\lambda_2}-e^{\delta t\lambda_3}}{\lambda_2-\lambda_3} \\ \frac{\lambda_2\lambda_3(e^{\delta t\lambda_2}-e^{\delta t\lambda_3})}{\lambda_2-\lambda_3} & A_b(4,2) & -\frac{\lambda_2\lambda_3(e^{\delta t\lambda_2}-e^{\delta t\lambda_3})}{\lambda_2-\lambda_3} & \frac{\lambda_2 e^{\delta t\lambda_2}-\lambda_3 e^{\delta t\lambda_3}}{\lambda_2-\lambda_3} \end{pmatrix} \tag{3.21}$$

where
$A_b(3,2) = -\frac{k_1(e^{\delta t\lambda_2}-e^{\delta t\lambda_3}-\delta t\lambda_2+\delta t\lambda_3)+k_2\lambda_2(1-e^{\delta t\lambda_3})-k_2\lambda_3(1-e^{\delta t\lambda_2})}{k_1(\lambda_2-\lambda_3)}$
and
$A_b(4,2) = \frac{k_1(\lambda_2-\lambda_3-\lambda_2 e^{\delta t\lambda_2}+\lambda_3 e^{\delta t\lambda_3})-k_2\lambda_2\lambda_3(e^{\delta t\lambda_2}-e^{\delta t\lambda_3})}{k_1(\lambda_2-\lambda_3)}$.

Furthermore, v_k in (3.19) is the discrete process noise with zero mean, and covariance matrix given by,

$$cov[v] = C_d = \begin{pmatrix} C_b & 0 \\ 0 & C_b \end{pmatrix} \tag{3.22}$$

The discrete time random component for direction "x" v_x is given by the integral:

$$v_x(k\delta t) = \int_{k\delta t}^{(k+1)\delta t} e^{A_p((k+1)\delta t-\tau)} G(\tau)\tilde{v}_x(\tau)d\tau \tag{3.23}$$

which represents a four dimensional multivariate Gaussian distribution parameterized by zero mean and covariance matrix:

$$C_b = \tilde{q}_x \int_0^{\delta t} e^{A_p(\delta t-\tau)} G [e^{A_p(\delta t-\tau)} G]^T d\tau. \tag{3.24}$$

where $\tilde{q}_x$ is the continuous-time process noise intensity in "x" direction.

3.3.3 Consideration of variable targets interacting behavior

Hidden interactions between the objects and the environment may vary and therefore the unknown parameters k_1 and k_2 should account for this variability as well. Objects may even gradually transition from independent motion to interacting motion when, for instance, targets that are initially far away from each other moving independently "decide" to gather and travel in group formation for a while.

Incorporation of the knowledge about objects interacting behavior requires an effort of on-line learning k_1 and k_2. This can be done directly by extending the state vector with k_1 and k_2 and their respective change rate. The extended state vector considered is $\underline{s}(t) = [s(t)\ k_1(t)\ \dot{k}_1(t)\ k_2(t)\ \dot{k}_2(t)]^T$. Indeed, k_1 and k_2 are not considered constants any more. Instead, k_1 and k_2 are considered variables and are assumed to evolve according to independent Continuous White Noise Acceleration models.

Then, the model considered for the new state vector can be expressed as,

$$\underline{s}_{k+1} = A_e \underline{s}_k + v_{e,k} \tag{3.25}$$

where,

$$A_e = \begin{pmatrix} A_d & 0 \\ 0 & A_k \end{pmatrix} \tag{3.26}$$

the blocks of A_e associated to coordinates k_1 and k_2 are straightforward to calculate as they are uncoupled from any other coordinate,

$$A_k = \begin{pmatrix} A_u & 0 \\ 0 & A_u \end{pmatrix} ; where \ \ A_u = \begin{pmatrix} 1 & \delta t \\ 0 & 1 \end{pmatrix} \tag{3.27}$$

being,

$$v_e = [v\ v_{k1}\ v_{\dot{k}1}\ v_{k2}\ v_{\dot{k}2}]^T \tag{3.28}$$

which represents a twelve dimensions multivariate Gaussian distribution parameterized by zero mean and covariance matrix,

$$cov[v_e] = \begin{pmatrix} C_d & 0 \\ 0 & C_k \end{pmatrix} \tag{3.29}$$

$$C_k = \begin{pmatrix} C_u & 0 \\ 0 & C_u \end{pmatrix} \tag{3.30}$$

again, the blocks C_u associated with coordinates k_1 and k_2 can be calculated straightforwardly,

$$C_u = \begin{pmatrix} \frac{\delta t^3}{3} & \frac{\delta t^2}{2} \\ \frac{\delta t^2}{2} & \delta t \end{pmatrix} \tilde{q}_k \tag{3.31}$$

where $\tilde{q}_k$ is the continuous-time process noise intensity of the variables modeling the interacting motion.

3.4 Integration of Interacting Motion Modeling in a TrBD Tracking Application

This section contains all necessary aspects to develop a particle filtering algorithm based on the formulated model of targets interaction.

Let s_k denote the state vector and z_k denote the TrBD measurements at time index k. Z_k denotes the set of measurements up to time k, including z_k: $Z_k = \{z_1, z_2, ..., z_k\}$. The state space model can be represented by two conditional probability densities:

$$s_{k+1} \sim p(s_{k+1}|s_k), \tag{3.32}$$

$$z_k \sim p(z_k|s_k), \tag{3.33}$$

where in our particular case, $p(s_{k+1}|s_k)$ is the dynamic model presented in previous subsection (Eq. (3.25)). $p(z_k|s_k)$ is the probability density of the measurements given the state. This density function is presented in Subsection 3.4.1.

3.4.1 Observation model: radar track-before-detect measurements

For the numerical experiments we consider a radar TrBD measurement model as in [52]. The used measurement model defines the power reflected by the tracking scenario for each radar cell. One measurement z_k is composed of $N_r \times N_b$ power measurements z_k^{ij}, where $k \in \mathbb{N}$ and N_r and N_b are the number of range and bearing cells.

$$z_k^{ij} = |z_{A,k}^{ij}|^2 = |A_k^{(1)} h_A^{(1)ij} + A_k^{(2)} h_A^{(2)ij} + n_I(t_k) + i n_Q(t_k)|^2 \tag{3.34}$$

where A_k^c is the complex amplitude of the target labeled as c.

$$A_k^c = \tilde{A}_k^{(c)} e^{i\phi_k},\ \phi_k \in U(0, 2\pi) \tag{3.35}$$

$$h_A^{(c)ij}(s_k^c) = e^{-\frac{(r_i - r_k^c)^2}{2R} - \frac{(b_j - b_k^c)^2}{2B}},\ i = 1, ..., N_r,\ j = 1, ..., N_b \tag{3.36}$$

r_k^c and b_k^c are the range and bearing of the target c. Note that c is used for the target labels, which could either be 1 or 2 as in Eq. (3.34). For sake of easier visualization of simulation results, target labels will be associated to colors *blue* and *red* in following subsections. R and B are constants related to the size of the cells. Additionally,

$$r_k^c = \sqrt{(x_k^c)^2 + (y_k^c)^2} \text{ and } b_k^c = arctan(\frac{y_k^c}{x_k^c}) \tag{3.37}$$

The noise in Eq. (3.34) is complex Gaussian, where $n_I(t_k)$ and $n_Q(t_k)$ are independent, zero-mean white Gaussian with variance σ_n^2 accounting for the in-phase and quadrature phase components respectively. These measurements, conditioned on the state are assumed to be exponentially distributed [53],

$$p(z^{ij}|s_k) = \frac{1}{\mu_0^{ij}} e^{-\frac{1}{\mu_0^{ij}} z_k^{ij}} \tag{3.38}$$

where

$$\mu_0^{ij} = (\tilde{A}_k^{(1)})^2 (h_A^{(1)ij}(s_k, t_k))^2 + (\tilde{A}_k^{(2)})^2 (h_A^{(2)ij}(s_k, t_k))^2 + 2\sigma_n^2 \tag{3.39}$$

Assuming that the noise is independent from cell to cell and that the reflections of the two targets are independent, the density model of the measurements given the state becomes:

$$p(z_k|s_k) = \prod_{ij} p(z^{ij}|s_k) \tag{3.40}$$

3.4.2 Algorithm

In the framework of recursive Bayesian estimation the prior density $p(s_{k+1}|Z_k)$ and the posterior density $p(s_{k+1}|Z_{k+1})$ can be obtained, according to the Chapman-Kolmogorov and Bayes equations, as:

$$p(s_{k+1}|Z_k) = \int p(s_{k+1}|s_k) p(s_k|Z_k) ds_k \tag{3.41}$$

$$p(s_{k+1}|Z_{k+1}) = \frac{p(z_{k+1}|s_{k+1}) p(s_{k+1}|Z_k)}{p(z_{k+1}|Z_k)} \tag{3.42}$$

A PF is selected for the implementation due to the non-linearity in the dynamic and measurement models (see Eqs. (3.25) and (3.34)). The particle cloud representation of the joint probability density at time k is given by the weighted set of particles $\{s_k^i, w_k^i\}_{i=1}^{N_p}$. An Importance-Sampling-based filter algorithm suffices to show the benefits of modeling target interactions. Algorithm 1 presents the SIR filter that will be used in the simulations in Subsection 3.5.1.

1 $k = 0$;
2 Draw N_p samples s_k^i from $p(s_k)$;
3 $k = k + 1$;
4 Draw N_p samples v_k^i from $p(v_k)$;
5 Obtain N_p samples s_k^i from $p(s_k^i | s_{k-1}^i, v_k^i)$;
6 Given z_k, obtain $\tilde{w}_k^i = p(z_k | s_k^i)$;
7 Normalize weights $w_k^i = \tilde{w}_k^i / \sum_{j=1}^{N_p} \tilde{w}_k^j$;
8 Resample from $\hat{p}(s_k | Z_k) = \sum_{i=1}^{N_p} w_k^i \delta(s_k - s_k^i)$;
9 Extract point estimates from $\hat{p}(s_k | Z_k)$, e.g. according to MMSE metric;
10 go to 3

Algorithm 1: Pseudo-code of the SIR filter. Simulations in next section incorporate the interacting motion and TrBD measurement models (from Sections 3.3.3 and 3.4.1) in the densities from lines 5 and 6.

3.5 Simulation examples

This section presents simulation results for different scenarios involving interacting targets. Based on these simulations, we compare the performance of a traditional filter based on independent motion assumptions (using the base-line model presented in the introduction of Section 3.3) with the proposed method (based on the interacting target motion model in Subsection 3.3.3).

3.5.1 Preliminary results

The initial set of interacting trajectories simulated could effectively depict the movement of a water-skier being towed by a rope attached to a boat. The trajectories of the water-skier and the boat are illustrated by the continuous red and blue lines in Fig. 3.3 respectively.

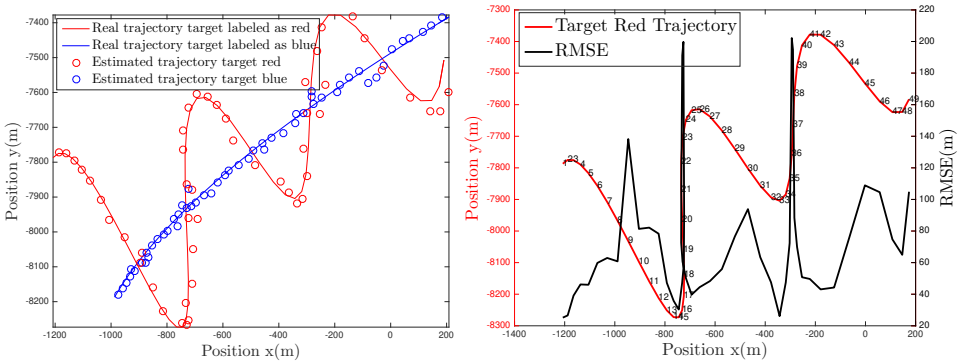

Figure 3.3: Position estimates of a traditional filter with independent motion assumptions on the left hand side. Estimation error of the track of target labeled as red on the right hand side.

The trajectories are generated using the dynamic model in (3.25) with evolution of k_1 and k_2 as represented by the continuous lines in Fig. 3.4.

Tracking results are shown in Figs. 3.3 and 3.5. Fig. 3.3 shows the estimation performance of a traditional filter assuming decoupled motion of the two targets. Fig. 3.5

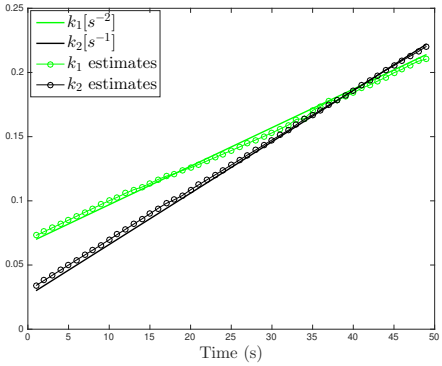

Figure 3.4: Estimation of the parameters in the interacting motion model.

shows the estimation performance of the formulated extension with inference of targets interaction.

Although the trajectories are strongly coupled, the traditional filter manages to keep the targets in track because the process noise covariance of the model is tuned in relation to the coupled maneuverability of the objects. Such prior information is not available in real operation, but has been used here so that the traditional filter keeps the r target in track. This is essential to produce a high quality base line for evaluation of the contribution in this chapter. Nevertheless, the traditional filter incurs in large estimation errors when large accelerations take place due to target interactions (in this case produced by physical tightening of the rope), see Fig. 3.3 right hand side. Fig. 3.5 shows the estimation error reduction in the position estimates when the information about target interaction is estimated and exploited on-line. Estimates of the coupling parameters k_1 and k_2 are illustrated in Fig. 3.4. This estimates can be readily exploited on-line, lowering the uncertainty in the prediction step.

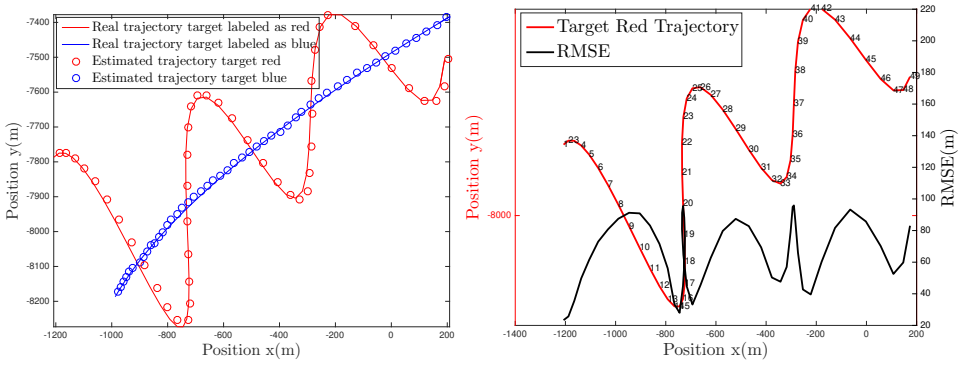

Figure 3.5: Position estimates of the proposed filter encapsulating interacting motion inference on the left hand side. Estimation error of the track of target labeled as red on the right hand side.

3.5.2 Final results: prevention of labeling confusion and detection of anomalous target behavior

Detecting certain types of coupled motion is relevant for the system to provide situational awareness at user level. The purpose of this section is not only improving tracking performance by exploiting real-time estimation of coupling parameters. We also aim at detecting changes between interactive/no-interactive targets behavior. A Multiple Mode (MM) filtering implementation can be used to integrate both aims. In order to evaluate the benefits of such MM implementation, we compare a traditional filter with a MM filter where the two models used in previous subsection are encapsulated. By these means, the posterior mode probabilities can be used as a measure of certainty about whether or not the objects have interacting behaviors. As the MM mechanism gives more importance to the mode with higher posterior probability, reduction in estimation error is expected disregarding the degree of target interaction.

Let $m_k = 1$ and $m_k = 2$ denote the non-interacting and interacting modes at time step k respectively. The posterior probability of each mode can be calculated using the particle-based approximation as follows,

$$p(m_k = 1|Z_k) \approx \sum_{i:m_k^{i*}=1} w_k^{i*} \approx \frac{\#\{m_k^{i*} = 1\}}{N_p} \tag{3.43}$$

$$p(m_k = 2|Z_k) \approx \frac{\#\{m_k^{i*} = 2\}}{N_p} \tag{3.44}$$

where w_k^{i*} and m_k^{i*} are used to denote the weight after resampling and the mode after resampling of particle i at time instant k respectively.

Algorithm 2 summarizes the MM SIR filter used in the simulation example in this subsection.

1 $k = 0$;
2 Draw N_p samples s_k^i from $p(s_k)$;
3 Draw N_p samples m_k^i from $p(m_k)$;
4 $k = k + 1$;
5 Draw N_p samples v_k^i from $p(v_k)$;
6 Obtain N_p samples s_k^i from $p(s_k^i|s_{k-1}^i, v_k^i, m_{k-1}^i)$;
7 Given z_k, obtain $\tilde{w}_k^i = p(z_k|s_k^i)$;
8 Normalize weights $w_k^i = \tilde{w}_k^i / \sum_{j=1}^{N_p} \tilde{w}_k^j$;
9 Resample from $\hat{p}(s_k|Z_k) = \sum_{i=1}^{N_p} w_k^i \delta(s_k - s_k^i)$;
10 Calculate $p(m_{k-1}|Z_k)$ according to Eqs. (3.43) and (3.44);
11 Extract point estimates from $\hat{p}(s_k|Z_k)$, e.g. according to MMSE metric;
12 Draw N_p samples m_k^i from $p(m_k|m_{k-1}^i)$;
13 go to 4

Algorithm 2: Pseudo-code of the MM SIR filter.

The final results show the performance of a MM particle filter exposed to periodical switches between interacting and independent target motion. The MM filter is compared with a traditional particle filter were no efforts are made to model interactions. For a fair

comparison, we run the traditional particle filter with the same amount of particles used in the MM filter. However, the variance of the process noise in the traditional filter should be tuned to a larger magnitude (in relation to targets maneuverability) than in the MM implementation due to the lack of interacting information. Otherwise, the traditional filter will not be able to maintain the targets in track.

In the upcoming simulation experiment the trajectory set is such that the targets maneuver coordinately every now and then, as represented by the continuous lines in Fig. 3.6 (left hand side).

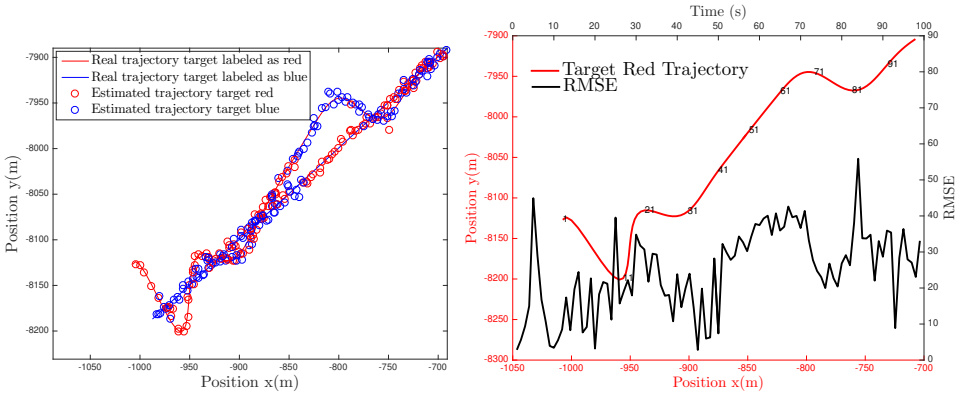

Figure 3.6: Estimated position of the targets by the traditional filter on the left hand side. Estimation error of target labeled as red in the right hand side, where each curve is referenced to the axis scale on its same color. Time scale is also shown over the trajectory.

Such type of on-off chasing behavior can be replicated with varying coupling parameters k_1 and k_2 as represented by the ground truth curves in Fig. 3.7. In the simulation segment

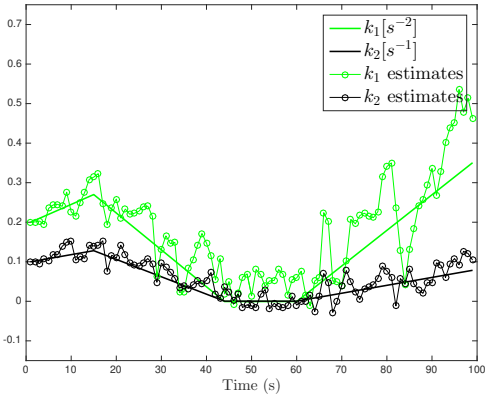

Figure 3.7: Estimation of the parameters in the interacting motion model.

between 43 and 61 seconds, the targets are moving independently. Over the first 42 seconds and the last 39 seconds, “r” target dynamics are dependent on “b” dynamic state.

Figs. 3.6 and 3.8 show the point estimates extracted from the traditional and MM filters respectively. The MM particle filter provides more accurate point estimates than the traditional filtering solution. In Fig. 3.6 it is also clear that the large uncertainty when using a traditional filter compromises labeling with respect to target identity if the targets get close enough (both in position and velocity space). This "labeling confusion" has been avoided by the proposed incorporation of interacting motion models in the filtering process.

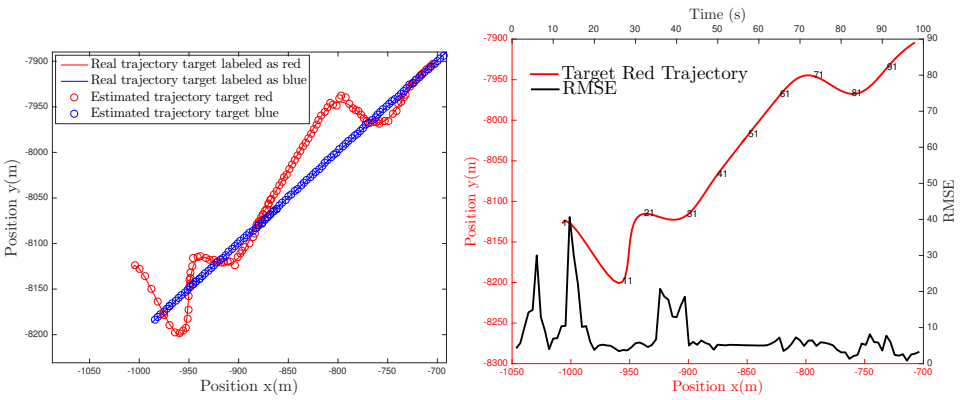

Figure 3.8: Estimated position of the targets by the MM filter on the left hand side. Estimation error of target labeled as red in the right hand side, where each curve is referenced to the axis scale on its same color. Time scale is also shown over the trajectory.

Fig. 3.7 shows the estimation of the coupling variables in the interacting motion model. Periods of interaction/no-interaction are correctly detected relying on the estimated posterior mode probabilities of the MM filter (see Fig. 3.9). Thresholding this posterior statistic allows for detection of anomalous amount of target interaction, which can be reflected as a suspicious target-behavior warning at higher system levels.

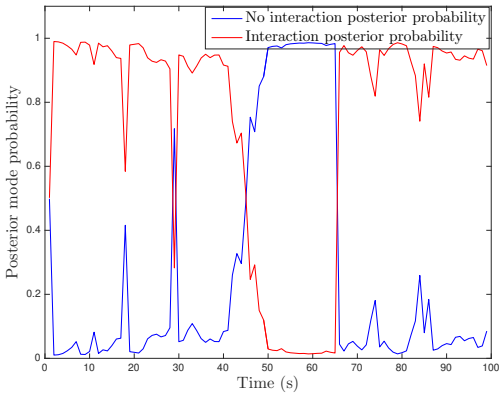

Figure 3.9: The posterior mode probability can be used to infer the amount of interaction between the targets. The interpretation in this case is that the motion of the targets is strongly coupled over the simulation, except from 50 to 65 seconds, where the targets perform independent motion.

The "curse" of dimensionality inherent in PF implementations with high-dimensional state vectors can be observed in the roughness of the estimation of the coupling parameters (see Fig. 3.7). Despite this, rough estimation of k_1 and k_2 still provides valuable information to enhance tracking performance as shown in Fig. 3.8. Since the main contribution in this chapter is on the modeling of interacting motion, these efficiency problems of the implementation (that will appear when considering larger number of targets) fall out of the scope of the study.

3.6 Conclusions

This chapter has looked at the labeling confusion problem in TrBD MOT from the dynamics point of view, which is especially effective when some structure can be extracted from the coupled motion of the targets. Detection of anomalous target behaviors is a related higher level challenge, which has also been considered in this chapter. Both challenges are tackled by means of modeling and estimating interacting target motion.

In this chapter we have provided a PF solution to estimate and exploit interacting targets behavior in a TrBD MOT application. The method uses parameters to model coupled accelerations along coordinates of different targets. The hidden parameters used to model interactive motion are estimated as part of the state vector and exploited on-line. For the first time in literature, the presented method exploits such information to close the sensing-tuning loop inside the tracker, resulting in enhanced tracking performance (including avoidance of labeling confusion). Additionally, this chapter proposes the incorporation of the interacting motion models in a Multiple Model (MM) Bayesian filtering implementation. This enables detection of suspicious target behavior correlated to non-regular degrees of targets interaction.

4

Performance evaluation criterion for TrBD MOT solutions

4.1 Introduction

In order to estimate the trajectories of the targets, various track-formation strategies can be adopted. Track-formation is the problem of connecting target state estimates that belong to the same target to form tracks. In order to take informed track-formation decisions in TrBD MOT, the labeling problem as defined in [27], needs to be solved. To solve the labeling problem, a method for labeling uncertainty characterization is required.

An optimal solution to the labeling problem is especially important when tracking closely-spaced objects. TrBD MOT copes with closely-spaced objects in cases where a traditional plot-based approach would have to deal with merged measurements. Due to integration over time, TrBD MOT provides an inherently increased resolution capability over Detect-before-track (DBT) MOT, which makes it all the more important to address the characterization of labeling uncertainty in the absence of detection plots.

Characterizing labeling uncertainty involves decomposing the multi-object Bayes posterior density. This decomposition has been traditionally done by solving the Data Association (DA) problem, the Multiple Hypotheses Tracking (MHT) decomposition [11] is an example. In TrBD context, association-dependent decompositions cannot be formulated due to the absence of detections (and plots). Nevertheless, labeling uncertainty still needs to be characterized. Therefore, a DA-free method to perform a label-dependent decomposition of the Bayes posterior is required. The contents in chapters 5, 6 and 7 propose various implementations for such a method.

The remainder of this thesis keeps the focus on the TrBD MOT problem for closely-spaced objects. This chapter revisits a sensible method for evaluation of TrBD DA-free

The contents provided in this chapter are based on the publication "Evaluation of Labeling Uncertainty in Multiple Target Tracking with Track-before-detect Radars," C. M. Leon and H. Driessen, in *Proceedings of the 22nd International Conference on Information Fusion*, Ottawa, 2019, pp. 1-8.

solutions. The evaluation method, published by the author of this thesis in [22] and revisited in [27], calculates the evaluation references relying on a label-dependent decomposition based on DA. Although this chapter does not provide a new contribution compared to the published results, it does provide a more compact and simplified formulation.

The method presented in this chapter departs from the current literature trend based on optimization over the Mean Optimal Sub-Pattern Assignment (MOSPA) metric. Instead, the presented criterion is based on traditional MSE optimization. In spite of this, the proposed generation of evaluation references prevents "track coalescence" and "track swap" underperformance. Additionally, the evaluation criterion does not suffer "combinatorial explosion" as it would be expected given its DA-based construction. This becomes possible when implementing the performance evaluation criterion with a PF due to the fact that several association-dependent PFs with the same particle support can be unified as a single PF. This differs from parametric methods, where the sum of different data association-dependent densities, for instance a Gaussian mixture, cannot be represented as one unified parametric density.

The main contribution of this chapter is a PF algorithm implementation providing optimal statistics relevant for track formation. These statistic are labeled tracks and corresponding labeling certainties. Additionally, such algorithm is incorporated as part of a criterion for performance evaluation of DA-free trackers. Despite its DA-based construction, the evaluation criterion can be used legitimately to evaluate solutions such as the UD-based and CMT algorithms provided in following chapters.

The chapter is organized as follows. In section 2, we provide the context and outline the trend in literature for performance evaluation of MOT algorithms. In section 3, the proposed generation of optimal references is presented. Also, the elaboration on how PF approximations enable a suitable performance evaluation, departing from optimization over MMOSPA, is provided. In section 4, the mathematical description of the proposed approach is formulated and the PF algorithm for practical implementation of the evaluation method is provided. Finally, numerical results are discussed before extracting conclusions and closing the chapter.

4.2 Related trends and context

In [54] Svensson et al. show that when targets are closely spaced, traditional tracking algorithms can be adjusted to perform better under a performance measure that disregards identity. This performance measure is MOSPA and it has become the standard benchmark metric for evaluation of tracking performance in the Information Fusion community. In a nutshell, optimizing over MOSPA in closely-spaced targets scenarios provides better results than optimizing over MSE or MAP as long as the research question is only "where are the targets now?" and the question of "which target corresponds to which estimated location?" does not matter at all or can be answered relying on additional classification processing or additional systems such as Identification Friend or Foe (IFF).

The main arguments supporting the use of MOSPA metric when labeling of the tracks does not matter can be traced back to chapter 2. The same arguments can be found in [55], where it is explained that optimizing over traditional metrics leads to estimation underperformance known as "track coalescence" (for MMSE) or "track swap" (for MAP) when considering multimodal PDFs. Such cases become problematic due to the existence of

multimodalities in the posterior PDF as a result of several association hypothesis holding non negligible probabilities. One heuristic way used to avoid track-coalescence while optimizing over traditional MMSE is taking the mean of the most likely hypothesis. However, this does not take into account the uncertainty of other (potentially non-negligible) hypotheses.

A theoretically complete solution for the evaluation method when tracking of identities matter (as it happens to be the case in our problem description from section 2.3) is an MHT-type of solution [11]. In fact, MHT-based algorithms generate optimal references for answering the two questions in the overall thesis problem description from section 2.3 (in DBT context). Firstly, reference labeled tracks can be extracted by optimizing over MMSE individually for each and every hypothesis. Secondly, not only every mode in the posterior density would have an unbiased point estimate representative, but also the corresponding labeling uncertainty would be analytically characterized by the MHT DA probabilities.

Unfortunately, practical implementation of this complete solution would not be feasible as DA hypotheses grow exponentially from one scan to the next one [11]. Additionally, left aside "combinatorial explosion" problems, displaying multiple DA-dependent solutions in the screen of the radar operator is not acceptable [44].

4.3 Proposed approach

The outcome of this chapter is a PF algorithm for the generation of the output Optimal references in Fig. 4.1. This optimal references are a key component in the complete plot-based framework for evaluation of DA-free trackers.

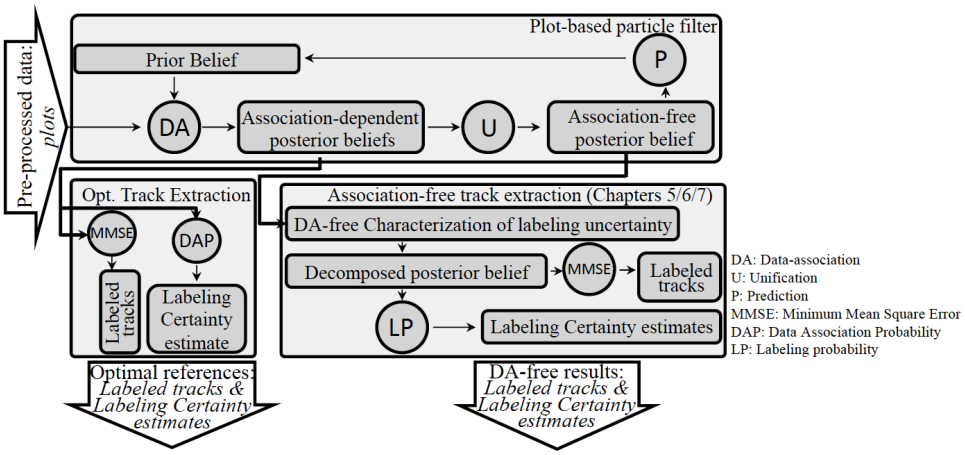

Figure 4.1: Plot-based labeled-MOT criterion for evaluation of DA-free decompositions.

The block diagram in Fig. 4.1 receives plots as input and produces two sets of outputs (represented by the two arrows). Each set of outputs contains several pairs. Being each pair composed of labeled tracks and corresponding labeling certainty estimate. To be precise, the arrow *Optimal references* "contains" as many pairs as the factorial of the number of targets, matching all possible ways of assigning labels to the tracks for an arbitrary discrete time-step. The output on the left hand side contains the analytic references calculated by

the desired evaluation algorithm. The output on the right hand side is formated in the exact same way, contains the final estimates provided by a generic DA-free solution. Examples of such solution, will be proposed in following chapters. The evaluation criterion quantifies the similarity between both sets of outputs, as will be presented in the performance evaluation of the various algorithms in chapters 5, 6 and 7.

The meaning of the major processes involved in the evaluation criterion are provided on the right hand side of Fig. 4.1. The description of the block diagram is as follows. The DA process takes a prior believe and a plot-set as inputs, and it generates an analytic DA-based decomposition (association-dependent posterior beliefs) as outputs. Optimal references for the labeled tracks and labeling certainties, are calculated for each independent component. According to fundamental analytical principles, these optimal references are calculated based on MMSE estimation and DAP processes and provided as outputs in the left downwards-pointing arrow.

The described procedure brings nothing new compared to MHT-based theory. In fact, the well known practical concern of MHT "combinatorial explosion" arises at this point as propagating all DA-dependent posterior densities is not tractable using parametric density representations. The novel contribution in the implementation of the evaluation algorithm resides on how to circumvent the "combinatorial explosion" problem without resorting to pruning, merging or capping techniques commonly used in MHT-based implementations. Instead of using these techniques, the problem is tacked by removing the DA structure in the DA-dependent decomposition through the Unification (U) process in Fig. 4.1. This U process can only be supported by PF implementations of the evaluation algorithm.

The U process is only supported by PF approximations as it produces the unification of several DA-dependent particle-based approximations into a single particle cloud. The reason why the U process is not supported with parametric implementations is because the unification of several DA-dependent parametric densities cannot result on a single unified parametric density, but on a mixture.

Choosing to implement the evaluation algorithm with particle-based approximations does not only circumvent the "combinatorial explosion" problem. Also, the unification of different DA-dependent particle-based approximations into a single particle cloud is a process that removes the DA structure. Hence, the outcome of this process resembles the type of DA-free posterior densities produced in TrBD filtering.

Overall, choosing a PF to implement the evaluation method provides: approximation of updated densities with explicit label-dependent structure and the ability to remove this structure. The first aspect enables generation of references for evaluation and the second aspect enables tractability and generation of inputs for the DA-free algorithms under evaluation. This way, the algorithm provided as the main contribution in this chapter gets incorporated into the performance evaluation criterion pictured in Fig. 4.1.

To finalize the high level description of the evaluation criterion, the functionality implemented in the bottom right block in Fig. 4.1 needs to be defined. This functionality can be described as the inference of the optimal references produced in the bottom left block, assuming one has only access to a PF approximation of the posterior density after unification, i.e. and approximation of the DA-free or non-decomposed posterior density. This block will be implemented by the DA-free tracking algorithms proposed in chapters 5, 6 and 7.

Circumventing "combinatorial explosion" in the evaluation algorithm

This subsection provides a deeper description on how the evaluation criterion circumvents the "combinatorial explosion" concern. Fig. 4.2 illustrates the exponential growth of components in the posterior density when considering implementations with parametric densities. The "combinatorial explosion" problem resulting from extending the hypotheses tree over time is due to the fact that all DA-dependent components cannot be unified as a single density after each measurement incorporation. For instance, a Gaussian mixture density cannot be described parametrically as one single parametric density. Therefore, one needs to propagate each parametric density in the mixture from one recursion to the next one.

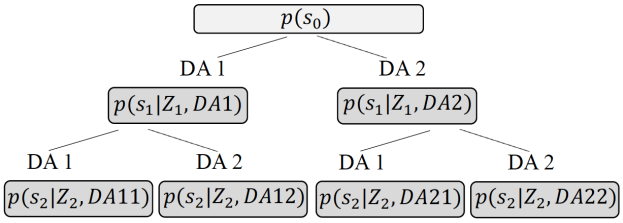

Figure 4.2: Hypotheses tree growth along first two scans by exact MHT, assuming two targets, no false alarm and perfect detection. Dropping these assumptions would result in an even quicker hypotheses growth.

The unification of association dependent densities can be performed when considering implementations based on particle-based approximations. The proposed evaluation algorithm prevents "combinatorial explosion" by unification of several DA-dependent particle clouds into a single particle cloud. This is possible provided all association-dependent clouds share the same particle basis as illustrated in Fig. 4.3. The notation s and w are used to refer to particles' states and weights respectively.

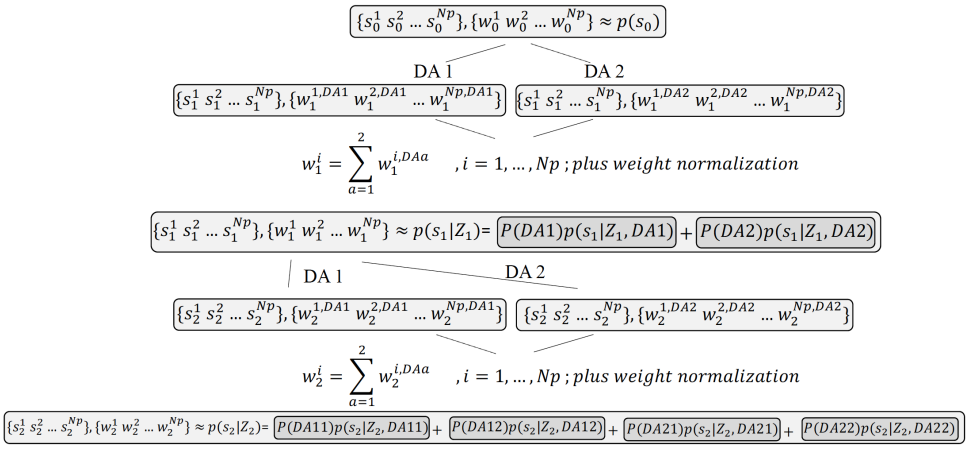

Figure 4.3: The use of PFs enables the approximation of the theoretically complete solution without running into "combinatorial explosion". The proposed hypotheses growth unification for PF implementations requires that all DA-dependent PFs share the same particle basis.

As illustrated in Fig. 4.3, two association-dependent PFs (with same particle support and different association-dependent weights) can be unified as a single PF taking the same sample support and adding up (followed by normalizing) the weights.

Association dependent PF approximations, for instance after incorporation of measurements in the second scan, $\{s_2^i, w_2^{i,DA1}\}_{i=1}^{Np}$ and $\{s_2^i, w_2^{i,DA2}\}_{i=1}^{Np}$ in Fig. 4.3, are used individually for extracting labeled tracks and labeling probabilities analytically. Labeled tracks are optimized over MMSE and labeling probabilities are calculated as the association probabilities. These labeled tracks and labeling probabilities will be considered as references for evaluation. Then the association-dependent PFs are unified as explained in previous paragraph. At this point the link can be made with the overall block diagram in Fig. 4.1. In fact, the unified particle cloud is fed as the DA-free density approximation for the algorithms that will be presented in following chapters.

For sake of fair evaluation, it is explicit in the design of the evaluation criterion that both the algorithm generating evaluation references and the algorithm under evaluation need to be executed using the same plot data-set. Although perhaps counterintuitive, the algorithms to be presented in following chapters, designed for operation in TrBD, need to be validated in DBT. This is not a contradiction, these DA-free algorithms support estimation of label tracks and labeling certainties from non-decomposed densities, disregarding whether the these densities are calculated in TrBD or DBT context.

It is precisely because no analytical solution of the desired decomposition can be derived analytically in TrBD, that we will be interested on using this criterion in order to compare the optimality of the solutions in chapters 5, 6 and 7.

4.4 Mathematical description

The essential theory required to build up optimal references for evaluation is directly linked to the relation between the labeling problem and the DA problem described in section 2.4. Based on this, the optimal references for the labeled tracks and labeling certainty estimates can be described mathematically as follows:

- In DBT context
  - Generate the analytical decomposition of $p(\boldsymbol{s}_k|\boldsymbol{Z}_k)$:

$$p(\boldsymbol{s}_k|\boldsymbol{Z}_k) \propto \sum_{m=1}^{t!} l(\pi_m(\boldsymbol{z}_k)|\boldsymbol{s}_k) p(\boldsymbol{s}_k|\boldsymbol{Z}_{k-1}) \tag{4.1}$$

  - For each DA-dependent component $l(\pi_m(\boldsymbol{z}_k)|\boldsymbol{s}_k)p(\boldsymbol{s}_k|\boldsymbol{Z}_{k-1})$
    - Extract MMSE labeled point estimates:

$$E[l(\pi_m(\boldsymbol{z}_k)|\boldsymbol{s}_k)p(\boldsymbol{s}_k|\boldsymbol{Z}_{k-1})] = \int_{\boldsymbol{s}_k} \boldsymbol{s}_k l(\pi_m(\boldsymbol{z}_k)|\boldsymbol{s}_k) p(\boldsymbol{s}_k|\boldsymbol{Z}_{k-1}) d\boldsymbol{s}_k \tag{4.2}$$

    - Extract labeling certainty associated:

$$p(\pi_m(\boldsymbol{z}_k)|\boldsymbol{Z}_k) = \frac{\int l(\pi_m(\boldsymbol{z}_k)|\boldsymbol{s}_k) p(\boldsymbol{s}_k|\boldsymbol{Z}_{k-1}) d\boldsymbol{s}_k}{\sum_{m=1}^{t!} \int l(\pi_m(\boldsymbol{z}_k)|\boldsymbol{s}_k) p(\boldsymbol{s}_k|\boldsymbol{Z}_{k-1}) d\boldsymbol{s}_k} \tag{4.3}$$

- Unify the decomposition in Equation (4.1) (only possible in PF implementations)
- Start new filtering iteration

Please note again that the optimal references in Equations (4.2) and (4.3) need to be derived from the DBT analytical expression in Equation (4.1). Nonetheless, the validation of the module in the lower right corner in Fig. 4.1 (using plots) guarantees equivalent inference quality in TrBD.

4.4.1 Algorithm implementation

Alg. 3 is the pseudo-code to generate the PF approximation of the optimal references described mathematically in section 4.4.

$k = 0$;
Draw N_p samples $\boldsymbol{s}_k^j$ from $p(\boldsymbol{s}_k)$;
Draw N_p samples $\boldsymbol{n}_k^j$ from $p(\boldsymbol{n}_k)$;
$k = k + 1$;
$\boldsymbol{s}_k^j = f(\boldsymbol{s}_{k-1}^j, \boldsymbol{n}_{k-1}^j)$;
Generate data-association-dependent posterior beliefs;
for i=1 until t!;
    Given $\boldsymbol{z}_k$, obtain $\tilde{w}_k^{i,j} = p(\pi_i(\boldsymbol{z}_k)|\boldsymbol{s}_k^j)$;
    Normalize weights $w_k^{i,j} = \tilde{w}_k^{i,j} / \sum_{j=1}^{N_p} \tilde{w}_k^{i,j}$;
    Extract Labeled Point Estimates (LPEs) according to the particle-based approximation of Equation (4.2);
    Obtain certainty measures of LPEs according to particle-based approximation of Equation (4.3);
Sum data-association-dependent posteriors in order to approximate $p(\boldsymbol{s}_k|\boldsymbol{Z}_k)$ with a single particle cloud;
for j=1 until N_p;
    $w_k'^j = \sum_{i=1}^{t!} w_k^{i,j}$;
Normalize weights $w_k^j = w_k'^j / \sum_{j=1}^{N_p} w_k'^j$;
Resample N_p times from $\hat{p}(\boldsymbol{s}_k|\boldsymbol{Z}_k) = \sum_{j=1}^{N_p} w_k^j \delta(\boldsymbol{s}_k - \boldsymbol{s}_k^j)$ to generate $\hat{p}(\boldsymbol{s}_k|\boldsymbol{Z}_k) = \frac{1}{N_p} \sum_{j=1}^{N_p} \delta(\boldsymbol{s}_k - \boldsymbol{s}_k^j)$;
go to 3

Algorithm 3: Pseudo-code for generation of optimal references

4.5 Numerical results

Implementation of Alg. 3 for a closely-spaced MOT scenario leads to the results in Figs. 4.4 and 4.5.

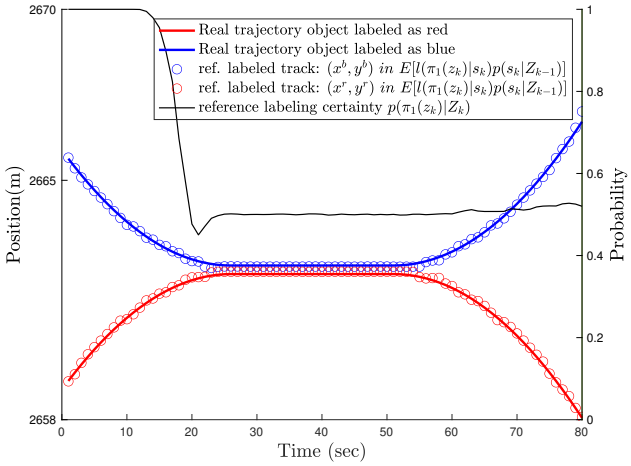

Figure 4.4: Generation of references (resulting from hypothesis π_1) for evaluation of DA-free algorithms.

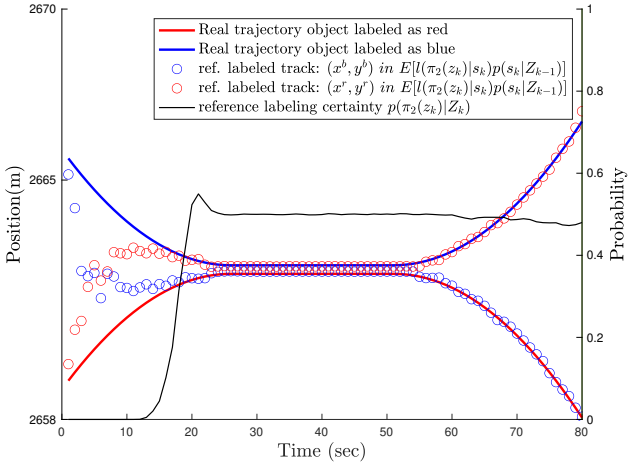

Figure 4.5: Generation of references (resulting from hypothesis π_2) for evaluation of DA-free algorithms.

The figures illustrate the two DA-dependent set of references. Not surprisingly, labeled-track references are very close to the real trajectories. In fact, when target identity is not of interest, one would simply use the ground-truth trajectories to measure estimation performance.

Unlike ground-truth trajectories, ground-truth labeling certainties are not known as a design choice of the simulation. Instead, the ground-truth labeling certainty needs to be calculated due to its dependency on all modeling aspects. In fact, the calculation of when and how quickly the ground-truth labeling certainty drops down to 0.5 depends on the parameters of the simulation. The choice of simulation parameters is shown in Table (4.1).

Table 4.1: Parameters of the simulation

parameter	value
d_i	1.66 m
d_m	0.22 m
σ_n	0.14 m/s$^{3/2}$
σ_v	0.045 m
τ	1 s
N_p	100000 particles

The evaluation can be reproduced by setting up the trajectories for the objects with initial and minimum distance as indicated by d_i and d_m in Table (4.1). The evaluation considers the dynamic and measurement models as nearly constant velocity [23] and linear-Gaussian. The standard deviations of the process noise and observation noise are indicated by σ_n and σ_v respectively in Table (4.1), where τ denotes the revisit time.

4.5.1 Discussion of numerical results

As expected, over the first 12 seconds of the simulation only one of the DA hypotheses holds full certainty. The certainty associated to the alternative DA hypothesis is so low that the first labeled point estimates in Fig. (4.5) can be disregarded. Also expected, the labeling certainty drops down to around 0.5 as soon as the objects get closely-spaced. This means that labeling information has been lost and cannot be recovered after the split under the assumption that the likelihood is permutation invariant (the measurements do not carry any information of identity).

4.6 Conclusions

This chapter presented a sensible method for evaluation of DA-free MOT solutions. The main contribution of this chapter is a PF algorithm implementation providing optimal statistics relevant for track formation. As no analytical form of such statistics exists in TrBD context, the evaluation algorithm provided in this chapter calculates them in DBT context, where a Data Association dependent decomposition can be formulated analytically. This analytical decomposition enables extraction of references both for the labeled tracks and corresponding labeling certainties.

The presented algorithm will be incorporated as part of a criterion for performance evaluation of DA-free trackers. Despite its DA-based construction, the evaluation criterion can be used legitimately to evaluate solutions such as the UD-based and CMT algorithms, which will be designed for operation in TrBD context in following chapters. This is because these algorithms will be designed to infer a relevant label-dependent decomposition of any posterior density, disregarding whether this density has been generated in the context of DBT or TrBD.

The algorithm presented in this chapter provides evaluation references departing from current trends based on MOSPA-based estimation. Special attention has been directed to prevent the problems of “track coalescence” and “track swap” commonly observed when MOT algorithms do not account for labeling uncertainty characterization.

The evaluation method prevents "combinatorial explosion" as well, which is expected in parametric implementations of exact MHT-like algorithms. This practical problem has been avoided by means of approximating the Bayes recursion with a PF. The convenience of a particle-based implementation of the evaluation method is twofold. Firstly, association-dependent PFs can be unified after extraction of association-dependent references for evaluation. Secondly, the unified PF is the type of input required by the labeling characterization algorithms to be presented in the last part of the thesis.

This chapter complements the rest of the thesis. It constructs the inputs for the algorithms in the last chapters in the form of a non-decomposed approximation of the posterior density. Also, it provides the reference outputs (expected from the algorithms in the last chapters) associated the optimal label-dependent decomposition.

in TrBD MOT by recovering a label-dependent decomposition from a non-decomposed TrBD posterior density.

Let us consider, for instance, that the measurements in the second scan have been incorporated and that we only have access to the unified posterior density approximated by particle cloud $\{s_2^i, w_2^i\}_{i=1}^{Np}$. The inference problem is about recovering the tracks and labeling probabilities extracted from the two association-dependent PF approximations $\{s_2^i, w_2^{i,DA1}\}_{i=1}^{Np}$ and $\{s_2^i, w_2^{i,DA2}\}_{i=1}^{Np}$.

5

DA-Free Tracking: Generalization of Blom and Bloem's Unique Decomposition

5.1 Introduction

This chapter presents a DA-free tracking solution for the TrBD MOT problem based on the Unique Decomposition (UD) by Blom and Bloem [25]. The UD is a theoretical method to decompose a two-targets PDF into its Permutation Invariant (PI) and Permutation Strictly Variant (PSV) components. Although applications, implementations and generalizations of the UD presented in 2009 have been published [56] [57], none of these results cover the implementation for non-linear and/or non-Gaussian (non-LG) problems. Without this implementation, the UD cannot be applied in the TrBD MOT problem due to the highly non-linear nature of the TrBD radar measurements.

The UD allows interpretation of the labeling problem in generic MOT contexts. This remains valid even when considering measurement models precluding formulation of DA – as illustrated in [33] for an MOT problem in the area of Wireless Sensor Networks (WSN).

This chapter derives two solutions to estimate separately the PI and the PSV components under non-LG conditions. One solution applies the decomposition at each scan in a single filter, the other solution tracks the decomposition over time, using a two filter implementation. The algorithm for the two-PFs solution will be provided as the preferred UD implementation due to its ability to tackle particle depletion.

The two algorithms are showcased in simulations, involving low-observable closely-spaced object scenarios in TrBD context. Simulation results illustrate the potential of the two-PFs algorithm to perform DA-free labeling uncertainty characterization and to aid at

The contents provided in this chapter have been submitted for publication in IEEE *Transactions on Aerospace and Electronic Systems* as "Implementation of the Unique PDF Decomposition for tracking closely-spaced objects with Track-Before-Detect radar systems," C. M. Leon, H. Driessen and A. Yarovoy.

taking informed track-formation decisions. Ultimately, this results in a novel approach to the TrBD MOT problem.

The chapter is organized as follows. Section 2 presents the related literature. Section 3 presents the estimation framework and modeling assumptions. Section 4 describes analytically the proposed single filter solution. Section 5 derives the dual filter solution presented as the main contribution of this chapter. Section 6 presents simulation results and section 7 concludes the chapter.

5.2 Related literature

In 2009, Blom and Bloem presented the existence and characterization of a unique decomposition for two-target densities [25]. Practical implementations under Gaussian assumptions were presented by the same authors in [56] and [57]. In [25], Blom and Bloem gave an interpretation of the UD in the context of MOT problems. In particular, Remarks 1 and 2 in [25] state the PDF conditions required to declare total labeling certainty or total labeling uncertainty.

The UD theory based on the problem described in [25] is indisputable. In fact, the UD (summarized by the first four equations in this chapter) is fully analytical. Despite theoretical correctness and interpretations in [25], it is not certain whether the UD theory can be applied for optimal characterization of labeling uncertainty in a TrBD MOT problem.

A sensible application of the UD theory to the labeling problem has been done in [33] by interpreting the invariance coefficient of the UD as a measure of labeling ambiguity. The same authors have illustrated that this interpretation cannot be extended to densities out of the scope of [25] such as multimodal-non-symmetric densities (see [58, A.17]).

A relevant question would be whether mentioned problematic densities can be reproduced from practical MOT scenarios. This does not seem to be the case as when the joint-multitarget density becomes multimodal due to closely-spaced targets, the modes tend show up in symmetric regions as the objects get sufficiently separated (after being closely-spaced) [1][30].

In [33], the authors tackle an MOT problem based on (strongly non-linear) signal intensity measurements from a WSN. As measurements are not modeled by detection points, labeling uncertainty cannot be characterized via DA probabilities. In order to characterize labeling uncertainty, [33] estimates the permutation invariance weight of the posterior PDF. This weight, defined in the UD by Blom and Bloem, was mapped into the probability of successful labeling for a non-LG MOT problem. Although proposed as future work in [33], the generalization of this solution for more than two objects has not been addressed.

Despite being based on the UD theory by Blom and Bloem, the contents in [33] do not derive the non-LG implementation of the UD "per sé". In fact, the implementation suggested in [33] considers a relaxed version of the problem. Due to this relaxation, estimation is only expected to be accurate if the targets have separated sufficiently after being closely-spaced. The present chapter aims at deriving a more generic implementation of the UD for non-LG problems.

The application of the UD expands the estimation of labeling probabilities (referred to as probability of "track swap" in [56] and [57], and as probability of "successful labeling" in [33]). Another application of the UD is to ease the optimization of point estimates over

the Mean Optimal Sub-Pattern Assignment (MOSPA) metric. In fact, some literature results show that calculation of Minimum-MOSPA (MMOSPA) point estimates can be eased by first doing a transformation of the posterior PDF into its UD. In particular, [43] derives an exact method to obtain the MMOSPA error estimate inspired by a proof in [59], and shows that the mean of the strictly permutation variant PDF can be shown to be an approximation to the MMOSPA estimate.

5.2.1 The Unique Decomposition theory

According to [25], any joint PDF $p(s_k)$ of a two target state vector $s_k = [s_k^1\ s_k^2]^T$ can be decomposed as a weighted sum of its permutation invariant component $p^I(s_k)$ and its permutation strictly variant component $p^V(s_k)$:

$$p(s_k) = \alpha_k^I p^I(s_k) + (1-\alpha_k^I)p^V(s_k) \tag{5.1}$$

where:

$$\alpha_k^I = \int_{s_k} min(p(s_k), p(\pi s_k))ds_k \tag{5.2}$$

$$p^I(s_k) = \frac{min(p(s_k), p(\pi s_k))}{\alpha_k^I} \tag{5.3}$$

$$p^V(s_k) = \frac{p(s_k) - \alpha_k^I p^I(s_k)}{1-\alpha_k^I} \tag{5.4}$$

where π denotes the permutation matrix. In our case of study, where two scalar targets are considered ($2-1D$ targets case):

$$\pi = \begin{pmatrix} 0 & 1 \\ 1 & 0 \end{pmatrix} \tag{5.5}$$

5.3 Estimation framework and modeling assumptions

In recursive Bayesian estimation, the posterior and predictive densities $p(s_k|Z_k)$ and $p(s_k|Z_{k-1})$, are desired. The general non-linear dynamic system and observation models can be denoted as f and q respectively:

$$s_k = f(s_{k-1}, q_{k-1}) \tag{5.6}$$

$$z_k = q(s_k, v_k),\ k \in \mathbb{N} \tag{5.7}$$

where s_k, q_k, z_k and v_k represent the state, process noise, the measurement, and the measurement noise respectively.

We tackle the MOT problem in the framework of recursive Bayesian filtering. The predicted and posterior densities of interest $p(s_k|Z_{k-1})$ and $p(s_k|Z_k)$ are obtained by iteration over the Chapman-Kolmogórov and Bayes equations:

$$p(s_k|Z_{k-1}) = \int p(s_k|s_{k-1})p(s_{k-1}|Z_{k-1})ds_{k-1} \tag{5.8}$$

$$p(s_k|Z_k) = \frac{p(z_k|s_k)p(s_k|Z_{k-1})}{p(z_k|Z_{k-1})} \tag{5.9}$$

in this framework, the models in Equations (5.6) and (5.7) are expressed in the form of $p(s_k|s_{k-1})$ and $p(z_k|s_k)$ respectively.

Due to the non-linear and non-Gaussian character of our TrBD problem, the densities are not known as an easy parametric function, though rather in a sample-based (particle) approximation. This poses the difficulty on how to compute the UD for the predictive and posterior densities (to be more precise how to compute the minimization as formulated in Equations (5.2) and (5.3)), since in many Particle Filters (PF) the evaluation of the density per particle is not readily available.

Particle filtering based on Sequential Importance Resampling (SIR) will be the choice for approximating the densities of interest. As computational efficiency is not on the focal point in this chapter, other filtering implementations, e.g. the ones based on rejection sampling or particle flow filters etc, are not considered.

This chapter derives and implements algorithms for computing the UD in a running filter that can deal with generic, i.e. non-LG problems. The derivations in this chapter assume that both dynamic and observation models are invariant with respect to label swapping. This means that there should be no distinction between the dynamic models used for the various objects, i.e. $p(s_k|s_{k-1}) = p(\pi s_k|s_{k-1})$, and that the likelihood function used to model measurements should not change when swapping the labels of the targets, i.e. $p(z_k|s_k) = p(z_k|\pi s_k)$. The first assumption holds in practical implementations when tracking similar targets, unless coupled motion is modeled explicitly. The second assumption is already described in the introductory chapter as it is equivalent to considering measurement models which do not carry any labeling information. This is the case in the TrBD models considered throughout this thesis .

Following sections will derive and provide implementations for two decomposition filters based on the UD theory. The structural difference between both algorithms is how the filters start each recursion. The first filter decomposes the predictive density based on a non-decomposed previous posterior density. The second filter runs a recursion on the decomposed density using two filters.

The first proposed filter can be regarded as a partially decomposed recursive solution whereas the second filter can be regarded as a fully decomposed recursive solution. In both filters the update step is the same, while the difference is in the prediction step. The description of the steps includes a derivation of the analytical formulas and a description of the particle-based approximation. For the sake of clarity, derivations are left to the appendix section A.2.

5.4 Analytic description and algorithm implementation of the partially decomposed filter

As the update step is the same for both proposed solutions, its description will only be provided in this section and referred to from next section.

5.4.1 Update step

This section provides a description of the update step for both the invariant and strictly variant parts of the predictive density. In particular, we are interested in computing the densities and weights required by the desired decomposition of the posterior:

$$p(s_k|Z_k) = \alpha^I_{k|k} p^I(s_k|Z_k) + \alpha^V_{k|k} p^V(s_k|Z_k) \tag{5.10}$$

Assuming the decomposition of $p(s_k|Z_{k-1})$ is available, i.e. $p^I(s_k|Z_{k-1})$, $p^V(s_k|Z_{k-1})$, $\alpha^I_{k|k-1}$ and $\alpha^V_{k|k-1} = 1 - \alpha^I_{k|k-1}$ are known, the update of the decomposition when receiving a new measurement for which the likelihood is invariant under permutation, i.e. $p(z_k|s_k) = p(z_k|\pi s_k)$ is given by (using $X \in \{I, V\}$):

$$p^X(s_k|Z_k) = \frac{p(z_k|s_k)p^X(s_k|Z_{k-1})}{p^X(z_k|Z_{k-1})} \tag{5.11}$$

with

$$\alpha^X_{k|k} = \frac{p^X(z_k|Z_{k-1})\alpha^X_{k|k-1}}{p(z_k|Z_{k-1})} \tag{5.12}$$

$$p^X(z_k|Z_{k-1}) = \int p(z_k|s_k)p^X(s_k|Z_{k-1})ds_k \tag{5.13}$$

$$p(z_k|Z_{k-1}) = p^I(z_k|Z_{k-1})\alpha^I_{k|k-1} + p^V(z_k|Z_{k-1})\alpha^V_{k|k-1} \tag{5.14}$$

Please refer to the appendix section A.2 for the derivation of Equations (5.11) and (5.12). This update step comprises two regular update steps for both invariant and variant densities $p^X(s_k|Z_k)$ including an update of the weights $\alpha^X_{k|k}$ associated with the invariant and variant densities.

Particle filtering description

In order to approximate the expression in (5.11), the update step proceeds as the independent updating of both available particle clouds $\{s^{X,i}_{k|k-1}, \gamma^{X,i}_{k|k-1}\}^{N_p}_{i=1}$ (with $X = \{I, V\}$):

$$\{s^{X,i}_{k|k}, \gamma^{X,i}_{k|k}\}^{N_p}_{i=1} \sim p^X(s_k|Z_k) \tag{5.15}$$

with $\{s^{X,i}_{k|k}\}^{N_p}_{i=1} = \{s^{X,i}_{k|k-1}\}^{N_p}_{i=1}$ and:

$$\gamma^{X,i}_{k|k} = \frac{p(z_k|s^{X,i}_{k|k-1})\gamma^{X,i}_{k|k-1}}{\hat{p}^X(z_k|Z_{k-1})} \tag{5.16}$$

The approximation of (5.13) can be written as

$$\hat{p}^X(z_k|Z_{k-1}) = \sum_i p(z_k|s^{X,i}_{k|k-1})\gamma^{X,i}_{k|k-1} \tag{5.17}$$

The updating of the weights from the expression in (5.12) then is done via:

$$\hat{\alpha}^X_{k|k} = \frac{\hat{p}^X(z_k|Z_{k-1})\hat{\alpha}^X_{k|k-1}}{\hat{p}(z_k|Z_{k-1})} \tag{5.18}$$

where

$$\hat{p}(z_k|Z_{k-1}) = \hat{p}^I(z_k|Z_{k-1})\hat{\alpha}^I_{k|k-1} + \hat{p}^V(z_k|Z_{k-1})\hat{\alpha}^V_{k|k-1} \tag{5.19}$$

5.4.2 Prediction step

This section provides a description of the prediction step for the partially decomposed PF. Both the description in this section and the one provided in the following section provide expressions for calculating the elements in the desired UD of the predictive density:

$$p(s_k|Z_{k-1}) = \alpha^I_{k|k-1} p^I(s_k|Z_{k-1}) + \alpha^V_{k|k-1} p^V(s_k|Z_{k-1}) \tag{5.20}$$

The differentiating feature of the filter in the current section is that it assumes a running conventional, i.e. non-decomposed, particle filter, where the decomposition of the density in Equation (5.20) is then based upon the previous non-decomposed posterior $p(s_{k-1}|Z_{k-1})$. As opposed to this, the second description provided for the fully decomposed filter in the following section relies on the availability of a decomposed previous posterior.

Analytic description using a non-decomposed previous posterior $p(s_{k-1}|Z_{k-1})$

The UD of the predictive density $p(s_k|Z_{k-1})$ immediately follows by applying the definition of the UD:

$$p^I(s_k|Z_{k-1}) = \frac{min(p(s_k|Z_{k-1}), p(\pi s_k|Z_{k-1}))}{\alpha^I_{k|k-1}} \tag{5.21}$$

$$p^V(s_k|Z_{k-1}) = \frac{p(s_k|Z_{k-1}) - min(p(s_k|Z_{k-1}), p(\pi s_k|Z_{k-1}))}{\alpha^V_{k|k-1}} \tag{5.22}$$

$$\alpha^I_{k|k-1} = \int_{s_k} min(p(s_k|Z_{k-1}), p(\pi s_k|Z_{k-1}))ds_k \tag{5.23}$$

$$\alpha^V_{k|k-1} = 1 - \alpha^I_{k|k-1} \tag{5.24}$$

Particle filtering description: In order to approximate Equations (5.21),(5.22) and (5.23), the ability to evaluate the predictive density $p(s_k|Z_{k-1})$ for each particle is required. To fulfill this requirement (given a PF approximation of $p(s_{k-1}/Z_{k-1})$ $\{s^i_{k-1|k-1}, \gamma^i_{k-1|k-1}\}_{i=1}^{N_p}$) one can use the Chapman-Kolmogórov equation:

$$p(s_k|Z_{k-1}) = \int p(s_k|s_{k-1}) p(s_{k-1}|Z_{k-1}) ds_{k-1} \tag{5.25}$$

to analytically produce a continuous approximation of the predictive density:

$$\hat{p}(s_k|Z_{k-1}) = \sum_i p(s_k|s^i_{k-1|k-1}) \gamma^i_{k-1|k-1} \tag{5.26}$$

Equation (5.23) can be rewritten introducing the importance density $q(s)$

$$\alpha^I_{k|k-1} = \int_{s_k} \frac{min(p(s_k|Z_{k-1}), p(\pi s_k|Z_{k-1}))}{q(s_k)} q(s_k) ds_k \tag{5.27}$$

using this importance density to sample particles allows the approximation of Equation (5.23) as:

$$\hat{\alpha}^I_{k|k-1} = \sum_i \tilde{\gamma}^{I,i}_{k|k-1} \tag{5.28}$$

where

$$\tilde{\gamma}^{I,i}_{k|k-1} = \frac{min(\hat{p}(s^i_k|Z_{k-1}), \hat{p}(\pi s^i_k|Z_{k-1}))}{q(s^i_k)} \gamma^i_{k|k-1} \tag{5.29}$$

with $\{s^i_{k|k-1}, \gamma^i_{k|k-1}\}_{i=1}^{N_p} \sim q(s_k)$. Assuming the distribution $q(s_k)$ is the predictive density, i.e. $p(s_k|Z_{k-1})$, like in a running SIR filter, the approximation in Equation (5.29) becomes:

$$\tilde{\gamma}^{I,i}_{k|k-1} = min\left(1, \frac{\hat{p}(\pi s^i_{k|k-1}|Z_{k-1})}{\hat{p}(s^i_{k|k-1}|Z_{k-1})}\right) \gamma^i_{k|k-1} \tag{5.30}$$

The invariant density from Equation (5.21) can then be represented with the particle cloud:

$$\{s^{I,i}_{k|k-1}, 0.5\gamma^{I,i}_{k|k-1}, \pi s^{I,i}_{k|k-1}, 0.5\gamma^{I,i}_{k|k-1}\}_{i=1}^{N_p} \sim p^I(s_k|Z_{k-1}) \tag{5.31}$$

with $\{s^{I,i}_{k|k-1}\}_{i=1}^{N_p} = \{s^i_{k|k-1}\}_{i=1}^{N_p}$ and $\{\gamma^{I,i}_{k|k-1}\}_{i=1}^{N_p} = \frac{\{\tilde{\gamma}^{I,i}_{k|k-1}\}_{i=1}^{N_p}}{\hat{\alpha}^I_{k|k-1}}$

in the above notation, it is implied that both the particle $s^{I,i}_{k|k-1}$ and its permuted version contribute to constructing the approximation. This results in a theoretically perfect invariant approximation, with each individual particle carrying half of the weight.

The variant density from Equation (5.22) can now be approximated by the particle cloud:

$$\{s^{V,i}_{k|k-1}, \gamma^{V,i}_{k|k-1}\}_{i=1}^{N_p} \sim p^V(s_k|Z_{k-1}) \tag{5.32}$$

with $\{s^{V,i}_{k|k-1}\}_{i=1}^{N_p} = \{s^i_{k-1}\}_{i=1}^{N_p}$ and $\{\gamma^{V,i}_{k|k-1}\}_{i=1}^{N_p} = \frac{\{\tilde{\gamma}^{V,i}_{k|k-1}\}_{i=1}^{N_p}}{1-\hat{\alpha}^I_{k|k-1}}$, where

$$\tilde{\gamma}^{V,i}_{k|k-1} = \frac{\hat{p}(s^i_k|Z_{k-1}) - min(\hat{p}(s^i_k|Z_{k-1}), \hat{p}(\pi s^i_k|Z_{k-1}))}{q(s^i_k)} \gamma^i_{k|k-1} \tag{5.33}$$

Assuming the distribution $q(s_k)$ is the predictive density, i.e. $p(s_k|Z_{k-1})$, Equation (5.33) becomes:

$$\tilde{\gamma}^{V,i}_{k|k-1} = \left(1 - min\left(1, \frac{\hat{p}(\pi s^i_{k|k-1}|Z_{k-1})}{\hat{p}(s^i_{k|k-1}|Z_{k-1})}\right)\right) \gamma^i_{k|k-1} = \gamma^i_{k|k-1} - \tilde{\gamma}^{I,i}_{k|k-1} \tag{5.34}$$

finally, the approximation of Equation (5.24) is

$$\hat{\alpha}^V_{k|k-1} = \sum_i \tilde{\gamma}^{V,i}_{k|k-1} = 1 - \hat{\alpha}^I_{k|k-1} \tag{5.35}$$

Notice that the invariant and variant particles in this decomposition are equal, only the weights are different.

5.5 Analytic description and algorithm implementation of the fully decomposed filter

The solution proposed in this section comprises an update and prediction steps in both invariant and variant densities. The update step is identical to the one provided in previous section. Regarding the prediction step, the algorithm presented in this section

assumes that the decomposition of the previous posterior density $p(s_{k-1}|Z_{k-1})$ is available, i.e. $p^I(s_{k-1}|Z_{k-1})$, $p^V(s_{k-1}|Z_{k-1})$, $\alpha^I_{k-1|k-1}$ and $\alpha^V_{k-1|k-1} = 1 - \alpha^I_{k-1|k-1}$ are known, and assuming the dynamic models are the same for both targets, i.e. $p(s_k|s_{k-1}) = p(\pi s_k|s_{k-1})$, a recursive decomposition of the predictive density is given by a three stages Extrapolation-Decomposition-Merging (EDM) step.

Extrapolation: The first stage amounts to extrapolating the invariant and variant densities:

$$p^{II}(s_k|Z_{k-1}) = \int p(s_k|s_{k-1})p^I(s_{k-1}|Z_{k-1})ds_{k-1} \tag{5.36}$$

and

$$p^{MV}(s_k|Z_{k-1}) = \int p(s_k|s_{k-1})p^V(s_{k-1}|Z_{k-1})ds_{k-1} \tag{5.37}$$

Together they describe the predictive density:

$$p(s_k|Z_{k-1}) = \alpha^I_{k-1|k-1}p^{II}(s_k|Z_{k-1}) + \alpha^V_{k-1|k-1}p^{MV}(s_k|Z_{k-1}) \tag{5.38}$$

Assuming permutation invariant target dynamics, the density $p^{II}(s_k|Z_{k-1})$ is invariant, therefore it is referred to with the superscript II. However, the density $p^{MV}(s_k|Z_{k-1})$ can be mixed (containing invariant and strictly variant components), therefore it is referred to with MV. For this density the unique decomposition is used.

Decomposition: The mixed predictive density $p^{MV}(s_k|Z_{k-1})$ is decomposed into an invariant density $p^{IV}(s_k|Z_{k-1})$ and a strictly variant density $p^{VV}(s_k|Z_{k-1})$ using the UD definition

$$p^{MV}(s_k|Z_{k-1}) = \alpha^{IV}_{k|k-1}p^{IV}(s_k|Z_{k-1}) + \alpha^{VV}_{k|k-1}p^{VV}(s_k|Z_{k-1}) \tag{5.39}$$

with,

$$\alpha^{IV}_{k|k-1} = \int_{s_k} min(p^{MV}(s_k|Z_{k-1}), p^{MV}(\pi s_k|Z_{k-1}))ds_k \tag{5.40}$$

$$p^{IV}(s_k|Z_{k-1}) = \frac{min(p^{MV}(s_k|Z_{k-1}), p^{MV}(\pi s_k|Z_{k-1}))}{\alpha^{IV}_{k|k-1}} \tag{5.41}$$

$$p^{VV}(s_k|Z_{k-1}) = \frac{p^{MV}(s_k|Z_{k-1}) - p^{IV}(s_k|Z_{k-1})}{\alpha^{VV}_{k|k-1}} \tag{5.42}$$

with $\alpha^{VV}_{k|k-1} = 1 - \alpha^{IV}_{k|k-1}$

This decomposition can be evaluated in a running particle filter using a sample-based evaluation of $p^{MV}(s_k|Z_{k-1})$ as was explained for the case with a non-decomposed previous posterior.

Merging: Finally the elements of the desired decomposition (see Equation (5.20)) can be written down. The invariant density $p^I(s_k|Z_{k-1})$ and its weight are the result of merging both invariant densities $p^{II}(s_k|Z_{k-1})$ and $p^{IV}(s_k|Z_{k-1})$

$$p^I(s_k|Z_{k-1}) = \frac{\alpha^I_{k-1|k-1}p^{II}(s_k|Z_{k-1}) + \alpha^V_{k-1|k-1}\alpha^{IV}_{k|k-1}p^{IV}(s_k|Z_{k-1})}{\alpha^I_{k|k-1}} \tag{5.43}$$

$$\alpha^I_{k|k-1} = \alpha^I_{k-1|k-1} + \alpha^V_{k-1|k-1}\alpha^{IV}_{k|k-1} \tag{5.44}$$

and the variant density and its weight are

$$p^V(s_k|Z_{k-1}) = p^{VV}(s_k|Z_{k-1}) \tag{5.45}$$

$$\alpha^V_{k|k-1} = \alpha^V_{k-1|k-1}\alpha^{VV}_{k|k-1} \tag{5.46}$$

A sample-based implementation of the merging step for the invariant density suggests itself. For the variant density only the weight needs to be adjusted.

Particle Filtering description: To approximate the expressions in Equations (5.36) and (5.37) from the extrapolation step, one needs to describe two particle clouds:

$$\{s^{II,i}_{k|k-1}, 0.5\gamma^{II,i}_{k|k-1}, \pi s^{I,i}_{k|k-1}, 0.5\gamma^{II,i}_{k|k-1}\}^{N_p}_{i=1} \sim p^{II}(s_k|Z_{k-1}) \tag{5.47}$$

$$\{s^{MV,i}_{k|k-1}, \gamma^{MV,i}_{k|k-1}\}^{N_p}_{i=1} \sim p^{MV}(s_k|Z_{k-1}) \tag{5.48}$$

Both clouds in Equations (5.47) and (5.48) are trivial to generate as the predicted clouds of the invariant and strictly variant components of the previous posterior approximation. The decomposition step needs to be applied to the cloud in Equation (5.48) in order to approximate Equations (5.40), (5.41) and (5.42). As the PF approximation of the invariant part of the previous posterior remains invariant under prediction (given the assumption that dynamic models are the same for all targets), no decomposition is required for the cloud in Equation (5.47).

The approximation of Equations (5.41) and (5.42) can be represented with the clouds

$$\{s^{XV,i}_{k|k-1}, \gamma^{XV,i}_{k|k-1}\}^{N_p}_{i=1} \sim p^{XV}(s_k|Z_{k-1}) \tag{5.49}$$

where

$$\begin{aligned} s^{XV,i}_{k|k-1} &= s^{MV,i}_{k|k-1} \\ \gamma^{XV,i}_{k|k-1} &= \frac{\tilde{\gamma}^{XV,i}_{k|k-1}}{\hat{\alpha}^{XV,i}_{k|k-1}} \\ \tilde{\gamma}^{IV,i}_{k|k-1} &= min\left(1, \frac{\hat{p}(\pi s^{MV,i}_{k|k-1}|Z_{k-1})}{\hat{p}(s^{MV,i}_{k|k-1}|Z_{k-1})}\right)\gamma^{MV,i}_{k|k-1} \end{aligned} \tag{5.50}$$

$$\tilde{\gamma}^{VV,i}_{k|k-1} = \left(1 - min\left(1, \frac{\hat{p}(\pi s^{MV,i}_{k|k-1}|Z_{k-1})}{\hat{p}(s^{MV,i}_{k|k-1}|Z_{k-1})}\right)\right)\gamma^{MV,i}_{k|k-1} \tag{5.51}$$

$$\hat{\alpha}^{XV}_{k|k-1} = \sum_i \tilde{\gamma}^{XV,i}_{k|k-1} \tag{5.52}$$

Now the merging of the two invariant densities will be specified. Computing the individual weights of the three terms:

$$\begin{aligned} \hat{\alpha}^{II} &= \hat{\alpha}^I_{k-1|k-1} \\ \hat{\alpha}^{IV} &= (1 - \hat{\alpha}^I_{k-1|k-1})\hat{\alpha}^{IV}_{k|k-1} \\ \hat{\alpha}^V &= (1 - \hat{\alpha}^I_{k-1|k-1})(1 - \hat{\alpha}^{IV}_{k|k-1}) = 1 - \hat{\alpha}^{II} - \hat{\alpha}^{IV} \end{aligned} \tag{5.53}$$

we have three particle clouds (represented by expressions in Equations (5.47) and (5.49)), two of which represent invariant densities that need to be merged into one. Let us first compute

$$\hat{\alpha}^{I}_{k|k-1} = \hat{\alpha}^{II} + \hat{\alpha}^{IV} \tag{5.54}$$

The merging can be done in several ways. We choose to use a two-step procedure, where we repeatedly randomly select between the invariant-invariant and the invariant-variant cloud according to their probabilities

$$\frac{\hat{\alpha}^{II}}{\hat{\alpha}^{I}_{k|k-1}}, \frac{\hat{\alpha}^{IV}}{\hat{\alpha}^{I}_{k|k-1}} \tag{5.55}$$

and then take a sample from the selected particle cloud according to the particle weights. This procedure eventually leads to a single merged invariant particle cloud,

$$\left\{ s^{I,i}_{k|k-1}, \gamma^{I,i}_{k|k-1} \right\}_{i=1}^{N_p} \sim p^{I}(s_k|Z_{k-1})) \tag{5.56}$$

with the corresponding $\hat{\alpha}^{I}_{k|k-1}$.

Due to the merging operation (and/or the following resampling steps) this algorithm will finally result in two densities that do not share the same particle basis anymore. The updating that was described in Section 5.4.1 (which can deal with particle clouds that do not have the same particle basis) and the prediction step of the two clouds described in this section, complete the specification of the recursive fully decomposed algorithm.

5.6 Simulation Results

This section provides simulation results for the two algorithms using the particle filtering descriptions from previous sections. The targeted clouds and weights for each step of both algorithms can be found in Table 5.1, s^i and γ^i are used to denote the state and weight of an arbitrary particle out of the N_p particles. The superscript X is used to denote both I and V. For instance, the abbreviation $\{s^{X,i}_{k|k-1}, \gamma^{X,i}_{k|k-1}\}_{i=1}^{N_p}, \hat{\alpha}^{X}_{k|k-1}$ in Table 5.1 is equivalent to: $\{s^{I,i}_{k|k-1}, \gamma^{I,i}_{k|k-1}\}_{i=1}^{N_p}, \hat{\alpha}^{I}_{k|k-1}$ and $\{s^{V,i}_{k|k-1}, \gamma^{V,i}_{k|k-1}\}_{i=1}^{N_p}, \hat{\alpha}^{V}_{k|k-1}$

Both algorithms are recursive in essence, the main difference is that the algorithm in the left column propagates a non-decomposed posterior from k to $k+1$, while the one in the right column propagates a decomposed posterior.

5.6.1 Simulation models and parameters

The simulations in this section consider nearly constant velocity for modeling dynamics [23] and a lower dimensional version of the TrBD measurement model in [52] for modeling observations.

The measurement model used defines the power reflected by the tracking scenario for each radar cell. One measurement z_k is composed of N_r power measurements z^n_k, where $k \in \mathbb{N}$ and N_r is the number of range cells.

$$z^n_k = |z^n_{A,k}|^2 = |A^{(1)}_k h^{(1)n}_A + A^{(2)}_k h^{(2)n}_A + n_I(t_k) + in_Q(t_k)|^2 \tag{5.57}$$

Table 5.1: Two algorithms to realize the non-LG implementation of the Unique Decomposition.

steps	partially decomposed algorithm:	fully decomposed algorithm:
1	$\{s^i_{k-1\|k-1}, \gamma^i_{k-1\|k-1}\}_{i=1}^{N_p}$	$\{s^i_{k-1\|k-1}, \gamma^i_{k-1\|k-1}\}_{i=1}^{N_p}$
2	$\{s^{X,i}_{k\|k-1}, \gamma^{X,i}_{k\|k-1}\}_{i=1}^{N_p}, \hat{\alpha}^X_{k\|k-1}$	$\{s^{X,i}_{k\|k-1}, \gamma^{X,i}_{k\|k-1}\}_{i=1}^{N_p}, \hat{\alpha}^X_{k\|k-1}$
3	$\{s^{X,i}_{k\|k}, \gamma^{X,i}_{k\|k}\}_{i=1}^{N_p}, \hat{\alpha}^X_{k\|k}$	$\{s^{X,i}_{k\|k}, \gamma^{X,i}_{k\|k}\}_{i=1}^{N_p}, \hat{\alpha}^X_{k\|k}$
4	$\{s^i_{k\|k}, \gamma^i_{k\|k}\}_{i=1}^{N_p}$	$k = k+1$
5	$k = k+1$ *go to step* 1	$\{s^{X,i}_{k-1\|k-1}, \gamma^{X,i}_{k-1\|k-1}\}_{i=1}^{N_p}, \hat{\alpha}^X_{k-1\|k-1}$ *go to step* 2

where $n = 1, ..., N_r$, A^c_k is the complex amplitude of the target labeled as c,

$$A^{(c)}_k = \tilde{A}^{(c)}_k e^{i\phi_k},\ \phi_k \in U(0, 2\pi) \tag{5.58}$$

and,

$$h^{(c)n}_A(s^c_k) = e^{-\frac{(x^n_k - x^c_k)^2}{2R}} \tag{5.59}$$

Note that c is used for the target labels, which could either be 1 or 2 as in Eq. (5.57). For sake of easier visualization of simulation results, target labels will be associated to colors *blue* and *red* in following subsections. The noise in Eq. (5.57) is complex Gaussian, where $n_I(t_k)$ and $n_Q(t_k)$ are independent, zero-mean white Gaussian with variance σ^2_n accounting for the in-phase and quadrature phase components respectively. These measurements, conditioned on the state are assumed to be exponentially distributed [53],

$$p(z^n|s_k) = \frac{1}{\mu^n_0} e^{-\frac{1}{\mu^n_0} z^n_k} \tag{5.60}$$

where

$$\mu^n_0 = (\tilde{A}^{(1)}_k)^2 (h^{(1)n}_A(s_k, t_k))^2 + (\tilde{A}^{(2)}_k)^2 (h^{(2)n}_A(s_k, t_k))^2 + 2\sigma^2_n \tag{5.61}$$

Assuming that the noise is independent from cell to cell and that the reflections of the two targets are independent, the density model of the measurements given the state becomes:

$$p(z_k|s_k) = \prod_n p(z^n|s_k) \tag{5.62}$$

The ground truth trajectories are defined by the initial dynamics denoted with subscript o in Table 5.2 . The standard deviations of the process noise (σ_q), the SNR of the targets, the revisit time (τ) and the number of particles used in the implementation are also provided in Table II. Labeled track estimates are calculated relying on traditional MMSE estimation considering only the permutation strictly variant density approximation. The associated labeling certainty is calculated as $1 - \frac{\hat{\alpha}^I_{k|k}}{2}$.

Table 5.2: Parameters of the simulation

parameter	value
x_o^1	22 m
$\dot{x}_o^1$	2 m
x_o^2	12 m
$\dot{x}_o^2$	2.8 m
σ_q	1.4142 m/s$^{3/2}$
SNR	11
τ	1 s
N_p	1000 particles

5.6.2 Partially decomposed recursive algorithm: simulation results

Relevant statistics such as labeled track estimates and labeling certainty estimates are plotted in Fig. 5.1. As expected, estimation of labeled tracks are more accurate when extracting them after measurement incorporation.

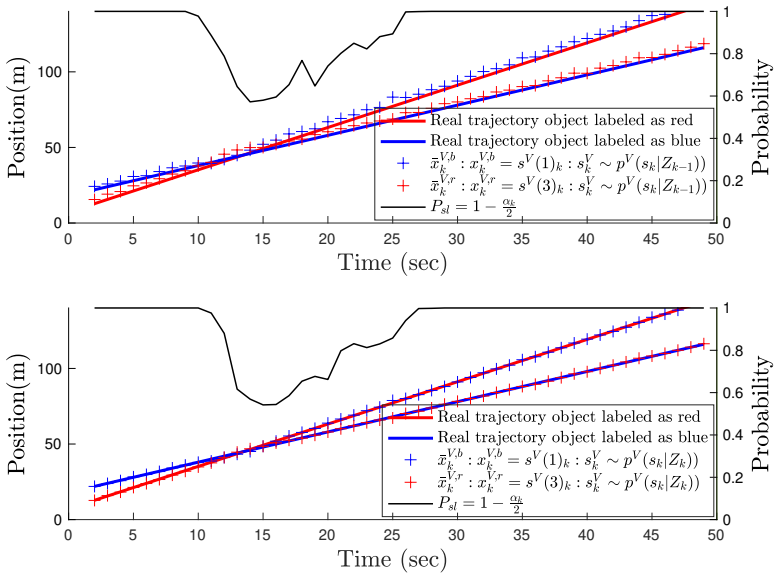

Figure 5.1: Estimation results of the partially decomposed recursive algorithm from Table 5.1. In the top figure, relevant statistics are extracted from the decomposition of the predicted density. In the bottom figure, relevant statistics are extracted from the decomposition of the filtering density.

The partially decomposed recursive algorithm becomes overconfident about the right labeling assignment (according to the P_{sl} curve) after targets separation. This overconfidence signals very poor labeling uncertainty estimation. In fact, the partially decomposed algorithm does run into labeling confusion very often, as it is the case in the particular simulation from Fig. 5.1. This happens because the resampling operation, essential to

prevent particle degeneracy of the cloud $\{s^i_{k|k}, \gamma^i_{k|k}\}_{i=1}^{N_p}$, makes the partially decomposed recursive algorithm vulnerable against particle "self-resolving" artifacts [1].

The term "self-resolving" sounds better than it is, since it does not resolve anything, it just destroys the potential theoretically correct partially invariant characteristics of a multi-target particle representation of the posterior density.

Same way as if we would have calculated the UD from the output of a regular SIR filter, self-resolving does not only negatively impacts (even potentially destroys) the filter operation but also the labeling uncertainty estimation as illustrated in Fig. 5.1.

In order to provide a non-LG implementation of Blom and Bloem's decomposition, circumventing the problem of PF "self-resolving", the two-PFs fully decomposed recursive algorithm was presented in section V. Its PF recursion is summarized in the right column of Table 5.1.

5.6.3 Fully-decomposed recursive algorithm: simulation results

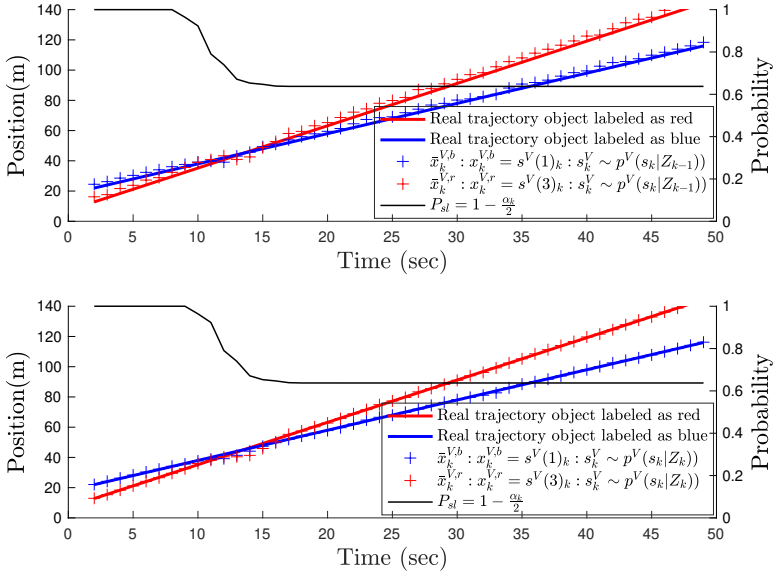

Figure 5.2: Estimation results of the fully decomposed recursive algorithm. In the top figure, relevant statistics are extracted from the decomposition of the predicted density. In the bottom figure, relevant statistics are extracted from the decomposition of the filtering density.

Regarding estimation of labeled tracks, both algorithms provide similar accuracy. The simulations show that the so-called "track-coalescence" effect does not seem to degrade tracking performance after target separation. As opposed to what happens with naive point estimates extraction from a multimodal PDF, the presented algorithms prevent "track-coalescence" by extracting MMSE estimates from the permutation strictly variant density approximation.

As expected from theory, Fig. 5.2 shows that the labeling probabilities by the two-PFs solution do not "self-resolve", leading to more stable estimation of track labeling uncertainty (compared to the results in Fig. 5.1). This was expected as in the fully decomposed recursive algorithm, the invariant component is propagated in isolation from the rest of the density between consecutive iterations. In fact, "self-resolving" is avoided by design. As a result, the multi-modalities inherent in the posterior density when tracking closely-spaced targets can be preserved.

5.7 Conclusions

This chapter derives an implementation of the Unique Decomposition (UD) theory [25] for non linear and/or non-Gaussian (non-LG) problems. Without this generalization, the UD cannot be applied in the TrBD MOT problem due to the highly non-linear nature of the TrBD radar measurements.

The filtering equations of the decomposition have been derived for two different SIR-based filtering implementations. One solution applies the decomposition at each scan in a single filter, the other solution tracks the decomposition over time, using a two filter implementation. Both algorithms have been simulated using synthetic radar TrBD measurements from low-observable targets.

Simulation results have shown that relevant statistics for track formation, namely labeled tracks estimates and respective labeling certainty estimates, can be exacted by both presented solutions. The algorithms prevent "track coalescence" by extracting track estimates based on traditional MMSE estimation applied to the permutation strictly variant component of the density. Regarding labeling uncertainty characterization, the single filter implementation is prone to labeling confusion as a result of not capturing existent labeling uncertainty due to particle "self-resolving" artifacts. Label confusion is prevented by the fully-decomposed 2-PF solution. This is accomplished by propagating the invariant component in isolation from the rest of the density.

Overall, application of the UD theory to the TrBD MOT problem for closely-spaced targets provides stable estimation of labeled tracks and labeling uncertainty. In particular, the dual-filter implementation allows to take informed track-formation decisions without formulating the pair-matching problem between plots and labels. This results in a novel contribution to the state-of-the-art in TrBD MOT.

6

DA-free Tracking: the Cross Modeling Tracker

6.1 Introduction

The track-formation problem needs to be tackled in any MOT solution. To take informed track-formation decisions, estimation of track point-estimates and characterization of labeling uncertainty is required. Extracting these estimates and characterization is not trivial in the context of Track-before-Detect (TrBD), especially when tackling closely-spaced target scenarios, as the formulation of DA hypotheses is ruled out.

The algorithm presented in previous chapter is especially suited for the TrBD MOT problem due to its ability to decompose the joint multiobject density without the need of formulating any DA problem. However, the current limitation of the UD theory is that it cannot be applied in scenarios with more than two objects.

The aim of next two chapters is to overcome the burden of UD-based algorithms. This will be done by providing a generic algorithm, with labeling characterization capabilities, suited for the TrBD MOT problem for an arbitrary number of targets. To this end, the algorithm coined as the The Cross Modeling Tracker (CMT) will be presented.

The CMT introduces a new decomposition of the Bayes posterior based on hypothesizing crosses between objects. A definition of cross-between-objects is taken here as a tool for characterizing labeling uncertainty in cases where the DA problem cannot be formulated. Among these cases, TrBD tracking is probably the most important one due to TrBD inherent capabilities for tracking low-observable objects and for handling closely-spaced object scenarios (in cases where detection-based trackers would have to deal with merged measurements).

The CMT results provided in this chapter are evaluated against the performance evaluation method presented in chapter 4. Simulation results involving challenging closely-spaced

The contents provided in this chapter have been published in "Efficient characterization of labeling uncertainty in closely-spaced targets tracking," C. M. Leon, H. Driessen and P. K. Mandal, in *proceedings of the 19th International Conference on Information Fusion*, Heidelberg, 2016, pp. 449-456. and in "Data-association-free Characterization of Labeling Uncertainty: the Cross Modeling Tracker," C. M. Leon, H. Driessen and A. Yarovoy, in *Journal of Advances in Information Fusion*, December 2021

objects scenarios will be provided. The results illustrate that the CMT is usable in the general $t-MD$ objects case provided that the number of targets t is known and constant in line with the first assumption in the introductory chapter. Therefore, the proposed solution extends the state-of-the-art of TrBD MOT by providing DA-free characterization of labeling uncertainty with validated estimation performance, which can be seamlessly used in generic $t-MD$ targets scenarios.

6.2 Proposed solution

The contents in this chapter are based on the first definition of cross-between-objects in [24, Section IV]. Although the decomposition proposed in [24, Section IV] is only usable for the $2-1D$ objects case, [27] gave analytical generalization to arbitrary $t-MD$ objects cases. Both [24, Section IV] and [27] are published results by the author of this thesis. In this chapter, a self contained presentation of these results is provided.

6.2.1 Modeling crosses in the $2-1D$ objects case

Figure 6.1 illustrates the idea of *cross modeling* in the most simple scenario where the labeling problem appears: two one-dimensional objects approach each other, stay closely-spaced for a while and finally split.

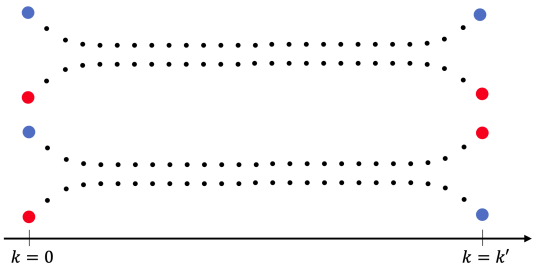

Figure 6.1: Representation on top hypothesizes that objects have (physically) crossed an even number of times from $k=0$ to $k=k'$. Representation at the bottom hypothesizes that objects have (physically) crossed an odd number of times from $k=0$ to $k=k'$.

At $k=0$, the tracker places a label to each object according to the tracker's convention: e.g. blue to the target that is further away and red to the other. At later point in time, for instance $k=k'$, two labeling possibilities are worth considering. One where the furthest object is blue and the nearest one red (example trajectories on top of the figure) and the other with opposite colors, positions being the same (example trajectories at the bottom of the figure).

We are using here color labels instead of number labels for sake of printing clarity. In order to align with the implicit label incorporation inherent in random vector formulations, one just needs to define the convention for mapping the set $\{blue, red\}$ to the two partitions in the stated vector.

Note that the questions in section 2.3 are not concerned with past states but only current information, for instance at $k=k'$. To answer the questions however, it is essential to estimate whether or not the objects have crossed an even or an odd number of times

from $k = 0$ to $k = k'$ in order to characterize the two possible labeling solutions. Based on described estimation of crosses, [24, Section IV] proposed a method to decompose the association-free TrBD posterior density.

The TrBD posterior density $p(\boldsymbol{s}_k|\mathbf{Z}_k)$ in Equation (6.1) displays symmetric multimodality for the closely-spaced target scenario exemplified in Fig. 6.2:

$$p(s_k|\mathbf{Z}_k) \approx l(\mathbf{z}_k|s_k)p(s_k|\mathbf{Z}_{k-1}) \tag{6.1}$$

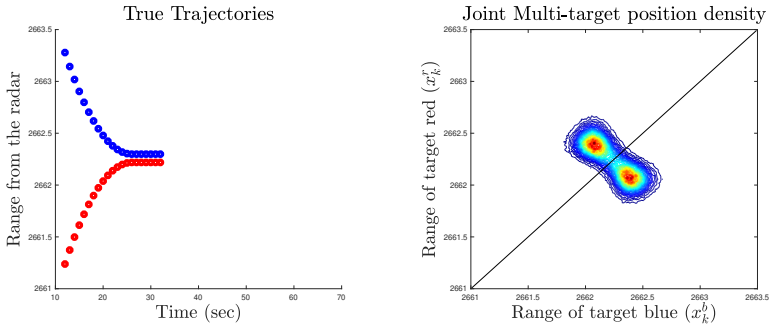

Figure 6.2: Illustration of a closely-spaced targets situation. Ground truth trajectories of two targets moving in a line ($2-1D$ objects scenario) in the left hand side. Last joint multiobject position density (position components of $p(\boldsymbol{s}_k|\mathbf{Z}_k)$) represented in the right hand side.

where $l(\mathbf{z}_k|s_k)$ is the likelihood function of the TrBD measurements conditioned on the state. One label-permutation-dependent decomposition can be formulated as in Equation (6.2). However, due to the assumption that $l(\mathbf{z}_k|s_k)$ is invariant with respect to label permutations, all components (indexed by m in Equation (6.2)) are identical disregarding whether the targets are closely-spaced or not. Therefore, the decomposition in Equation (6.2) cannot be relevant for characterizing labeling uncertainty.

$$p(s_k|\mathbf{Z}_k) \propto \sum_{m=1}^{t!} l(\mathbf{z}_k|\pi_m(s_k))p(s_k|\mathbf{Z}_{k-1}) \propto l(\mathbf{z}_k|s_k)p(s_k|\mathbf{Z}_{k-1}) \tag{6.2}$$

One physical interpretation of the multimodality in $p(\boldsymbol{s}_k|\mathbf{Z}_k)$ (illustrated in Fig. 6.2) is that the objects may have well crossed each other from one time scan to the next one. As one can see in Figure 6.2, the probability mass of $p(\boldsymbol{s}_k|\mathbf{Z}_k)$ concentrates in separated regions of the joint state space. These regions represent different labeling permutations of the information of interest.

In [24, Section IV], it is assumed that the state variable is a vector where partitions are stacked: $\boldsymbol{s}_k = [x_k^b\ \dot{x}_k^b\ x_k^r\ \dot{x}_k^r]^T$. Positions of each partition are denoted as x_k and velocities as $\dot{x}_k$. b and r are the labels for the first and second partition respectively (blue and red for printing clarity). In order to hypothesize crosses between objects, the concept of *order* at time step k was defined in [24, Section IV] as:

$$o_k = d(\boldsymbol{s}_k) = \begin{cases} 1 & \text{if } x_k^b > x_k^r \\ 2 & \text{otherwise} \end{cases} \tag{6.3}$$

For two objects moving in one dimension, the variable *order* determines whether the position of one 1D object is larger or less than the position of another 1D object. Additionally, it is trivial to interpret a permutation of *order* in the state vector as a cross of objects between time steps $k-1$ and k (see Figure 6.3).

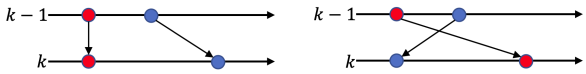

Figure 6.3: No permutation of *order* (left hand side), permutation of *order* (right hand side)

This trivial notion of order/cross in 1D, escapes to physical interpretation in higher dimensional problems. One cannot tell whether the position of one 2D object is larger or less than the position of another 2D object as the definition of ">" and "<" is only valid in the 1D line. In fact, although one *order* definition was provided in [24, Section V] for the $2-2D$ objects case, counterexamples were found proving its lack of generality.

6.3 Generalized characterization of Cross Modeling

Figure 6.4 illustrates the generic block diagram of a TrBD MOT solution based on cross modeling. [24, Section IV] provided an algorithm according to this block diagram to solve the formulated problem in section 2.3 for the $2-1D$ objects case.

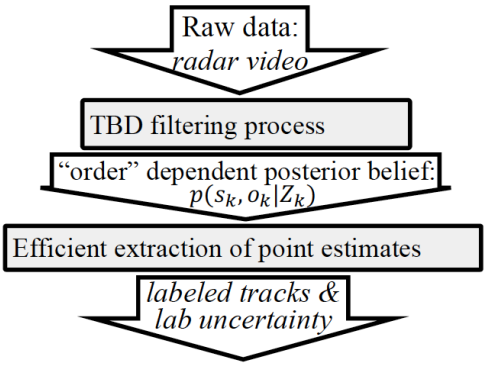

Figure 6.4: The illustrated block diagram describes the operation of the CMT. The block diagram is generic in the sense that it should be applicable in any arbitrary $t-MD$ objects case. However, the definition of o_k provided in Equation (6.3) does not allow its use out of the $2-1D$ objects case. Hence, the importance of generalizing the definition of o_k.

As the definition of o_k provided in Equation (6.3) does not apply out of the $2-1D$ objects case, the generalization of o_k Equation (6.3) is essential in order to model crosses for any arbitrary $t-MD$ object problems. The solution based on Equation (6.3) was designed in [24, Section IV] for particle-based implementations of the Bayesian filter. In particle filtering, "particle mixing" is a characteristic phenomenon inherent in approximations of multimodal densities [60]. Interestingly in the context of our labeling problem, when "particle mixing" happens at least two particles are represented with permuted order of

partitions in the state vector [61]. In order to generalize the definition of order/cross in [24, Section IV] to arbitrarily high dimensional problems, this chapter proposes to analyze and exploit "particle mixing" effects in the particle cloud. Exploitation of such "particle mixing" analysis is realized by means of clustering the particle cloud.

Clustering the particle cloud will result in a relevant decomposition aiding at extracting relevant statistics. This decomposition will enable straightforward extraction of labeling certainty estimates and trouble-free use of computationally efficient MMSE estimation (even when $p(s_k|\mathbf{Z}_k)$ is multimodal).

6.3.1 State space model

The general nonlinear dynamic system and observation models can be denoted as f and q respectively:

$$\boldsymbol{s}_k = f(\boldsymbol{s}_{k-1}, \boldsymbol{n}_{k-1}) \tag{6.4}$$

$$\mathbf{z}_k = q(\boldsymbol{s}_k, \boldsymbol{v}_k),\ k \in \mathbb{N} \tag{6.5}$$

where $\boldsymbol{s}_k$, $\boldsymbol{n}_k$, $\mathbf{z}_\mathbf{k}$ and $\boldsymbol{v}_k$ represent the state, process noise, the measurement and the measurement noise respectively.

We tackle the MOT problem in the framework of recursive Bayesian filtering. The predicted and posterior densities of interest $p(\boldsymbol{s}_k|\mathbf{Z}_{k-1})$ and $p(\boldsymbol{s}_k|\mathbf{Z}_k)$ are obtained by iteration over the Chapman-Kolmogórov and Bayes equations:

$$p(\boldsymbol{s}_k|\mathbf{Z}_{k-1}) = \int p(\boldsymbol{s}_k|\boldsymbol{s}_{k-1}) p(\boldsymbol{s}_{k-1}|\mathbf{Z}_{k-1}) d\boldsymbol{s}_{k-1} \tag{6.6}$$

$$p(\boldsymbol{s}_k|\mathbf{Z}_k) = \frac{p(\mathbf{z}_k|\boldsymbol{s}_k) p(\boldsymbol{s}_k|\mathbf{Z}_{k-1})}{p(\mathbf{z}_k|\mathbf{Z}_{k-1})} \tag{6.7}$$

in this framework, the models in Equations (6.4) and (6.5) are expressed in the form of $p(\boldsymbol{s}_k|\boldsymbol{s}_{k-1})$ and $p(\mathbf{z}_k|\boldsymbol{s}_k)$ respectively.

Due to the nonlinear nature of TrBD measurement models, the Bayesian recursion formulated in Equations (6.6) and (6.7) cannot be implemented via (stochastic) parametric models [28]. For this reason, a PF will be used to approximate the recursion.

6.3.2 A generic decomposition of $p(\boldsymbol{s}_k|\mathbf{Z}_k)$ in TrBD

As detailed in the subsection 2.4, the underlying concern to answer the questions in section 2.3 is how to decompose $p(\boldsymbol{s}_k|\mathbf{Z}_k)$ in TrBD. A generic decomposition of $p(\boldsymbol{s}_k|\mathbf{Z}_k)$ can be formulated by introducing an auxiliary variable o_k:

$$p(\boldsymbol{s}_k|\mathbf{Z}_k) = \sum_{i=1}^{t!} p(\boldsymbol{s}_k, o_k = i|\mathbf{Z}_k) \tag{6.8}$$

Please note that the desired definition of o_k is not the one in Equation (6.3) as we are targeting its generalization to the $t - MD$ objects case. The new density of interest $p(\boldsymbol{s}_k, o_k|\mathbf{Z}_k)$, can be factorized as:

$$p(\boldsymbol{s}_k, o_k|\mathbf{Z}_k) = p(\boldsymbol{s}_k|o_k, \mathbf{Z}_k) P(o_k|\mathbf{Z}_k) \tag{6.9}$$

where $p(\boldsymbol{s}_k|o_k,\mathbf{Z}_k)$ is the posterior density of the state vector given o_k and the measurements, while $P(o_k|\mathbf{Z}_k)$ is the posterior probability of o_k. Both can be computed using the association-free (non-decomposed) TrBD filter output $p(\boldsymbol{s}_k|\mathbf{Z}_k)$ and a certain probabilistic definition of the auxiliary variable o_k:

$$p(\boldsymbol{s}_k|o_k,\mathbf{Z}_k) = \frac{P(o_k|\boldsymbol{s}_k,\mathbf{Z}_k)p(\boldsymbol{s}_k|\mathbf{Z}_k)}{P(o_k|\mathbf{Z}_k)} \tag{6.10}$$

$$P(o_k|\mathbf{Z}_k) = \int_{\boldsymbol{s}_k} P(o_k|\boldsymbol{s}_k)p(\boldsymbol{s}_k|\mathbf{Z}_k)d\boldsymbol{s}_k \tag{6.11}$$

Assuming that the generalized definition of o_k is conditionally independent on $\mathbf{Z}_k$ given $\boldsymbol{s}_k$ (as it is the case in the $2-1D$ targets case definition from Equation (6.3)), Equation (6.10) can be rewritten as:

$$p(\boldsymbol{s}_k|o_k,\mathbf{Z}_k) = \frac{P(o_k|\boldsymbol{s}_k)p(\boldsymbol{s}_k|\mathbf{Z}_k)}{P(o_k|\mathbf{Z}_k)} \tag{6.12}$$

The generic decomposition in Equation (6.8) together with the desired definition of $P(o_k|\boldsymbol{s}_k)$ should allow answering the questions of interest for generic $t-MD$ problems. When MMSE estimation is the choice for extracting point estimates, the desired definition of $P(o_k|\boldsymbol{s}_k)$ should ensure that each component in Equation (6.8) $p(\boldsymbol{s}_k|o_k=m,\mathbf{Z}_k)$ is unimodal. Under this condition, the list of $t!$ label point estimates (question 1 in section 2.3) can be provided avoiding track-coalescence. Finally, the desired definition $P(o_k|\boldsymbol{s}_k)$ should be such that $P(o_k=m|\mathbf{Z}_k)$ represents the certainty of labeling association m (question 2 in section 2.3).

Labeled Point Estimates and labeling certainties of the CMT

In a particle-based implementation of the Bayesian recursion, $p(\boldsymbol{s}_k|\mathbf{Z}_k)$ is represented with a weighted set of particles $\{\boldsymbol{s}_k^i, w_k^i\}_{i=1}^{N_p}$. According to the decomposition in Equation (6.8), order-dependent Labeled Point Estimates (LPEs) can be calculated as the expected value of $\boldsymbol{s}_k$ given the *order* and measurements:

$$\begin{aligned} E[\boldsymbol{s}_k|o_k,\mathbf{Z}_k] &= \int_{\boldsymbol{s}_k} \boldsymbol{s}_k p(\boldsymbol{s}_k|o_k,\mathbf{Z}_k)d\boldsymbol{s}_k \\ &\underset{\text{Eq (6.12)}}{=} \frac{1}{P(o_k|\mathbf{Z}_k)} \int_{\boldsymbol{s}_k} \boldsymbol{s}_k P(o_k|\boldsymbol{s}_k)p(\boldsymbol{s}_k|\mathbf{Z}_k)d\boldsymbol{s}_k \\ &\approx \frac{1}{P(o_k|\mathbf{Z}_k)} \sum_i w_k^i \boldsymbol{s}_k^i P(o_k|\boldsymbol{s}_k^i) \end{aligned} \tag{6.13}$$

Order-dependent labeling certainties are necessarily in the second factor of Equation (6.9)

$$P(o_k|\mathbf{Z}_k) = \int_{\boldsymbol{s}_k} P(o_k|\boldsymbol{s}_k)p(\boldsymbol{s}_k|\mathbf{Z}_k)d\boldsymbol{s}_k \approx \sum_i w_k^i P(o_k|\boldsymbol{s}_k^i) \tag{6.14}$$

Evaluation of $E[\boldsymbol{s}_k|o_k, \mathbf{Z}_k]$ for each possible realization of o_k provides a different vector of LPEs (answer to question 1 in section 2.3):

$$E[\boldsymbol{s}_k|o_k = m, \mathbf{Z}_k] \approx \frac{1}{P(o_k = m|\mathbf{Z}_k)} \sum_i w_k^i \boldsymbol{s}_k^i P(o_k = m|\boldsymbol{s}_k^i) \approx \frac{1}{P(o_k = m|\mathbf{Z}_k)} \sum_{i|o_k^i = m} w_k^i \boldsymbol{s}_k^i \quad \text{where } m \in \{1, 2, .., t!\} \tag{6.15}$$

In the same way, evaluation of $P(o_k|\mathbf{Z}_k)$ for each possible realization of o_k provides a scalar with the associated labeling probability (answer to question 2 in section 2.3):

$$P(o_k = m|\mathbf{Z}_k) \approx \sum_i w_k^i P(o_k = m|\boldsymbol{s}_k^i) \approx \sum_{i|o_k^i = m} w_k^i \tag{6.16}$$

Algorithm implementation

Algorithm 4 is the practical implementation of the functionalities illustrated in Figure 6.4. Same way as in Figure 6.4, the algorithm is generic given a generic definition of "order" (o_k^i at particle level).

1 $k = 0$;
2 Draw N_p samples $\boldsymbol{s}_k^i$ from $p(\boldsymbol{s}_k)$;
3 Draw N_p samples $\boldsymbol{n}_k^i$ from $p(\boldsymbol{n}_k)$;
4 $k = k + 1$;
5 $\boldsymbol{s}_k^i = f(\boldsymbol{s}_{k-1}^i, \boldsymbol{n}_{k-1}^i)$;
6 Calculate o_k^i according to the definition of "order" under test;
7 Given $\mathbf{z_k}$, obtain $\tilde{w}_k^i = p(\mathbf{z}_k|s_k^i)$;
8 Normalize weights $w_k^i = \tilde{w}_k^i / \sum_{j=1}^{N_p} \tilde{w}_k^j$;
9 Resample from $\hat{p}(\boldsymbol{s}_k|\mathbf{Z}_k) = \sum_{i=1}^{N_p} w_k^i \delta(\boldsymbol{s}_k - \boldsymbol{s}_k^i)$:;
10 Extract LPEs according to Equation 6.15;
11 Obtain certainty measures of LPEs according to Equation 6.16;
go to 3

Algorithm 4: Pseudo-code of the PF algorithm for implementation of the CMT. Extensions over the plain SIR TrBD particle filter and traditional MMSE estimate extraction are highlighted in blue color. $p(\boldsymbol{s}_k)$ and $p(\boldsymbol{n}_k)$ denote the initial prior and the process noise models.

6.3.3 Performance evaluation of the CMT for the $2-1D$ objects case

Before delving into the problem of generalizing the solution in [24, Section IV], it is relevant to understand the performance evaluation of the low dimensional CMT solution. In fact, although [24, Section IV] presented numerical results, these were not evaluated against the references described in chapter 4. Namely, reference labeled tracks and reference labeling probabilities.

Table 6.1: Parameters of the simulation

parameter	value
d_i	1.66 m
d_m	0.22 m
σ_n	0.14 m/s$^{3/2}$
σ_v	0.045 m
τ	1 s
N_p	10000 particles

The choice of simulation parameters to evaluate the solution in [24, Section IV] is shown in Table 6.1. This parametrization generates a high amount of labeling uncertainty in order to challenge the MOT algorithm. This becomes apparent when considering the overlapping in between partitions of different colors (labels) of the predicted and posterior particle cloud in Figure 6.5.

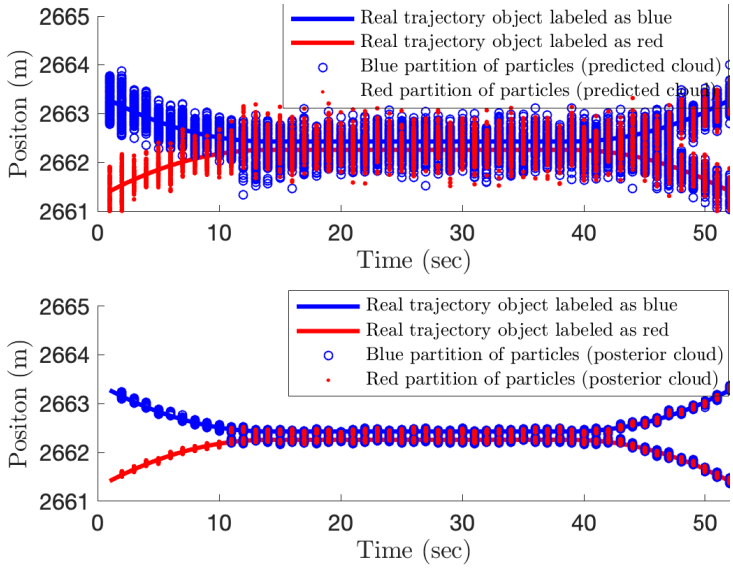

Figure 6.5: Illustration of real trajectories as well as predicted and posterior particle clouds along all simulation time steps. The particle mixing effect can be observed, for instance, in the posterior particle clouds after object separation. In fact, different particles hypothesize the state of the same physical object with different partitions.

The evaluation can be reproduced by setting up the trajectories for the objects with initial and minimum distance as indicated by d_i and d_m in Table 6.1. The evaluation considers the dynamic and measurement models as nearly constant velocity [23] and linear-Gaussian. The standard deviations of the process noise and observation noise are indicated by σ_n and σ_v respectively in Table 6.1, where τ denotes the revisit time. Without loss of generality, choosing these simple models suffices to validate Alg. 4 against the evaluation references calculated by Alg. 3.

The definition of o_k in Equation (6.3) can be rewritten in a probabilistic form:

$$\begin{aligned} P(o_k = 1|\mathbf{s}_k) &= 1 \;\; if \;\; x_k^b > x_k^r \\ P(o_k = 2|\mathbf{s}_k) &= 0 \;\; if \;\; x_k^b \leq x_k^r \end{aligned} \tag{6.17}$$

The definition in (6.17) can be plugged into Equations (6.12) and (6.11) in order to decompose $p(\mathbf{s}_k|\mathbf{Z}_k)$ using the CMT (Algorithm 4). By these means, LPEs and associated labeling certainties can be generated with Algorithm 4 and evaluated with the optimal reference generated by Algorithm 3. Simulation results illustrated in Figures 6.6 and 6.7 validate the cross modeling solution for the $2-1D$ objects case using the evaluation method described in chapter 4.

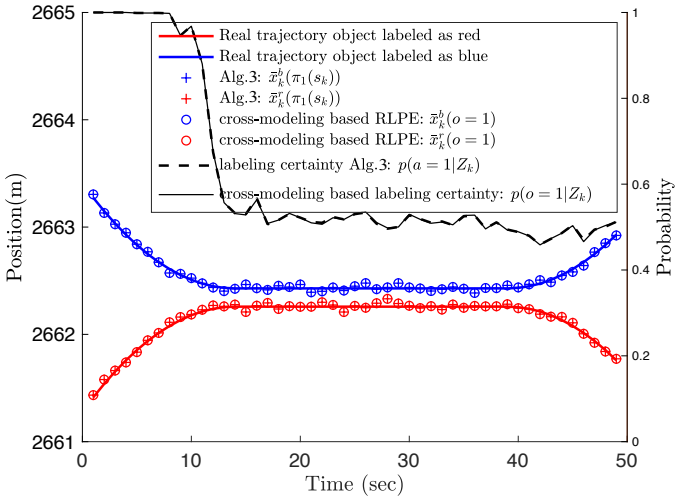

Figure 6.6: Evaluation of estimation performance of the CMT for a $2-1D$ objects scenario. Cross modeling based estimates are extracted only from the cluster associated to "order" 1.

Comments on the results

Algorithm 4 decomposes the particle cloud in two ($t!$) clusters. These clusters explicitly approximate the DA-free decomposition in Equation (6.8). The cluster associated to "order" 1 supports the hypothesis that the maneuvers of the two labeled objects lead to non-crossed trajectories with respect to the initialization $\forall k$. This cluster produces LPEs represented in Figure 6.6 as $\bar{x}_k^{b,r}(o=1)$. The certainty measure associated ($P(o=1|\mathbf{Z}_k)$ curve) is extracted from the particle approximation of the joint multiobject posterior in step 11 of Algorithm 4.

Over the first 6 seconds of the simulation, the LPE($o=1$) holds full certainty. No single particle belongs to the cluster $o=2$ and therefore, no representative can be extracted from there (see Figure 6.7). As expected, $P(o_k=1|\mathbf{Z}_k)$ drops down to around 0.5 after the objects remain closely-spaced for some time. This means that labeling information has been completely lost. Labeling information cannot be recovered after the split as suggested by the measure of certainty. The LPE($o=2$) supports the hypothesis that the maneuvers of the two labeled objects lead to crossed trajectories with respect to the initialization $\forall k$.

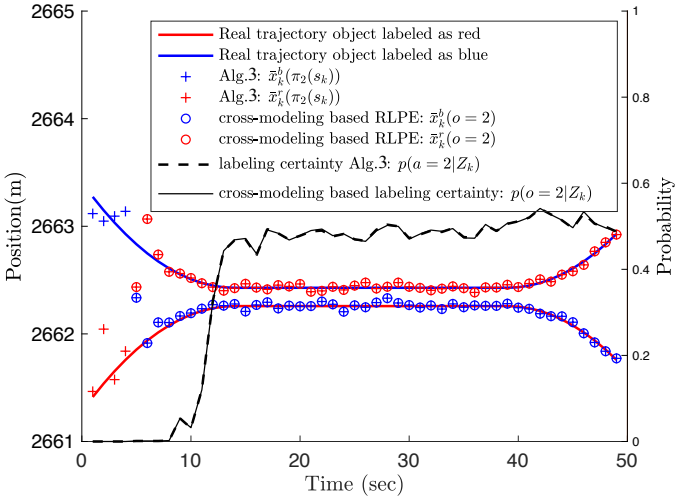

Figure 6.7: Evaluation of estimation performance of the CMT for a $2-1D$ objects scenario. Cross modeling based estimates are extracted only from the cluster associated to "order" 2.

6

Estimation results produced by the CMT closely match the ground truths generated by Algorithm 3. This validates the CM method as a solution to the problem defined in the Section 2.4 for the $2-1D$ objects scenario.

6.4 First generalization of the definition of *cross*: scenarios with arbitrary number t of 1D objects

In a $2-1D$ objects setting, given the state of one particle at time step k, Equation (6.3) provides its *order*. We will refer to this calculation as an absolute evaluation of *order*. Unlike 1-D points, 2-D points cannot be ordered making use of the operators $\leq$ and $>$. For this reason, finding an absolute evaluation of "order" in 2-D is not a trivial concern.

6.4.1 Absolute versus relative *order* calculation and the definition of *cross*:

An alternative method to obtain the *order* can be realized by relative evaluation: relying on the prior *order* at time step $k-1$ and detecting whether or not the objects have crossed from time step $k-1$ to k,

	$P(o_k=1\|\boldsymbol{s}_k)=1$	$P(o_k=2\|\boldsymbol{s}_k)=1$
$P(o_{k-1}=1\|\boldsymbol{s}_{k-1})=1$	no cross	cross
$P(o_{k-1}=2\|\boldsymbol{s}_{k-1})=1$	cross	no cross

For $2-1D$ objects scenarios:

	$x_k^r < x_k^b$	$x_k^r \geq x_k^b$
$x_{k-1}^r < x_{k-1}^b$	no cross	cross
$x_{k-1}^r \geq x_{k-1}^b$	cross	no cross

Hence, to declare a cross, either of the two following conditions must be met:

$$x_{k-1}^1 < x_{k-1}^2 \quad and \quad x_k^1 \geq x_k^2 \tag{6.18}$$

$$x_{k-1}^1 \geq x_{k-1}^2 \quad and \quad x_k^1 < x_k^2 \tag{6.19}$$

The relative *order* evaluation method shifts the generalization problem from the definition of *order* to the definition of *cross*. A *cross* detector for $2-1D$ objects can be derived from the absolute definition in Equation (6.3). Let us denote $\boldsymbol{s}_k^{'p}$ as the position part of the state vector $\boldsymbol{s}_k = [x_k^b\ \dot{x}_k^b\ x_k^r\ \dot{x}_k^r]$ of particle p at time step k: $\boldsymbol{s}_k^{'p} = [x_k^{p,b}\ x_k^{p,r}]$. Since $\boldsymbol{s}_k^{'p}$ and $\boldsymbol{s}_{k-1}^{'p}$ are vectors in a 2D space (2 objects placed along 1D spacial dimension), one can calculate the Euclidean distance or $l2-norm$ between them in the joint space as (superscript p is dropped for notation simplicity):

$$norm(\boldsymbol{s}'_k - \boldsymbol{s}'_{k-1}) = \sqrt{(x_k^r - x_{k-1}^r)^2 + (x_k^b - x_{k-1}^b)^2} \tag{6.20}$$

$$= \sqrt{(x_k^r)^2 - 2(x_k^r x_{k-1}^r) + (x_{k-1}^r)^2 + (x_k^b)^2 - 2(x_k^b x_{k-1}^b) + (x_{k-1}^b)^2} \tag{6.21}$$

$$= \sqrt{(x_k^b - x_{k-1}^r)^2 + (x_k^r - x_{k-1}^b)^2 + 2(x_{k-1}^r - x_{k-1}^b)(x_k^b - x_k^r)} \tag{6.22}$$

Then,

$$norm^2(\boldsymbol{s}'_k - \boldsymbol{s}'_{k-1}) = (x_k^b - x_{k-1}^r)^2 + (x_k^r - x_{k-1}^b)^2 + 2(x_{k-1}^r - x_{k-1}^b)(x_k^b - x_k^r) \tag{6.23}$$

$$norm^2(\boldsymbol{s}'_k - \boldsymbol{s}'_{k-1}) = norm^2(\Pi \boldsymbol{s}'_k - \boldsymbol{s}'_{k-1}) + K \tag{6.24}$$

where $K = 2(x_{k-1}^r - x_{k-1}^b)(x_k^b - x_k^r)$ and Π denotes the permutation matrix:

$$\Pi = \begin{pmatrix} 0 & 1 \\ 1 & 0 \end{pmatrix} \tag{6.25}$$

Each of the Equations (6.18) and (6.19) define the conditions to declare a cross. Interestingly, when any of these equations is applied to the function K, the result is $K > 0$ as long as x_{k-1}^r, x_{k-1}^b, x_k^r and x_k^b take positive values. Variables x_{k-1}^r, x_{k-1}^b, x_k^r and x_k^b can only take positive values in our application problem as these are range magnitudes. Therefore, Inequation (6.26) holds as long as a cross in the state vector of particle p takes place:

$$norm^2(\boldsymbol{s}_k^{'p} - \boldsymbol{s}_{k-1}^{'p}) > norm^2(\Pi \boldsymbol{s}_k^{'p} - \boldsymbol{s}_{k-1}^{'p}) \tag{6.26}$$

Equivalently, the next *order switch* condition can be used to find out whether or not a cross should be declared for the particle p between time instants $k-1$ and k.

$$norm(\boldsymbol{s}_k^{'p} - \boldsymbol{s}_{k-1}^{'p}) > norm(\Pi \boldsymbol{s}_k^{'p} - \boldsymbol{s}_{k-1}^{'p}) \tag{6.27}$$

The result in Equation (6.27) can be pictured in a physically meaningful way as in Figure 6.8.

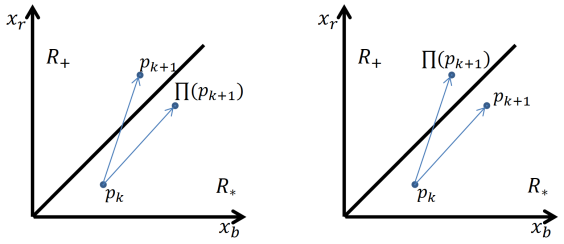

Figure 6.8: The illustration in the left hand side represents an *order switch* as the points p_k and p_{k+1} belong in different sides of the diagonal $x_r = x_b$. Indeed, Inequation (6.27) holds in this case. In the right hand side the point p does not cross the line $x_r = x_b$ between time instants k and $k+1$ meaning that the order remains the same in this case. Indeed, Inequation (6.27) does not hold.

6.4.2 Generalization of *cross* from $2-1D$ to $t-1D$ cases

This generalization considering $1D$ objects makes use of the relative definition of "order" based on Inequation (6.27), applied to all possible pairs of partitions in the state vector. As the number of possible labeling solutions is $t!$, only the extension from two to three targets will be exemplified due to space limitations. Nevertheless, there is no loss of generality as the same technique can be applied to any arbitrary number of targets t.

For a three-object scenario, the three partitions in the state vector can be ordered in six different ways according to, for instance, the convention in Table 6.2:

	1D magnitude increasing direction $\rightarrow$		
$o = 1$	1^{st}	2^{nd}	3^{rd}
$o = 2$	1^{st}	3^{rd}	2^{nd}
$o = 3$	2^{nd}	1^{st}	3^{rd}
$o = 4$	3^{rd}	1^{st}	2^{nd}
$o = 5$	2^{nd}	3^{rd}	1^{st}
$o = 6$	3^{rd}	2^{nd}	1^{st}

Table 6.2: Order convention for the 3 scalar-targets case

The convention in Table 6.2 groups in cluster 1 those particles complying with: position of the first partition is less than the position of the second partition, being the position of the second partition less than the position of the third partition. For the sake of printing clarity in forthcoming simulation experiments, the first, second and third partitions will be identified with colors green, red and blue respectively.

Between the time steps $k-1$ and k, there are eight distinct types of crosses that could occur. Each cross type is composed of three boolean variables. These are used to codify whether or not a cross is declared between pairs of partitions. When the boolean variable

is set to 1, a cross is declared between the corresponding pair of objects. For instance, one can adopt the following convention:

	cross of partitions $1^{st}-2^{nd}$	cross of partitions $1^{st}-3^{rd}$	cross of partitions $2^{nd}-3^{rd}$
C1	0	0	0
C2	0	0	1
C3	1	0	0
C4	0	1	1
C5	1	1	0
C6	1	1	1
C7	1	0	1
C8	0	1	0

These cross-type codes can be used now for relative evaluation of the *order* at time step k, given the order at time step $k-1$:

	$o_k=1$	$o_k=2$	$o_k=3$	$o_k=4$	$o_k=5$	$o_k=6$
$o_{k-1}=1$	C1	C2	C3	C4	C5	C6
$o_{k-1}=2$	C2	C1	C7	C8	C6	C5
$o_{k-1}=3$	C3	C7	C1	C6	C8	C4
$o_{k-1}=4$	C4	C8	C6	C1	C7	C3
$o_{k-1}=5$	C5	C6	C8	C7	C1	C2
$o_{k-1}=6$	C6	C5	C4	C3	C2	C1

6.4.3 Simulation results

The estimation performance of the CM method for a $3-1D$ objects scenario, using Inequation (6.27) as the "cross detector", is illustrated in this subsection. Note that the validation method summarized in chapter 4 is based on evaluation of data association hypotheses. Therefore, Algorithm 2 can be used right away to generate optimal LPEs and labeling probabilities in any arbitrary $t-MD$ objects case. Figure 6.9 illustrates the estimation performance of the CMT.

Discussion of results

The results in Figure 6.9 reveal remarkably accurate estimation performance of the CMT both in the computation of LPEs and labeling probabilities. This validates the CMT as a convenient solution to answer the questions in section 2.3 for scenarios where an arbitrary number of objects move in one dimension.

The choice of the particular ground truth trajectories in Figure 6.9 results in complete loss of labeling information (1/3! certainty for all LPEs). Although Figure 6.9 illustrates this worst case scenario, it is apparent that the CMT accurately estimates labeling uncertainty also in more favorable scenarios. For instance, scenarios where the objects remain closely-spaced for a shorter time and labeling certainty is lost only partially.

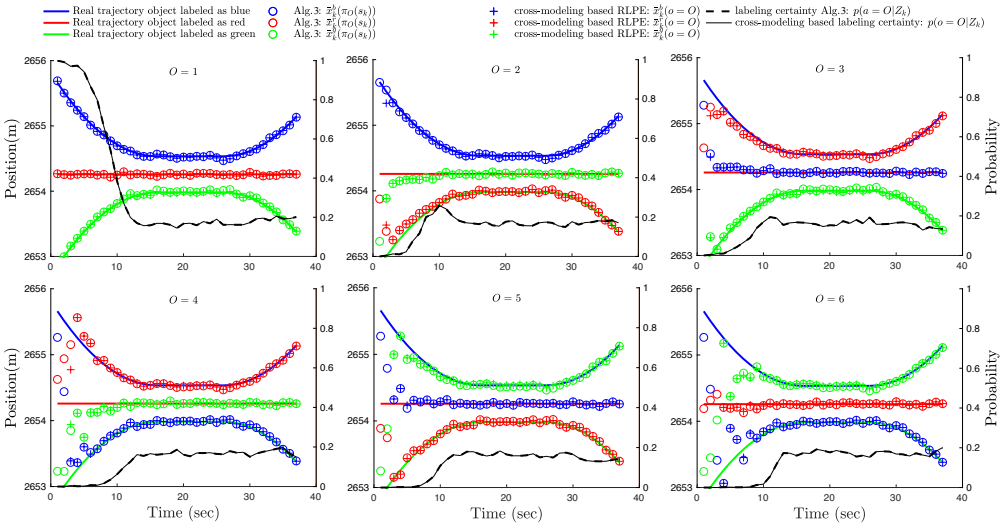

Figure 6.9: Evaluation of estimation results provided from the clusters associated to all states of "order" in Table 6.2

Losing labeling information is a physical limitation inherent in closely-spaced object scenarios. Furthermore, once labeling certainty is lost, it is mathematically not possible to recover it (assuming that the objects cannot be differentiated in measurements/maneuverability). In this context, all what can be expected from the tracker is that it captures the uncertainty produced by the combination scenario/sensor-limitations as accurately as possible. The best indicator of the DA-free decomposition quality is how good the CMT can estimate when and how quickly the 100% labeling certainty (in the beginning of the simulation) drops as the targets get closer to each other. While regular TrBD filters such as the one in [52] cannot capture this, the CMT reports successful results for the cases simulated so far.

6.5 Second generalization of the definition of *cross* from $t-1D$ to $t-MD$ objects

Subsection 6.3.2 presented a generic DA-free decomposition of $p(\boldsymbol{s}_k|\mathbf{Z}_k)$ by introducing the (not yet defined for the generic $t-MD$ case) variable o_k. An analytical expression for the LPEs and labeling probabilities (dependent on the definition of o_k) was provided in Equations (6.15) and (6.16). Another analytical derivation provided in Subsection 6.4.1 has proved that the relative calculation of o_k for the $2-1D$ objects case, based on Inequation (6.27), leads to identical results than the absolute calculation of o_k based on Equation (6.3).

Section 6.4.2 illustrated how the relative calculation of o_k (based on Inequation (6.27)) can be extended seamlessly to cope with more than two objects moving in a one-dimensional space. This section covers the generalization of the relative calculation of o_k from 1D to MD objects. In practice, simulation experiments will be limited to cases where M is 2 and 3 to illustrate that the CMT can be used for tracking of land/sea objects (2D) and air objects

(3D).

The reader is referred to Appendix A.3 at this point in order to understand the complexity of extending the definition of o_k in Equation (6.3) to objects moving in 2 and 3 spacial dimensions.

6.5.1 Generalization of the *cross* detector to $2-2D$ objects settings

Inequation (6.27) does not extend straightforwardly from $2-1D$ to $2-2D$ objects scenarios as illustrated in Appendix A.3. However, the reason why Inequation (6.27) works well for the $2-1D$ case can be found after analyzing the function K derived in Subsection 6.4.1. Given the 2D points $\boldsymbol{s}_{k-1}^{'p}$ and $\boldsymbol{s}_{k}^{'p}$ (2 objects in a 1D space), the function $K = 2(x_{k-1}^{r} - x_{k-1}^{b})(x_{k}^{b} - x_{k}^{r})$ complies with a very particular condition:

$$K(\boldsymbol{s}_{k-1}^{'p}, \boldsymbol{s}_{k}^{'p}) = -K(\boldsymbol{s}_{k-1}^{'p}, \Pi(\boldsymbol{s}_{k}^{'p})) \tag{6.28}$$

as $\boldsymbol{s}_{k}^{'p}$ and $\Pi(\boldsymbol{s}_{k}^{'p})$ are crossed with respect to each other, K can be regarded as an odd function in the "order" of $\boldsymbol{s}_{k}^{'p}$. In other words, two different evaluations of K, using the current state of particle p and its permuted version are equal in absolute value but different in sign:

$$\begin{aligned} |K(\boldsymbol{s}_{k-1}^{'p}, \boldsymbol{s}_{k}^{'p})| &= |K(\boldsymbol{s}_{k-1}^{'p}, \Pi(\boldsymbol{s}_{k}^{'p}))| \\ sgn(K(\boldsymbol{s}_{k-1}^{'p}, \boldsymbol{s}_{k}^{'p})) &= sgn(-K(\boldsymbol{s}_{k-1}^{'p}, \Pi(\boldsymbol{s}_{k}^{'p}))) \end{aligned} \tag{6.29}$$

Additionally, as we already pointed out in Subsection 6.4.1:

$$K(\boldsymbol{s}_{k-1}^{'p}, \boldsymbol{s}_{k}^{'p}) > 0 \quad \Leftrightarrow \quad \boldsymbol{s}_{k-1}^{'p}, \boldsymbol{s}_{k}^{'p} \textit{ are crossed} \tag{6.30}$$

The condition $K(\boldsymbol{s}_{k-1}^{'p}, \boldsymbol{s}_{k}^{'p}) > 0$ and Inequation (6.27) are equivalent "cross detectors" for the $2-1D$ case due to Equation (6.24). Our problem formulation can be narrowed down to the following question: What is the $2-2D$ counterpart of the K function which can be applied to the two 4D points $\boldsymbol{s}_{k-1}^{'p}$ and $\boldsymbol{s}_{k}^{'p}$?

Let us consider an equivalent expression of K introducing the *norm* function, which we denote as K_{2-1D}:

$$K_{2-1D} = 2(norm(\boldsymbol{s}_{k-1}^{'r}) - norm(\boldsymbol{s}_{k-1}^{'b}))(norm(\boldsymbol{s}_{k}^{'b}) - norm(\boldsymbol{s}_{k}^{'r})) \tag{6.31}$$

The desired function $K_{2-2D} : \mathbb{R}^8 \rightarrow \mathbb{R}$ can be found by considering the counterpart of K_{2-1D} for the $2-2D$ case:

$$K_{2-2D} = 2(norm(\boldsymbol{s}_{k-1}^{'r}) - norm(\boldsymbol{s}_{k-1}^{'b}))(norm(\boldsymbol{s}_{k}^{'b}) - norm(\boldsymbol{s}_{k}^{'r})) \tag{6.32}$$

where now $\boldsymbol{s}_{k}^{'p} = [x_k^{p,b} \; y_k^{p,b} \; x_k^{p,r} \; y_k^{p,r}]^T$, $\boldsymbol{s}_{k}^{'p,r} = [x_k^{p,r} \; y_k^{p,r}]^T$ and $\boldsymbol{s}_{k}^{'p,b} = [x_k^{p,b} \; y_k^{p,b}]^T$. K_{2-2D} is indeed the odd function (in the "order" of $\boldsymbol{s}_{k}^{'}$) which complies with the conditions in Equations (6.28) and (6.30). Therefore, the extension of the definition of "cross" for the $2-2D$ objects case is:

$$K_{2-2D} > 0 \tag{6.33}$$

Simulations results

The results provided by the CMT for the $2-2D$ objects case using Inequation (6.33) as the "cross detector" are shown in Figure 6.10:

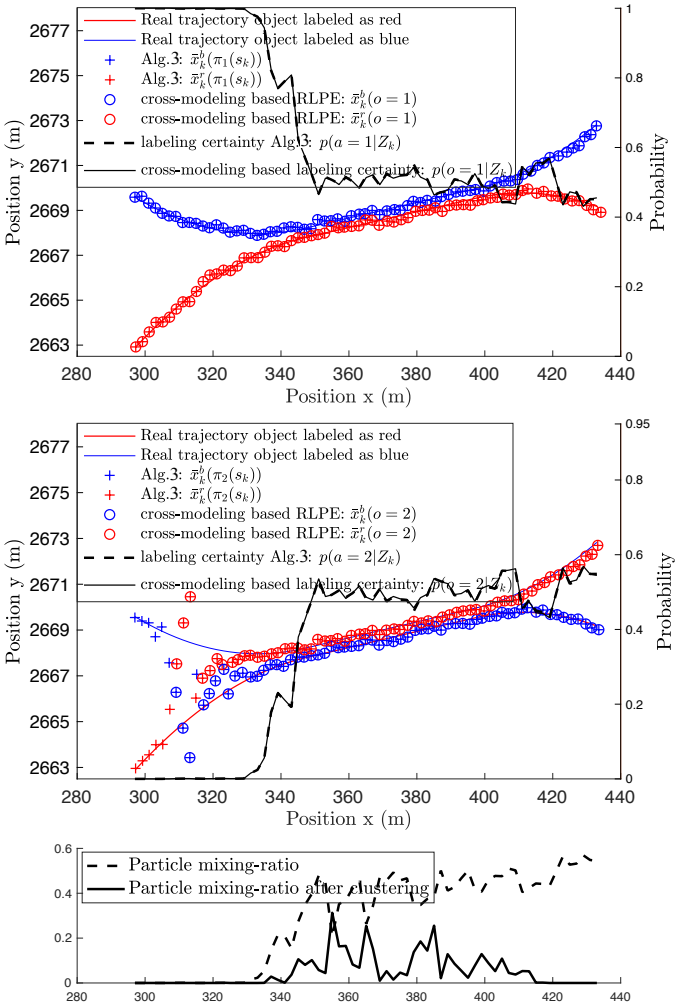

Figure 6.10: Evaluation of estimation performance of the CMT when Inequation (6.33) is used as the "cross detector". LPEs and labeling uncertainties are extracted from the clusters "order" 1 and 2, illustrated on top and middle figures. Alg. 3 is the performance evaluator algorithm. The figure at the bottom confirms that the "order detector" in Inequation (6.33) is appropriate. In fact, the associated clustering method removes particle mixing within clusters after objects separation.

Discussion of the results

The results reveal remarkably accurate estimation performance of the CMT both in the computation of LPEs and labeling probabilities. This validates the CMT as a convenient

solution to answer the questions in section 2.3 for 2D objects. In fact, LPEs result in low OSPA errors. This becomes possible even when extracting cost efficient MMSE (see Equation (6.15)) point estimates thanks to the clustering method, which separates particles in different state of "order". These results support our argument that the design of the proper "cross detector" should produce a decomposition of $p(\boldsymbol{s}_k|\mathbf{Z}_k)$ where each component is unimodal. Also, very accurate estimation of labeling uncertainty is provided, which can be calculated by simply considering the proportion of particles within each order-dependent cluster (see Equation (6.16)).

6.5.2 Generalization of the *cross* detector to $2-3D$ objects settings

The function $K_{2-3D} : \mathbb{R}^{12} \rightarrow \mathbb{R}$ is the counterpart of K_{2-1D} for the $2-3D$ objects case:

$$K_{2-3D} = 2(norm(\boldsymbol{s}_{k-1}^{'r}) - norm(\boldsymbol{s}_{k-1}^{'b}))(norm(\boldsymbol{s}_{k}^{'b}) - norm(\boldsymbol{s}_{k}^{'r})) \tag{6.34}$$

where now $\boldsymbol{s}_k^{'p} = [x_k^{p,b}\ y_k^{p,b}\ z_k^{p,b}\ x_k^{p,r}\ y_k^{p,r}\ z_k^{p,b}]^T$. As $\boldsymbol{s}_k^{'p}$ and $\Pi(\boldsymbol{s}_k^{'p})$ are in different states of "order", K_{2-3D} is also an odd function (in the "order" of $\boldsymbol{s}_k^{'p}$) which complies with the conditions in Equations (6.28) and (6.30). The evaluations of the current state and its permuted version are equal in absolute value but different in sign. Therefore, the counterpart definition for the "cross detector" from K_{2-1D} and K_{2-2D} cases can be used in the K_{2-3D} case:

$$K_{2-3D} > 0 \tag{6.35}$$

Simulations results

The results provided by the CMT for the $2-3D$ objects case using Inequation (6.35) as the "cross detector" are shown in Figures 6.11 and 6.12:

Discussion of the results

The results reveal remarkably accurate estimation performance of the CMT both in the computation of LPEs and labeling probabilities. This validates the CMT as a convenient solution to answer the questions in section 2.3 also for 3D objects.

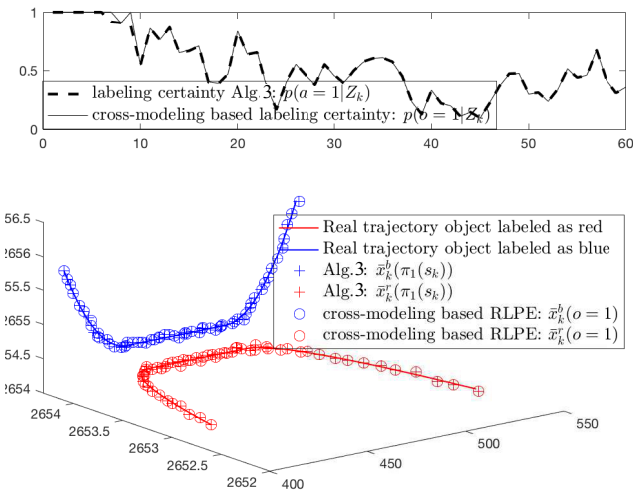

Figure 6.11: Evaluation of estimation performance of the CM method when Inequation (6.35) is used as the "order switch" detector. Labeled point estimates are extracted from the cluster "order" 1. Alg. 3 is the performance evaluator algorithm.

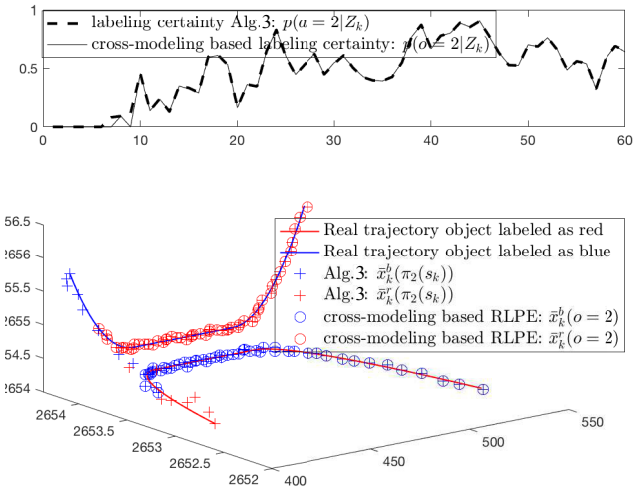

Figure 6.12: Evaluation of estimation performance of the CM method when Inequation (6.35) is used as the "cross detector". Labeled point estimates are extracted from the cluster "order" 2. Alg. 3 is the performance evaluator algorithm.

6.6 Conclusions

The problem of track formation needs to be tackled by any MOT solution. To take informed track formation decisions, estimation of track point-estimates and characterization of labeling uncertainty is required. Extracting these estimates and characterization is not trivial in the context of Track-before-Detect (TrBD), especially when tackling closely-spaced target scenarios, as the formulation of DA hypotheses is ruled out.

This chapter provides a TrBD MOT algorithm with labeling characterization capabilities offering wider applicability than the non-LG implementation of the UD presented in previous chapter. The Cross Modeling Tracker (CMT) has been presented in this chapter as a DA-free solution applicable in arbitrarily high dimensional problems.

Both this and previous chapters solve the underlying problem of decomposing the multitarget Bayes posterior density in a low dimensional case with two scalar targets. Unlike the UD-based implementation, where the decomposition is based on the permutation invariance characteristics of the density, the CMT introduces a novel label-dependent decomposition by hypothesizing physical crosses between the targets. The main contribution of the paper is the non-trivial generalization of the cross-between-objects concept from the two scalar targets case, where the concept of cross-between-objects has physical interpretation, to arbitrary number of vector targets case.

The CMT results provided in this chapter are evaluated against the performance evaluation method presented in chapter 4. Simulation results involving challenging closely-spaced objects scenarios have been provided. The results illustrate that the CMT is usable in the general $t - MD$ objects case, provided the number of targets t is known and constant in line with the first assumption in the introductory chapter. Therefore, the proposed solution extends the state-of-the-art of TrBD MOT by providing DA-free characterization of labeling uncertainty, with validated estimation performance and efficient scalability, which can be seamlessly used in generic $t - MD$ targets scenarios in TrBD MOT context.

7

Performance comparison of solutions in chapters 5 and 6 and optimization of the CMT for unresolved targets

7.1 Introduction

Track formation is an essential task in any MOT solution. In order to take informed track-formation decisions, the labeling problem needs to be solved. An optimal solution to the labeling problem is especially important when tracking closely-spaced objects. A solution to the labeling problem involves estimation of labeled tracks and labeling certainties. Therefore, a method for labeling uncertainty characterization is required.

Characterizing labeling uncertainty involves decomposing the multi-object Bayes posterior density. This decomposition has been traditionally done by solving the DA problem (MHT decomposition is an example). In Track-before-detect (TrBD) systems, association-dependent decompositions cannot be formulated due to the absence of detections. Still, labeling uncertainty needs to be characterized. Therefore, an association-free method to perform a label-dependent decomposition of the Bayes posterior is required.

The distinguishing characteristic of the algorithms presented in chapters 5 and 6 is their DA-free approach to the MOT problem, including the subproblem of estimating labeling uncertainty. Due to their DA-free nature, both algorithms are suited to solve the TrBD MOT problem.

This chapter starts by comparing the estimation performance of the algorithms presented in chapters 5 and 6 against the evaluation method presented in chapter 4. The algorithm proposed in chapter 5 is an application of the UD theory for non Linear and/or

The contents provided in this chapter are to be submitted for review in JAIF as "Optimization of the Cross Modeling Tracker for unresolved targets," C. M. Leon, H. Driessen and A. Yarovoy in *Journal of Advances in Information Fusion*, 2023

non-Gaussian (non-LG) systems, recently submitted for review in TAESS [62]. The algorithm proposed in chapter 6 is the Cross Modeling Tracker (CMT), already published in JAIF [27].

After showcasing the pros and cons of each algorithm, the focus of this chapter is on optimizing the CMT algorithm presented in [27]. Aside of pure estimation performance aspects, the CMT has wider applicability than the non-LG implementation of the UD presented in [62]. In fact, until now the UD theory has not been extended for more than two targets.

The CMT provides accurate estimates of labeled tracks and corresponding labeling certainties for the closely-spaced trajectories simulated in previous chapter. However, this chapter provides initial results motivating that the CMT in [27] is not an exact solution, meaning that the CMT statistics do not converge to the evaluation references as the number of particles tend to infinity. This is specially noticeable when considering unresolved targets. Two target are unresolved when they are located in the same resolution cell of range, angle and velocity [63] [64]. Depending on their SNR, targets can also be unresolved when they are in neighboring resolution cells. Besides discussing estimation performance comparison between the two DA-free solutions presented in this thesis, the purpose of this chapter is twofold. Firstly, we aim at theoretically identifying the approximations taken implicitly by the CMT algorithm presented in [27]. Secondly, we aim at reducing the impact of such approximations on estimation performance for scenarios involving unresolved targets, without degradation on estimation performance for all other scenarios.

In order to identify the approximations taken by the CMT, we bridge the gap between an exact solution (only accessible in Detect-before-Track (DBT) context) and the expressions provided by the CMT operating in DBT context. In order to mitigate the impact of the approximations, we propose the use of a new proposal density at PF implementation level.

The chapter is organized as follows. Section II provides evaluation results comparing the estimation performance of the CMT and the non-LG implementation of the UD. Section III derives the approximations implicit in the CMT and illustrates their impact on estimation performance with numerical simulations. Section IV introduces the optimization of the CMT algorithm for tracking unresolved targets. Section V provides results of the optimized CMT algorithm illustrating better estimation performance than the original CMT solution. Section VI concludes the chapter.

7.2 Estimation performance comparison between the non-LG UD and CMT algorithms

The main contribution in [27] was giving analytical generalization for the concept of cross-between-objects, so that the CMT algorithm can be extended to arbitrarily high-dimensional problems. This extension refers for both the number of targets and the transition from considering scalar targets to vector targets. The wider applicability of the CMT is a practical advantage compared to UD-based solution, which cannot deal with more than two-target densities. Nevertheless, this section starts by comparing the estimation performance of the non-LG UD and the CMT algorithms in a low dimensional problem, where both approaches can be applied.

The optimal references for evaluation are calculated analytically according to the

evaluation criterion presented in the chapter 4. These references (illustrated in Figs. 7.1, 7.2 and 7.3) are provided in the form of statistics of interest. Namely labeled track references and associated labeling certainty references. Note that such references can only be calculated in DBT context as explained in chapter 4. For the purpose of evaluating the non-LG UD and the CMT algorithms, both decomposition algorithms should be run in DBT context. More specifically, the algorithms under evaluation should be fed with the same plot set used in the generation of the optimal references.

Preliminary numerical results in Fig. 7.1 show estimation performance comparison between the non-LG implementation of the UD provided in [62] and the CMT presented in [27]. In particular, Fig. 7.1 illustrates labeling uncertainty characterization ability. Although both algorithms under evaluation produce tracks, these will be evaluated in following figures for sake of clarity in the visualization of results.

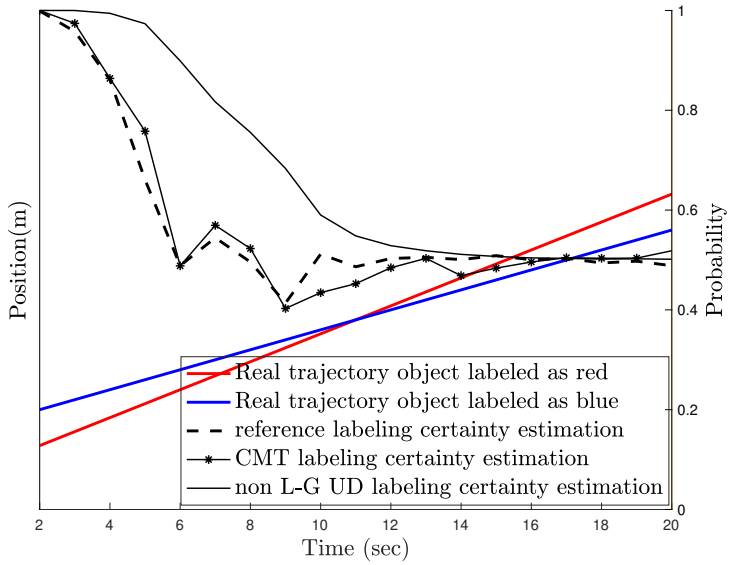

Figure 7.1: Visual inspection of labeling uncertainty estimation performance by the non-LG UD and the CMT trackers. The labeling certainty reference is generated by the Alg. 3 from chapter 4. The CMT labeling certainty estimates are generated using Alg. 4 in chapter 6 and the non-LG UD labeling certainty estimates are generated by the so-called fully decomposed algorithm summarized in the right column of Table 5.1. in chapter 5.

The non-LG implementation of the UD provides accurate estimation of the probability of successful labeling after target separation. However, it seems to underestimate the existent labeling uncertainty captured by the optimal labeling certainty reference before that point. As opposed to this, the CMT captures very accurately the drop of labeling certainty calculated by the reference.

To provide a complete picture, estimation performance by the CMT and the non-LG implementation of the UD should be assessed also in terms of track estimates. To this end, Figs. 7.2 and 7.3 provide additional visualizations of estimation error. Firstly, Fig. 7.2 shows the reference trajectories and reference labeling certainties used for evaluation as a function of different degrees of plots accuracy. Based on these references, Fig. 7.3

provides a thorough comparison of estimation results for both algorithms under evaluation. Overall, both algorithms produce degraded estimation performance when targets are very closely-spaced as compared to when they are not. As expected, this degradation applies to both labeling certainty estimates and corresponding track estimates.

Despite the illustrated performance degradation, the comparative results show that estimation performance of the CMT is better than the one of the non L-G implementation of the UD. In particular, the difference in track estimation performance is one order of magnitude (both in bias and dispersion) for the case with accurate plots. Better performance of the CMT is consistent (but less accentuated) along tested simulations with poorer plot accuracy.

The estimation of the probability of successful labeling by the CMT is also better than the one by the non-LG UD implementation (see first row of Fig. 7.3). Once more, the CMT seems to estimate very accurately the drop of the reference labeling certainty. Although the non-LG implementation of the UD calculates the invariance characteristics of the Bayes posterior in a theoretically sound manner, such solution does not outperform the CMT when targets are too closely-spaced.

The use of the non-LG implementation of the UD is convenient for cases where one is interested in target labeling information after target separation. Although the CMT implementation outperforms the non-LG implementation overall, the former solution is not exact. To be more specific, the CMT is very accurate unless the targets are extremely close to each other, or unresolved.

The remainder of this chapter considers the optimization of the CMT. Firstly, the approximations implicit in the CMT algorithm need to be analyzed. Then, the impact of such approximations on estimation performance will be studied. Finally, modifications to the original CMT tracking algorithm will be provided in order to mitigate the degradation of the CMT approximations on estimation performance.

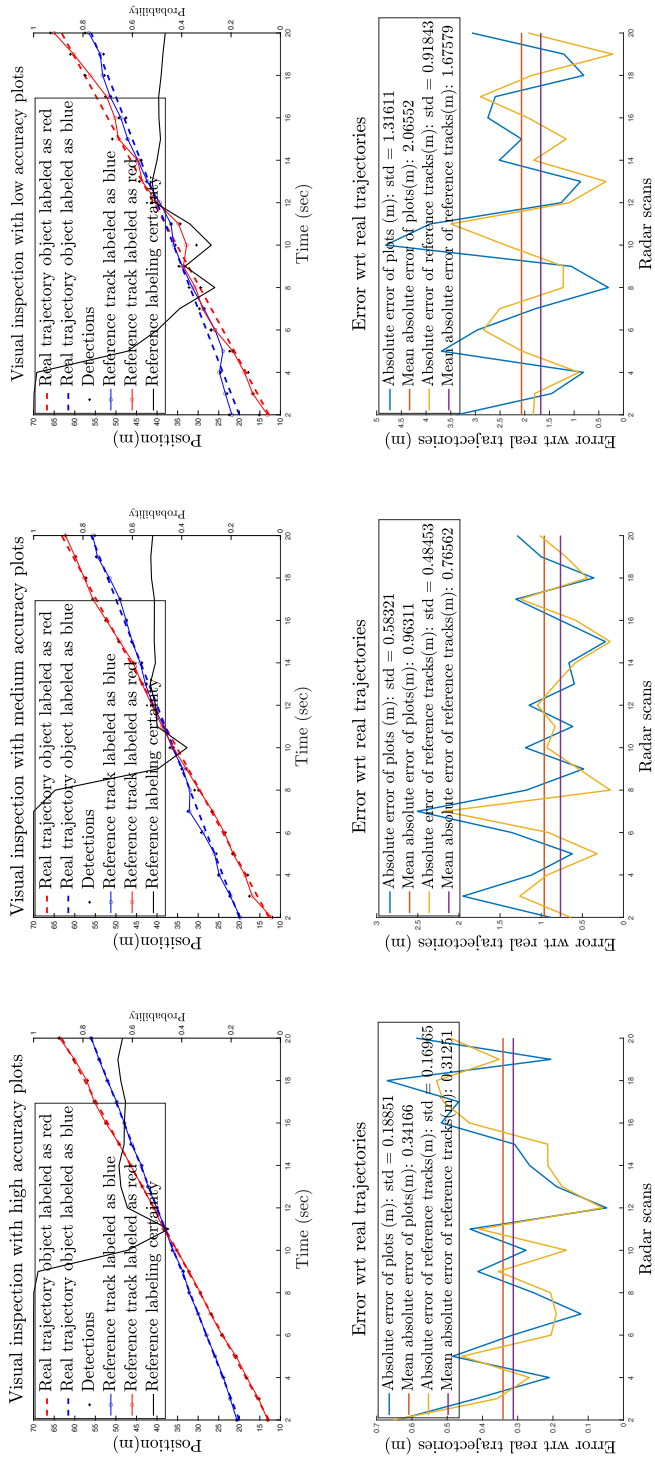

Figure 7.2: Effect of plot quality on the tracks references and labeling-certainty references. The references are generated using Alg. 3 from chapter 4.

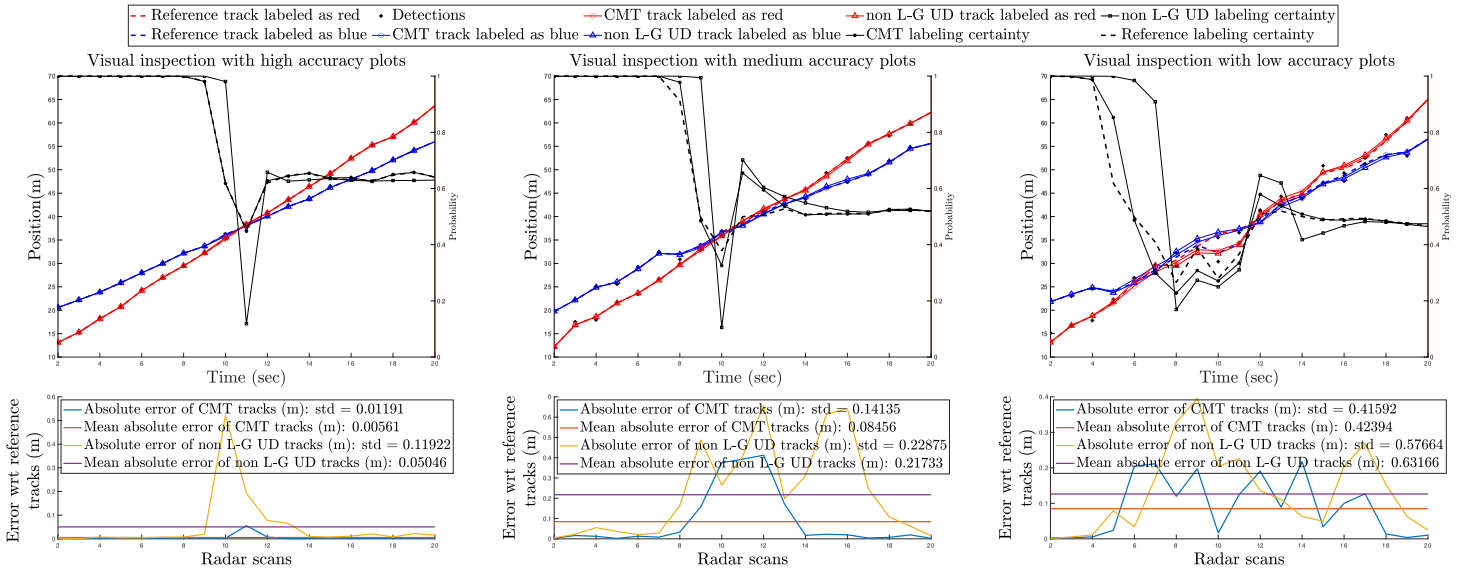

Figure 7.3: Evaluation of CMT and non-LG UD estimation results based on similarity with the analytical references from Fig. 7.2. The reference tracks are generated using Alg. 3 from chapter 4. The CMT labeled tracks are generated using Alg. 4 in chapter 6 and the non-LG UD labeled tracks are generated by the so-called fully decomposed algorithm summarized in the right column of Table 5.1. in chapter 5.

7.3 Approximations in the CMT and their impact on estimation performance

The approximations inherent in the CMT algorithm have not been identified in [27]. In this chapter, it is argued that the unknown approximations taken by the CMT must be implicit in the definition of cross-between-objects from the low dimensional solution presented in [24, Section IV], as the generalization in [27] is fully analytical.

In order to identify the approximations taken by the CMT, this chapter bridges the gap between the exact expressions of the desired decomposition and the ones provided by the CMT. An exact expression for the decomposition is only accessible in DBT context. In order to provide a fair comparison of the CMT decomposition with respect to the exact decomposition, the CMT decomposition needs to be exercised taking as input the posterior density produced in DBT context. Additionally, for the purpose of isolating the problem of identifying the approximations, we consider a simple two targets case, assuming perfect detectability and no false alarm.

7.3.1 The exact density decomposition

The exact decomposition in Equation (7.1) is only accessible in DBT context as it is generated considering the two possible plot-label DA hypotheses.

$$p(s_k|Z_k) = \frac{p(s_k|Z_{k-1})l_{DBT}(z_k|s_k)}{L(z_k)}P(z_k) + \frac{p(s_k|Z_{k-1})l_{DBT}(\pi(z_k)|s_k)}{L(\pi(z_k))}P(\pi(z_k)) \tag{7.1}$$

where $\pi(z_k)$ permutes the order in the measurement vector z_k,

$$P(z_k) = \frac{L(z_k)}{L(z_k) + L(\pi(z_k))} \tag{7.2}$$

and

$$P(\pi(z_k)) = \frac{L(\pi(z_k))}{L(z_k) + L(\pi(z_k))} \tag{7.3}$$

where

$$L(z_k) = \int_{s_k} p(s_k|Z_{k-1})l_{DBT}(z_k|s_k)ds_k \tag{7.4}$$

and

$$L(\pi(z_k)) = \int_{s_k} p(s_k|Z_{k-1})l_{DBT}(\pi(z_k)|s_k)ds_k \tag{7.5}$$

7.3.2 The approximate density decomposition by the CMT

The decomposition in Equation (7.6) is the CMT approximation of the decomposition in Equation (7.1). Note that Equation (7.6) incorporates the observation model in DBT context. This is because although the CMT can be used in TrBD context, the identification of approximations needs to be done in DBT context (for sake of fair comparison with the exact expressions which are only accessible in DBT context). It is convenient for this purpose that the CMT allows to calculate decompositions independently from the context, i.e. the CMT decomposes the Bayes posterior density disregarding whether this density has been obtained in DBT or TrBD contexts.

$$p(s_k|Z_k) = \frac{p(s_k|Z_{k-1})(l_{DBT}(z_k|s_k) + l_{DBT}(\pi(z_k)|s_k))}{\int_{s_k} p(s_k|Z_{k-1})(l_{DBT}(z_k|s_k) + l_{DBT}(\pi(z_k)|s_k))ds_k} \mathbb{1}_{s_k|x_k^b \geq x_k^r} + \frac{p(s_k|Z_{k-1})(l_{DBT}(z_k|s_k) + l_{DBT}(\pi(z_k)|s_k))}{\int_{s_k} p(s_k|Z_{k-1})(l_{DBT}(z_k|s_k) + l_{DBT}(\pi(z_k)|s_k))ds_k} \mathbb{1}_{s_k|x_k^b < x_k^r} \tag{7.6}$$

7.3.3 Approximations by the CMT decomposition at density level

The approximation of the CMT decomposition in Equation (7.6) given the exact decomposition in Equation (7.1) can be split as:

$$\frac{p(s_k|Z_{k-1})(l(z_k|s_k) + l(\pi(z_k)|s_k))}{\int_{s_k} p(s_k|Z_{k-1})(l(z_k|s_k) + l(\pi(z_k)|s_k))ds_k} \mathbb{1}_{s_k|x_k^b \geq x_k^r} \approx \frac{p(s_k|Z_{k-1})l(z_k|s_k)}{\int_{s_k} p(s_k|Z_{k-1})l(z_k|s_k)ds_k} P(z_k) \tag{7.7}$$

$$\frac{p(s_k|Z_{k-1})(l(z_k|s_k) + l(\pi(z_k)|s_k))}{\int_{s_k} p(s_k|Z_{k-1})(l(z_k|s_k) + l(\pi(z_k)|s_k))ds_k} \mathbb{1}_{s_k|x_1^b < x_k^r} \approx \frac{p(s_k|Z_{k-1})l(\pi(z_k)|s_k)}{\int_{s_k} p(s_k|Z_{k-1})l(\pi(z_k)|s_k)ds_k} P(\pi(z_k)) \tag{7.8}$$

where the subindex *DBT* has been dropped from l_{DBT} for simplicity as it cannot be confused with l_{TrBD} because the identification of approximations is formulated in DBT context.

7.3.4 Identification of CMT approximations relevant for track formation

Estimation performance is quantified at the output of the tracker. The tracker does not output densities but tracks. Therefore, the approximations formulated in Equations (7.7) and (7.8) at density level do not provide a clear idea of the impact of the CMT approximations on the estimation performance. This section aims at studying how the density level approximations propagate to the output of the tracker. In particular, how they affect track-formation.

A common way to perform track-formation involves the calculation of two statistics of interest: labeled tracks and corresponding labeling certainty estimates. Along the rest of this section we study how the density level approximations (introduced by Equations (7.7) and (7.8)) propagate to the statistics-of-interest level.

Exact solution for the statistics of interest

According to the exact decomposition from Equation (7.1), it is possible to calculate MMSE-based labeled point estimates and labeling probabilities. The exact solution for the (MMSE) labeled point estimates is:

$$E_{s_k|z_k} = \int_{s_k} s_k \frac{p(s_k|Z_{k-1})l(z_k|s_k)}{L(z_k)} ds_k \tag{7.9}$$

$$E_{s_k|\pi(z_k)} = \int_{s_k} s_k \frac{p(s_k|Z_{k-1})l(\pi(z_k)|s_k)}{L(\pi(z_k))} \tag{7.10}$$

The exact solution for the labeling probabilities is:

$$lp_{s_k|z_k} = P(z_k) \tag{7.11}$$

$$lp_{s_k|\pi(z_k)} = P(\pi(z_k)) \tag{7.12}$$

Approximate CMT solution for the statistics of interest

According to the CMT decomposition in Equation (7.6), it is possible to calculate MMSE-based labeled point estimates and labeling probabilities approximations. In particular, the CMT approximations for the exact solutions $E_{s_k|z_k}$ and $E_{s_k|\pi(z_k)}$ are:

$$\hat{E}_{s_k|z_k} \approx \frac{1}{\hat{lp}_{s_k|z_k}} \int_{s_k|x_k^b \geq x_k^r} s_k \frac{p(s_k|Z_{k-1})(l(z_k|s_k) + l(\pi(z_k)|s_k))}{\int_{s_k} p(s_k|Z_{k-1})(l(z_k|s_k) + l(\pi(z_k)|s_k))ds_k} ds_k \tag{7.13}$$

$$\hat{E}_{s_k|\pi(z_k)} \approx \frac{1}{\hat{lp}_{s_k|\pi(z_k)}} \int_{s_k|x_k^b < x_k^r} s_k \frac{p(s_k|Z_{k-1})(l(z_k|s_k) + l(\pi(z_k)|s_k))}{\int_{s_k} p(s_k|Z_{k-1})(l(z_k|s_k) + l(\pi(z_k)|s_k))ds_k} ds_k \tag{7.14}$$

Equivalently, the CMT approximations for the exact labeling probabilities $lp_{s_k|z_k}$ and $lp_{s_k|\pi(z_k)}$ are:

$$\hat{lp}_{s_k|z_k} \approx \int_{s_k|x_k^b \geq x_k^r} \frac{p(s_k|Z_{k-1})(l(z_k|s_k) + l(\pi(z_k)|s_k))}{\int_{s_k} p(s_k|Z_{k-1})(l(z_k|s_k) + l(\pi(z_k)|s_k))ds_k} ds_k \tag{7.15}$$

$$\hat{lp}_{s_k|\pi(z_k)} \approx \int_{s_k|x_k^b < x_k^r} \frac{p(s_k|Z_{k-1})(l(z_k|s_k) + l(\pi(z_k)|s_k))}{\int_{s_k} p(s_k|Z_{k-1})(l(z_k|s_k) + l(\pi(z_k)|s_k))ds_k} ds_k \tag{7.16}$$

7.3.5 Study of CMT approximations at statistics-of-interest level

For the sake of simplicity, we first study the approximation for the labeling probabilities. Then, we do the same for the (MMSE) labeled point estimates.

Analytical comparison of exact labeling probabilities and CMT labeling probabilities

The goal is to bridge the gap between the exact expression in Equation (7.11) and its CMT approximation in Equation (7.15). Please note that:

$$L(z_k) + L(\pi(z_k)) = \int_{s_k} p(s_k|Z_{k-1})(l(z_k|s_k) + l(\pi(z_k)|s_k))ds_k \tag{7.17}$$

Therefore, we only need to compare the labeling likelihoods (numerators in Equation (7.2) and (7.15)). Namely $L(z_k)$ and $\int_{s_k|x_k^b \geq x_k^r} p(s_k|Z_{k-1})(l(z_k|s_k) + l(\pi(z_k)|s_k))$

The exact expression for one of the two labeling likelihoods is:

$$L(z_k) = \int_{s_k} p(s_k|Z_{k-1}) l(z_k|s_k) ds_k \tag{7.18}$$

This can be manipulated to match the region of integration used by the CMT approximation of the labeling likelihood:

$$\begin{aligned} L(z_k) &= \int_{s_k} p(s_k|Z_{k-1}) l(z_k|s_k) ds_k \\ &= \int_{s_k} p(s_k|Z_{k-1}) l(z_k|s_k) \mathbb{1}_{s_k|x_k^b \geq x_k^r} + p(s_k|Z_{k-1}) l(z_k|s_k) \mathbb{1}_{s_k|x_k^b < x_k^r} ds_k \\ &= \int_{s_k} p(s_k|Z_{k-1}) l(z_k|s_k) \mathbb{1}_{s_k|x_k^b \geq x_k^r} + \pi\{p(s_k|Z_{k-1}) l(z_k|s_k)\} \mathbb{1}_{s_k|x_k^b \geq x_k^r} ds_k \\ &= \int_{s_k|x_k^b \geq x_k^r} p(s_k|Z_{k-1}) l(z_k|s_k) + \pi\{p(s_k|Z_{k-1}) l(z_k|s_k)\} ds_k \end{aligned} \tag{7.19}$$

Where π transforms any density into its symmetric (with respect to the diagonal $x_k^b = x_k^r$) version. The last expression shows that there exists an exact formulation for $L(z_k)$ when forcing the integration region to be $s_k | x_k^b \geq x_k^r$. Based on this exact formulation, one can analyze the CMT approximation for $L(z_k)$:

$$\begin{aligned} &\int_{s_k|x_k^b \geq x_k^r} p(s_k|Z_{k-1}) l(z_k|s_k) + \pi\{p(s_k|Z_{k-1}) l(z_k|s_k)\} ds_k \\ &\quad \approx \int_{s_k|x_k^b \geq x_k^r} p(s_k|Z_{k-1}) (l(z_k|s_k) + l(\pi(z_k)|s_k)) \end{aligned} \tag{7.20}$$

Equation (7.20) should be interpreted as the first line being an exact expression and the second line being its CMT approximation. After removing identical contributions on both sides of the approximation sign:

$$\int_{s_k|x_k^b \geq x_k^r} \pi\{p(s_k|Z_{k-1}) l(z_k|s_k)\} ds_k \approx \int_{s_k|x_k^b \geq x_k^r} p(s_k|Z_{k-1}) l(\pi(z_k)|s_k) \tag{7.21}$$

An equivalent derivation for $l p_{s_k|\pi(z_k)}$ and $l \hat{p}_{s_k|\pi(z_k)}$ leads to:

$$\begin{aligned} &\int_{s_k|x_k^b < x_k^r} \pi\{p(s_k|Z_{k-1}) l(\pi(z_k)|s_k)\} + p(s_k|Z_{k-1}) l(\pi(z_k)|s_k) ds_k \\ &\quad \approx \int_{s_k|x_k^b < x_k^r} p(s_k|Z_{k-1}) (l(z_k|s_k) + l(\pi(z_k)|s_k)) \end{aligned} \tag{7.22}$$

Same way as before, the first line is an exact expression (of $L(\pi(z_k)$ in this case) and the second line is the CMT solution. Since both expressions are not identical, we write an approximation sign in between. After removing identical contributions on both sides of the approximation sign:

$$\int_{s_k|x_k^b < x_k^r} \pi\{p(s_k|Z_{k-1}) l(\pi(z_k)|s_k)\} ds_k \approx \int_{s_k|x_k^b < x_k^r} p(s_k|Z_{k-1}) l(z_k|s_k) \tag{7.23}$$

How good approximations in Equations (7.21) and (7.23) are will be the focus of discussions in upcoming sections. For the moment, note that the CMT approximates $\int_{s_k|x_k^b \geq x_k^r} \pi\{p(s_k|Z_{k-1}) l(z_k|s_k)\} ds_k$ by calculating $\int_{s_k|x_k^b \geq x_k^r} p(s_k|Z_{k-1}) l(\pi(z_k)|s_k)$ in the process of estimating $L(z_k)$ and similarly for $L(\pi\{z_k\})$ based on Equation (7.23).

Analytical comparison of exact labeled point estimates and CMT labeled point estimates

The exact expression for one of the two labeled point estimates is:

$$E_{s_k|z_k} = \int_{s_k} s_k \frac{p(s_k|Z_{k-1})l(z_k|s_k)}{L(z_k)} ds_k \tag{7.24}$$

This expression can be manipulated to match the region of integration used by the CMT approximation of the labeled point estimate:

$$\begin{aligned} E_{s_k|z_k} &= \int_{s_k} s_k \frac{p(s_k|Z_{k-1})l(z_k|s_k)}{L(z_k)} ds_k \\ &= \frac{1}{L(z_k)} \int_{s_k} s_k p(s_k|Z_{k-1})l(z_k|s_k)\mathbb{1}_{s_k|x_k^b \geq x_k^r} + s_k p(s_k|Z_{k-1})l(z_k|s_k)\mathbb{1}_{s_k|x_k^b < x_k^r} ds_k \\ &= \frac{1}{L(z_k)} \int_{s_k} s_k p(s_k|Z_{k-1})l(z_k|s_k)\mathbb{1}_{s_k|x_k^b \geq x_k^r} + \pi\{s_k\}\pi\{p(s_k|Z_{k-1})l(z_k|s_k)\}\mathbb{1}_{s_k|x_k^b \geq x_k^r} ds_k \\ &= \frac{1}{L(z_k)} \int_{s_k|x_k^b \geq x_k^r} s_k p(s_k|Z_{k-1})l(z_k|s_k) + \pi\{s_k\}\pi\{p(s_k|Z_{k-1})l(z_k|s_k)\} ds_k \end{aligned} \tag{7.25}$$

The last expression shows that there exists an exact formulation for $E_{s_k|z_k}$ when forcing the integration region to be $x_k^b \geq x_k^r$. Based on this, $E_{s_k|z_k}$ is approximated by $\hat{E}_{s_k|z_k}$ as:

$$\begin{aligned} &\frac{1}{L(z_k)} \int_{s_k|x_k^b \geq x_k^r} s_k p(s_k|Z_{k-1})l(z_k|s_k) + \pi\{s_k\}\pi\{p(s_k|Z_{k-1})l(z_k|s_k)\} ds_k \\ &\approx \frac{1}{\hat{lp}_{s_k|z_k}} \int_{s_k|x_k^b \geq x_k^r} s_k \frac{p(s_k|Z_{k-1})(l(z_k|s_k) + l(\pi(z_k)|s_k))}{\int_{s_k} p(s_k|Z_{k-1})(l(z_k|s_k) + l(\pi(z_k)|s_k)) ds_k} ds_k \end{aligned} \tag{7.26}$$

Which can be simplified as:

$$\begin{aligned} &\int_{s_k|x_k^b \geq x_k^r} s_k p(s_k|Z_{k-1})l(z_k|s_k) + \pi\{s_k\}\pi\{p(s_k|Z_{k-1})l(z_k|s_k)\} ds_k \\ &\approx \int_{s_k|x_k^b \geq x_k^r} s_k p(s_k|Z_{k-1})(l(z_k|s_k) + l(\pi(z_k)|s_k)) \end{aligned} \tag{7.27}$$

and further simplified as:

$$\begin{aligned} &\int_{s_k|x_k^b \geq x_k^r} \pi\{s_k\}\pi\{p(s_k|Z_{k-1})l(z_k|s_k)\} ds_k \\ &\approx \int_{s_k|x_k^b \geq x_k^r} s_k p(s_k|Z_{k-1})l(\pi(z_k)|s_k) \end{aligned} \tag{7.28}$$

Same way as before, the first line is an exact expression, and the second line is its CMT approximation. Since both expressions are not identical, we write and approximation sign in between. An equivalent derivation for $E_{s_k|\pi(z_k)}$ and $\hat{E}_{s_k|\pi(z_k)}$ leads to:

$$\begin{aligned} &\int_{s_k|x_k^b < x_k^r} \pi\{s_k\}\pi\{p(s_k|Z_{k-1})l(\pi(z_k)|s_k)\} + s_k p(s_k|Z_{k-1})l(\pi(z_k)|s_k) ds_k \\ &\approx \int_{s_k|x_k^b < x_k^r} s_k p(s_k|Z_{k-1})(l(z_k|s_k) + l(\pi(z_k)|s_k)) \end{aligned} \tag{7.29}$$

which can be simplified as:

$$\int_{s_k|x_k^b<x_k^r} \pi\{s_k\}\pi\{p(s_k|Z_{k-1})l(\pi(z_k)|s_k)\}ds_k \approx \int_{s_k|x_k^b<x_k^r} s_k p(s_k|Z_{k-1})l(z_k|s_k) \tag{7.30}$$

7.3.6 Numerical impact of the CMT approximations

Not many expressions need be remembered to follow the rest of this chapter: only the four discovered approximations in Equations (7.21), (7.23), (7.28) and (7.30). These formulate explicitly the (so far unknown) approximations required to bridge the gap between the exact DBT solution and the CMT solution at statistics-of-interest level. This subsection uses numerical examples to showcase the estimation errors introduced by these approximations.

We start by revisiting the results in [27] to observe that the estimation errors are indeed negligible in the case of the problem illustrated in Fig. 7.4. For these particular set of

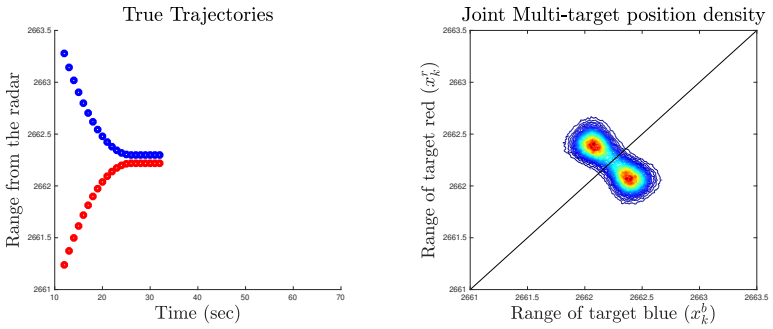

Figure 7.4: Illustration of a closely-spaced objects scenario where the objects are close enough to introduce labeling uncertainty, but can still be resolved.

trajectories, the visualization of the CMT estimation performance is provided in Fig. 7.5 (where the exact solution is implemented by Alg. 3 in chapter 4).

As illustrated in the first 10 seconds of the simulation in Fig. 7.5, the CMT approximations do not affect estimation performance in easy scenarios when objects are far apart from each other. The approximations do not seem to produce underperformance when labeling certainty is compromised as illustrated in Fig. 7.5 either. This type of labeling uncertainty is, in practice, generated by scenarios where the objects are closely-spaced with respect to maneuverability/update-rate of the system, but they can still be resolved in the measurements.

Following simulation results show that the error introduced by the CMT approximations is especially noticeable when the objects are so close to each other that the Bayes posterior becomes unimodal. This happens in practice when the objects get closely-spaced with respect to sensor resolution (the objects cannot be resolved in the measurements). The visualization of estimation underperformance of the CMT for the scenario in Fig. 7.6 is presented in Fig. 7.7

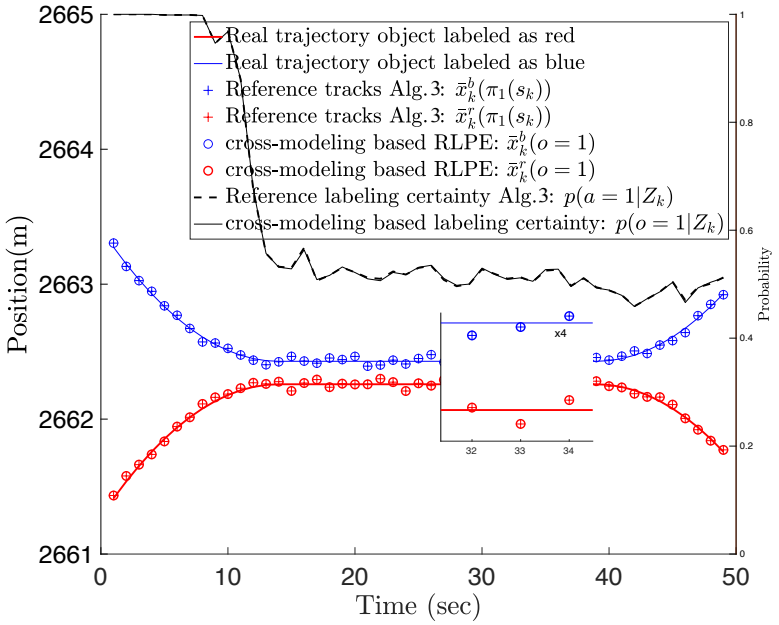

Figure 7.5: Illustration of a closely-spaced targets situation. Cross Modeling Tracker point estimates perfectly match the references for evaluation (+ points generated using Alg. 3). Also, the CMT labeling certainty associated to this particular assignment of labels seems to be very accurate. Note that this is done by the CMT without using any data-association method.

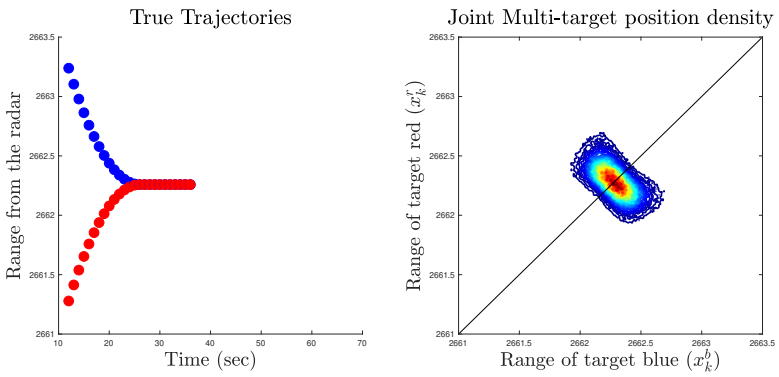

Figure 7.6: Illustration of a extremely closely-spaced objects scenario (closer than sensor resolution) where the joint multiobject posterior density becomes unimodal.

It is in scenarios such as the one in Fig. 7.7 where the approximations introduced by the CMT result in noticeable estimation error. Especially, along the simulation time steps where the objects are closer than the sensor resolution. These results are consistent with the ones observed in Fig. 7.3 with other type closely-spaced target trajectories.

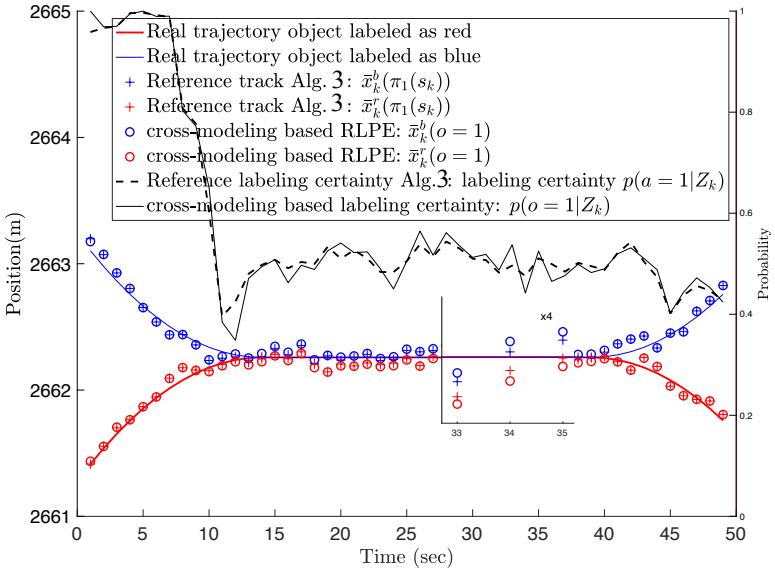

Figure 7.7: Illustration of extremely closely-spaced targets situation. Cross modeling based point estimates do not match the references for evaluation (+ points generated using Alg.3). Labeling certainty estimation is also biased.

7.3.7 Relevant analytic remarks

The CMT approximations have been formulated analytically (see Equations (7.21), (7.23), (7.28) and (7.30)) and their impact has been showcased with numerical simulations (see Figs. 7.5 and 7.7). For practical closely-spaced target scenarios, the joint multitarget density tends to adopt permutation invariant shapes as illustrated in Figs. 7.4 and 7.6. This observation has been also reported in [42][30]. This subsection provides analytical remarks to further understand the effects of the approximations in practice. The interpretation of these remarks will lead the optimization process in the following section.

- Remark 1: Provided $p(s_k|Z_{k-1})$ is permutation invariant, the approximations in Equations (7.21) and (7.23) become exact:
  assume $p(s_k|Z_{k-1}) = \mathrm{p}(\pi(s_k)|Z_{k-1})$,
  then,

$$\int_{s_k|x_k^b \geq x_k^r} \pi\{p(s_k|Z_{k-1})l(z_k|s_k)\}ds_k = \int_{s_k|x_k^b \geq x_k^r} p(s_k|Z_{k-1})l(\pi(z_k)|s_k)ds_k \tag{7.31}$$

$$\int_{s_k|x_k^b < x_k^r} \pi\{p(s_k|Z_{k-1})l(\pi(z_k)|s_k)\}ds_k = \int_{s_k|x_k^b < x_k^r} p(s_k|Z_{k-1})l(z_k|s_k)ds_k \tag{7.32}$$

- Remark 2: Provided $p(s_k|Z_{k-1})$ is permutation invariant, the exact expressions in the left hand side of Equations (7.28) and (7.30) can be calculated with no error as the permuted version of the results in the right hand side of Equations (7.28) and (7.30),

assume $p(s_k|Z_{k-1}) = \mathrm{p}(\pi(s_k)|Z_{k-1})$,
then,

$$\int_{s_k|x_k^b \geq x_k^r} \pi\{s_k\}\pi\{p(s_k|Z_{k-1})l(z_k|s_k)\}ds_k = \pi\{\int_{s_k|x_k^b \geq x_k^r} s_k p(s_k|Z_{k-1})l(\pi(z_k)|s_k)ds_k\} \tag{7.33}$$

$$\int_{s_k|x_k^b < x_k^r} \pi\{s_k\}\pi\{p(s_k|Z_{k-1})l(\pi(z_k)|s_k)\}ds_k = \pi\{\int_{s_k|x_k^b < x_k^r} s_k p(s_k|Z_{k-1})l(z_k|s_k)ds_k\} \tag{7.34}$$

7.3.8 Interpretation of the remarks in the context of the optimization problem

The first remark justifies that the plain CMT provides very accurate labeling uncertainty estimation. In fact, under the assumption of permutation invariant $p(s_k|Z_{k-1})$ densities, Equations (7.31) and (7.32) prove analytically that the labeling uncertainty estimates become asymptotically exact as the number of particles grows to infinity.

Although having permutation invariant $p(s_k|Z_{k-1})$ is a sufficient condition for the CMT to provide exact labeling certainty estimates, this is not a necessary condition. In fact, by considering Equation (7.31) one can also conclude that permutation strictly variant $p(s_k|Z_{k-1})$ densities lead to exact CMT labeling certainty estimation. To give an example, consider a strongly asymmetric $p(s_k|Z_{k-1})$ such as the one in in Fig. 7.8, the product of $p(s_k|Z_{k-1})$ and $l(z_k|s_k)$ (in Equation (7.31)) leads to non-zero probability mass only under the diagonal ($x_k^b = x_k^r$). Note that $l(z_k|s_k)$ is one of the two association likelihoods defined by convention, e.g. let $l(z_k|s_k)$ be the association likelihood hypothesizing that the detection of the object blue is the one at the larger range.

Taking into account mention asymmetric $p(s_k|Z_{k-1})$ density and convention, the first integral in Equation (7.31) becomes zero as all the probability mass is swapped above the diagonal after the operator π is applied. Finally, the second integral is also zero due to the lack of overlapping between $p(s_k|Z_{k-1})$ and $l(\pi z_k|s_k)$. For this reason, the CMT produces almost exact estimates along the first 10 seconds of the simulations in Figs. 7.5 and 7.7.

The second remark proves that the calculation of the labeled tracks by the CMT is not exact. This theoretical mismatch seems to be negligible in practice when the targets are far away from each other or relatively closely-spaced (but still resolved). This can be concluded from the numerical results in Fig. 7.5. The same theoretical mismatch becomes non-negligible in practice when the targets are extremely closely-spaced, as illustrated by the artificial "track separation" observed in the numerical results from Fig. 7.7.

In order to correct the theoretical mismatch in the labeled point estimates, the result of the integrals in the right hand side in Equations (7.28) and (7.30) needs to be label-swapped. Introducing this modification in the process of calculating CMT labeled tracks is not possible by design. This is because the CMT does not have access to the individual likelihoods $l(z_k|s_k)$ and $l(\pi(z_k)|s_k)$. Due to its DA-free nature, the CMT only has access to the sum

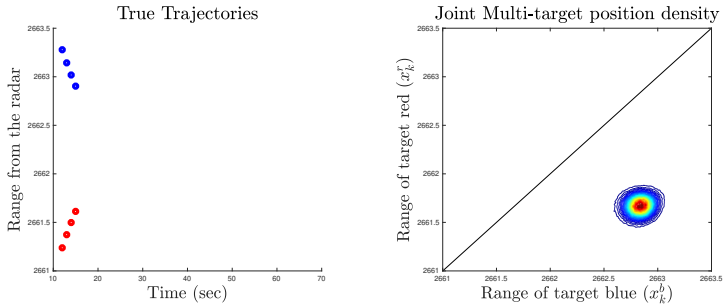

Figure 7.8: Illustration of distanced objects scenario, where the objects are not yet close enough to introduce labeling uncertainty.

of likelihoods $l(z_k|s_k)+l(\pi(z_k)|s_k)$. Factorizing $l(z_k|s_k)+l(\pi(z_k)|s_k)$ is not possible when calculating the CMT track estimates after introducing the label swap from Equations (7.33) and (7.34). Therefore, compensating for the bias in the CMT labeled tracks is not a trivial concern.

7.4 Mitigation of the impact of the CMT approximations on estimation performance

The previous section has provided theoretical interpretations and practical observations. As a conclusion, the focal point of the optimization problem should be on the extraction of CMT labeled point estimates or tracks. In particular, the goal is to mitigate the artificial "track separation" when considering unresolved targets.

The optimization strategy proposed in this section is based on the assumptions that $p(s_k|Z_{k-1})$ is permutation invariant and that $\pi(s_k)$ is a good approximation for s_k when the targets are extremely closely-spaced.

The former assumption seems to be realistic based on the shape of the density observed in Fig. 7.6. The later assumes that the multitarget state vector remains unaltered under label permutation, which is a realistic condition when the joint multitarget position estimates lay on one point of the diagonal. Under these assumptions, the CMT becomes exact also in the calculation of labeled tracks when tracking extremely closely-spaced targets. Note that when the second assumption does not hold (for non-closely-spaced targets), the theoretical mismatch exposed by the second remark has negligible degradation effect as commented in previous section.

7.4.1 Proposed optimization

The fact that the CMT labeled tracks suffer from artificial "track separation" when considering extremely closely spaced targets is a clear indication that the assumptions of permutation invariant $p(s_k|Z_{k-1})$ and/or $s_k \approx \pi(s_k)$ do not hold to the full extent. Firstly, the particle-based approximations in the implementation of the CMT algorithm may not capture the symmetric shape of the $p(s_k|Z_{k-1})$ density (including the tails) due to particle depletion, even when the exact density $p(s_k|Z_{k-1})$ is symmetric. Secondly, although most

of the probability mass of $p(s_k|Z_{k-1})$ is spread very close to the diagonal (see Fig. 7.6), the tails of the density may spread over regions of the joint space where $\pi(s_k)$ is certainly not a good approximation for s_k (see Fig. 7.6).

In this section we present an optimized CMT algorithm using a new proposal density prioritizing the quality of the approximation of $p(s_k|Z_{k-1})$ in the region close to the diagonal ($x_k^b = x_k^r$) and diminishing its sampling on the tails. As a result, the approximation $s_k \approx \pi(s_k)$ applied to each particle becomes more accurate. Additionally, the higher concentration of samples in the region of highest probability mass produces a more symmetric approximation of $p(s_k|Z_{k-1})$.

The claim in this section is that the use of a customized proposal density will improve significantly the estimation performance of the CMT when considering extremely closely-spaced targets, without producing significant degradation of performance in all other cases. The optimized particle-based filtering algorithm is provided in the following subsection. The modifications required for optimization will be derived according to the Importance Sampling principle. Finally, numerical simulations will be used to evaluate the accuracy of the claim.

7.4.2 The Optimal CMT algorithm

Alg 4. in chapter 6 describes the original CMT algorithm, only steps 5 and 7 need to be modified to describe the optimized CMT algorithm. In a recursive Bayesian method implemented with a PF, the density $p(s_k|Z_{k-1})$ has an exact formulation given the PF approximation of the previous posterior $p(s_{k-1}|Z_{k-1})$. In fact, $p(s_k|Z_{k-1})$ is a weighted sum of known densities:

$$\begin{aligned} p(s_k|Z_{k-1}) &\approx \int_{s_{k-1}} p(s_k|s_{k-1}) \sum_{i=1}^{N_p} w_{k-1}^i \delta(s_{k-1}^i - s_{k-1}) ds_{k-1} \\ &\approx \int_{s_{k-1}} \sum_{i=1}^{N_p} p(s_k|s_{k-1}^i) w_{k-1}^i \delta(s_{k-1}^i - s_{k-1}) ds_{k-1} \approx \sum_{i=1}^{N_p} w_{k-1}^i p(s_k|s_{k-1}^i) \end{aligned} \tag{7.35}$$

To approximate each $p(s_k|s_{k-1}^i)$, the original CMT algorithm used the following proposal density in step 5 in Alg.4 from chapter 6:

$$s_k^i \sim q(s_k) = p(s_k|s_{k-1}^i) \tag{7.36}$$

The optimization presented in this chapter consists on sampling from the proposal density:

$$q(s_k) = p(s_k|s_{k-1}^i)(p(s_k|s_{k-1}^i) + p(\pi(s_k)|s_{k-1}^i)) \tag{7.37}$$

The use of this proposal density widens the sampling space when the targets are not close to each other and adaptively sharpens it as the targets are approaching. Therefore, this proposal density results in a better approximation of $p(s_k|Z_{k-1})$ in the area close to the diagonal $x_k^b = x_k^r$ when the targets are extremely close to each other. By these means, the approximation $s_k \approx \pi(s_k)$ applied at particle level becomes more accurate, bringing the optimized CMT implementation closer to exactness in terms of track estimates.

Step 7 of Alg 4. needs to be modified according the Importance Sampling principle. In particular, the new calculation of the particle weight should be done as described in Alg.5:

1 $k = 0$;
2 Draw N_p samples $\boldsymbol{s}_k^i$ from $p(\boldsymbol{s}_k)$;
3 Draw N_p samples $\boldsymbol{n}_k^i$ from $p(\boldsymbol{n}_k)$;
4 $k = k + 1$;
5 Draw N_p samples $\boldsymbol{s}_k^i$ from $p(s_k|s_{k-1}^i)(p(s_k|s_{k-1}^i) + p(\pi(s_k)|s_{k-1}^i))$;
6 Calculate o_k^i according to the definition of "order" under test;
7 Given $\mathbf{z_k}$, obtain $\tilde{w}_k^i = p(\mathbf{z}_k|s_k^i)/(p(\mathbf{s}_k^i|s_k^i) + p(\pi(\mathbf{s}_k^i)|s_k^i))$;
8 Normalize weights $w_k^i = \tilde{w}_k^i / \sum_{j=1}^{N_p} \tilde{w}_k^j$;
9 Resample from $\hat{p}(\boldsymbol{s}_k|\mathbf{Z}_k) = \sum_{i=1}^{N_p} w_k^i \delta(\boldsymbol{s}_k - \boldsymbol{s}_k^i)$:;
10 Extract LPEs according to Equation 6.15;
11 Obtain certainty measures of LPEs
according to Equation 6.16;
go to 3

Algorithm 5: Pseudo-code of the PF algorithm for the optimized CMT. Modification over the original algorithm are in steps 5 and 7.

7.4.3 Discussion on estimation performance: regular CMT Vs optimized CMT

As illustrated in Figs. 7.9 and 7.10, estimation results are more accurate when using the optimized CMT algorithm. The use of convenient proposal densities aids at mitigating the impact of the CMT approximations. In particular, the "track separation" artifact produced by the regular CMT when the targets are extremely close to each other can be reduced significantly.

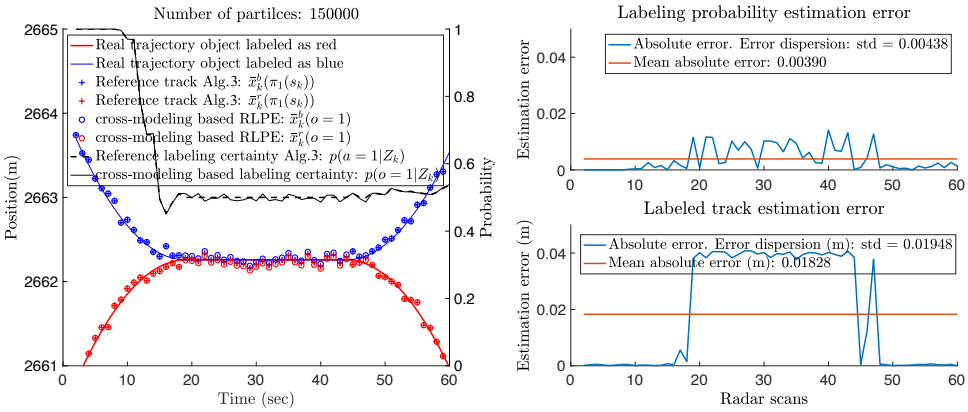

Figure 7.9: Regular CMT estimation performance for extremely-close targets.

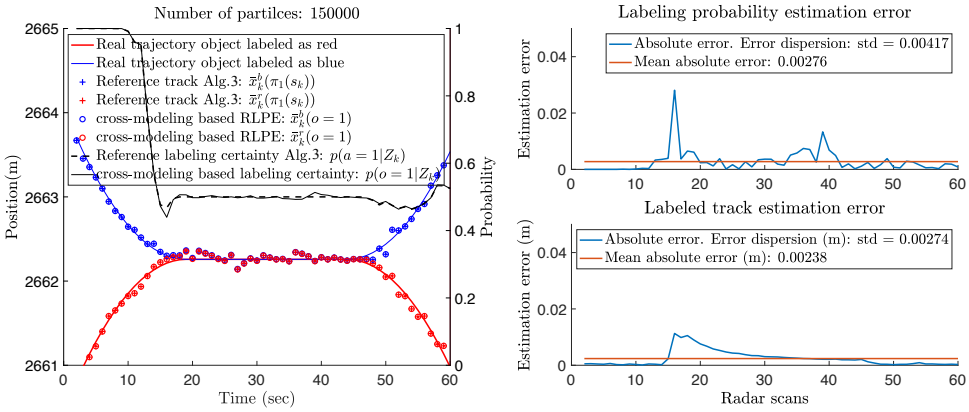

Figure 7.10: Optimized CMT estimation performance for extremely-close targets.

7.5 Conclusions

Evaluation results of the algorithms in chapters 5 and 6 for data-association-free tracking have been provided with simulations involving closely-spaced trajectories. These algorithms are the non-linear and/or non-Gaussian (non-LG) implementation of the Unique Decomposition (UD) derived in chapter 5 and submitted for publication as [62] and the Cross Modeling Tracker (CMT) derived in chapter 6 and published in [27]. Both algorithms subject to evaluation provide complete solutions for the Track-before-detect (TrBD) MOT problem, including characterization of labeling uncertainty without formulating any type of Data Association (DA) problem.

In spite of the non-LG implementation of the UD providing accurate estimation after closely-spaced targets have separated sufficiently, the CMT outperforms the non-LG implementation of the UD overall, especially when targets are in closely-space. Nevertheless, initial results have shown that the CMT is not an exact solution. This chapter has focused on optimizing the CMT from the base line solution derived in chapter 6.

To achieve the optimization of the CMT, this chapter has followed a two-steps approach. Firstly, the CMT approximations have been analytically formulated and the impact of such approximations has been illustrated with numerical examples. Secondly, the degradation due to the CMT approximations has been mitigated by using a convenient proposal density at PF implementation level. Simulation results have shown that the proposed optimized algorithm outperforms the original CMT algorithm presented in chapter 6 [27].

8

Conclusions and future lines

8.1 Conclusions

In this thesis the Multiple Object Tracking (MOT) problem involving closely-spaced objects is treated based on intensity map measurements. Although many sensor systems may produce these type of measurements, the contributions in this thesis are illustrated on the basis of raw radar measurements, such as e.g. range-azimuth maps. This particular problem has been coined in literature as Track-before-Detect (TrBD) MOT. TrBD MOT solutions have been reported to be especially relevant in the tracking of low SNR objects and in the tracking of closely-spaced targets, where a traditional detection-based tracker would have to deal with merged measurements. At a higher level, this thesis also tackles the problem of detecting anomalous target behavior. Solutions to this problem are relevant in societal applications such as for instance security assessment.

Despite the existence of many prior solutions for the detection-based MOT problem, also known as Detect-before-Track (DBT) MOT, the contributions in this thesis do not rely on any of such results. This is because TrBD MOT problems preclude the formulation of Data Association (DA), an essential component in traditional DBT context which turns the filtering process into a tracker by explicitly characterizing labeling uncertainty. As no existent characterization of labeling uncertainty can be applied to the TrBD MOT problem due to the absence of detections, we are left with no solution to the labeling problem when using raw data to track the targets. This results in degraded tracking performance when tracking closely-spaced targets, as showcased in the preliminary chapters of the thesis. The most important conclusion extracted from these preliminary studies is that while DBT MOT solves the labeling problem in a pre-filtering stage (via DA), TrBD MOT is forced to solve it in a post-filtering stage by inferring a labeling-dependent decomposition of the Bayes posterior. Therefore, it is a recurrent focus of the thesis to deal with the underlying problem of decomposing the Bayes posterior density, as it is in this decomposition where the information about labeling can be found.

Some general considerations hold along the thesis. Firstly, this thesis considers the worst case scenario assuming that intensity map measurements do not provide any labeling information. In other words, it is assumed that the likelihood model for the measurements given the state is invariant under label permutations. Nevertheless, although techniques

based on identification through measurements fall out of the scope of this thesis, they can be integrated seamlessly in order to reduce labeling uncertainty when tracking objects of different radar signatures. Secondly, this thesis considers the TrBD MOT problem assuming the number of targets is fixed and known, which aids at isolating the problem of DA-free characterization of labeling uncertainty. Nevertheless, this assumption does not restrict generality as the proposed approaches can be integrated seamlessly with existent solutions for the cardinality estimation problem in TrBD MOT.

The first novel contribution of the thesis is given in chapter 3, where the incorporation of interacting target dynamic models is used to solve the problem of detecting anomalous target behavior. Additionally, an automatic parameter tuning method is incorporated in the recursive Bayesian framework to estimate coupled accelerations between targets. The method exploits such information to close the sensing-tuning loop inside the tracker, resulting in enhanced tracking performance including reduction of labeling uncertainty. Such an adaptive method for modeling interacting target dynamics is relevant in this thesis as objects get/remain closely-spaced only by performing coordinated maneuvering. Additionally, interesting societal applications of this method can be found as many anomalous target behaviors involve some kind of interaction between the targets. For instance, safety assessment warnings can be generated when the estimated amount of target interaction exceeds the threshold of regular activity.

Chapter 4 presents a sensible method for evaluation of DA-free MOT solutions. The main contribution of chapter 4 is a PF algorithm implementation providing optimal statistics relevant for track formation. As no analytical form of such statistics exists in TrBD context, the evaluation algorithm provided calculates them in DBT context, where a Data Association dependent decomposition can be formulated analytically. This analytical decomposition enables extraction of references both for the labeled tracks and corresponding labeling certainties.

The presented algorithm will be incorporated as part of a criterion for performance evaluation of DA-free trackers. Despite its DA-based construction, the evaluation criterion can be used legitimately to evaluate solutions such as the UD-based and CMT algorithms, which are designed for operation in TrBD context. This is because these algorithms are designed to infer a relevant label-dependent decomposition of any posterior density, disregarding whether this density has been generated in the context of DBT or TrBD.

Moving on from modeling and evaluation aspects to TrBD MOT algorithm design, chapters 5, 6 and 7 deal with the almost-unexplored problem of characterizing labeling uncertainty without relying on DA. In particular, the presented novel solutions tackle the underlying problem of decomposing the Bayes posterior, trying to mimic the functionality of inaccessible DA-dependent decompositions, such as e.g. the MHT decomposition.

Chapter 5 considers the Unique Decomposition (UD) by Blom and Bloem as the only existent theoretical formulation capable of tackling the labeling problem without relying on any type of DA. The main contribution of Chapter 5 is the application of the UD to the TrBD MOT problem. This contribution deals with generalizing existent implementations of the UD to non-linear and non-Gaussian problems. In particular, a two-PF recursive solution is derived in order to estimate separately the Permutation Invariant and the Permutation Strictly Variant components of the UD.

While the decomposition of the Bayes posterior targeted in chapter 5 is based on

permutation invariance characteristics of the multitarget density, the main contribution of chapters 6 and 7 is decomposing the Bayes posterior by means of hypothesizing crosses between objects. This concept has physical meaning in the low dimensional case, where two objects move in a $1D$ space. However, hypothesizing crosses between objects out of the $2-1D$ case is certainly not trivial. In order to make the so-called Cross Modeling Tracker (CMT) usable for the general $t-MD$ targets case, chapter 6 generalizes the concept of cross-between-objects analytically. The novel CMT algorithm proposed here is validated using the evaluation method from chapter 4 by simulating $t-MD$ closely-spaced objects scenarios.

Overall, this thesis provides novel tools to solve the TrBD MOT problem for closely-spaced targets. In particular, two new methods to infer label-dependent decompositions of the joint multiobject Bayes posterior density have been derived. The CMT can be considered as the first step towards the TrBD counterpart of DBT Multiple Hypotheses Tracking (MHT). The non-linear non-Gaussian implementation of the UD and the CMT have been validated against the evaluation method in chapter 4.

Both approaches provide comparable results in terms of track estimation and labeling uncertainty characterization. The advantage of applying the UD theory is that particle self-resolving artifacts are prevented by design, allowing stable estimation with less amount of particles than the CMT. The CMT outperforms the application of the UD for extremely closely-spaced targets, especially in cases where the multitarget density becomes unimodal. Moreover, the main advantage of the CMT is its wider applicability in arbitrarily high dimensional cases. This is a current limitation of the UD theory, which has no existent generalization for joint densities with more than 2 targets.

8.2 Future lines

As for future work, the formulation of the CMT within the RFS framework can be investigated in order to add built-in cardinality estimation capabilities. This is required for the CMT to be declared as a solution for the complete MOT problem, where the assumption of known and constant number of objects does not hold. Additionally, studying the use of the CMT in the context of DBT may lead to interesting advantages. This may be specially the case when comparing with DBT methods in scenarios where DA needs to account for large number of non-negligible hypotheses.

An interesting extension of the formulation in chapter 5 would be deriving the equivalent algorithm dropping the assumption of invariance with respect to target dynamics. Finally, a very interesting theoretical problem would be the extension of UD theory to account for joint densities involving more than two targets.

A

Appendices

A

A.1 Calculation of A_b

The solution of the differential stochastic equation in Fig. (3.2) for "x" direction is,

$$s_x(t) = e^{A_p(t)t} \int G(t)\tilde{v}_x(t)e^{-A_p(t)t}dt \tag{A.1}$$

The discretization for a revisit time δt results in,

$$s_x((k+1)\delta t) = e^{A_p(t)\delta t}s_x(k\delta t) + \int_{k\delta t}^{(k+1)\delta t} e^{A_p((k+1)\delta t-\tau)}G(\tau)\tilde{v}_x(\tau)d\tau \tag{A.2}$$

Therefore, the block A_b in (3.18) is given by the exponential matrix $e^{A_p(t)\delta t}$.

From linear algebra theory we know that for any continuous scalar-valued function $f(x) : \mathbb{C} \to \mathbb{C}$ and for any square matrix $X \in \mathbb{R}^{nxn}$ (or $\in \mathbb{C}^{nxn}$):

$$f(X\delta t) = M \begin{pmatrix} f(J_{k1}(\lambda_1)\delta t) & & 0 \\ & \ddots & \\ 0 & & f(J_{km}(\lambda_m)\delta t) \end{pmatrix} M^{-1}, \tag{A.3}$$

where δt is a scalar, M is nonsingular and $J_{k1}(\lambda_1)$,...,$J_{km}(\lambda_1)$ are the so-called Jordan Blocks associated to eigenvectors $\lambda_1, ..., \lambda_m$. Each of them defined as an upper triangular matrix such that $J_k(\lambda) \in \mathbb{C}^{kxk}$ is,

$$J_k(\lambda) = \begin{pmatrix} \lambda & 1 & & 0 \\ & \ddots & \ddots & \\ & & \lambda & 1 \\ 0 & & & \lambda \end{pmatrix} \tag{A.4}$$

$f(J_k(\lambda)\delta t)$ is defined as,

$$f(J_k(\lambda)\delta t) = \begin{pmatrix} f(\lambda\delta t) & \delta t f'(\lambda\delta t) & \frac{\delta t^2}{2!}\delta t f''(\lambda\delta t) & \dots & \frac{\delta t^{k-1}}{(k-1)!}\delta t f^{(k-1)}(\lambda\delta t) \\ & \ddots & \ddots & \ddots & \vdots \\ & & \ddots & \ddots & \frac{\delta t^2}{2!}\delta t f''(\lambda\delta t) \\ & & & \ddots & \delta t f'(\lambda\delta t) \\ 0 & & & & f(\lambda\delta t) \end{pmatrix} \tag{A.5}$$

Given these definitions, the matrix J is the Jordan canonical form of the matrix X through the similarity transformation M, which existence is ensured in linear algebra theory.

$$J = \begin{pmatrix} J_{k1}(\lambda_1) & & 0 \\ & \ddots & \\ 0 & & J_{km}(\lambda_m) \end{pmatrix} = M^{-1}XM \tag{A.6}$$

X is, in our particular case, the continuous time system function for any of the "x", "y" directions,

$$A_p = \begin{pmatrix} 0 & 1 & 0 & 0 \\ 0 & 0 & 0 & 0 \\ 0 & 0 & 0 & 1 \\ k_1 & 0 & -k_1 & -k_2 \end{pmatrix}$$

The similarity transformation,

$$M = \begin{pmatrix} 1 & 0 & 0 & 0 \\ 0 & 1 & 0 & 0 \\ 1 & -\frac{k_2}{k_1} & 1 & 1 \\ 0 & 1 & \lambda_2 & \lambda_3 \end{pmatrix}, with\ \lambda_2 = \frac{-k_2 - \sqrt{k_2^2 - 4k_1}}{2},\ \lambda_3 = \frac{-k_2 + \sqrt{k_2^2 - 4k_1}}{2} \tag{A.7}$$

satisfies $J = M^{-1}A_pM$ as long as k_1 and k_2 are non zero and $k_2^2 \neq 4k_1$. We can neglect these particular cases as k_1 and k_2 are considered unknowns (part of the state vector) and a

particle filter is considered for the implementation. Because of that, components k_1 and k_2 of the particles are affected by the process noise in Eq. (3.25), therefore the mentioned particular cases have probability zero.
Then, A_b can be put in the form of Eq. (A.3) as,

$$A_b = e^{A_p \delta t} = M \begin{pmatrix} 1 & \delta t & 0 & 0 \\ 0 & 1 & 0 & 0 \\ 0 & 0 & e^{\lambda_2 \delta t} & 0 \\ 0 & 0 & 0 & e^{\lambda_3 \delta t} \end{pmatrix} M^{-1}$$

which results in,

$$\begin{pmatrix} 1 & \delta t & 0 & 0 \\ 0 & 1 & 0 & 0 \\ \frac{\lambda_2(1-e^{\delta t \lambda_3})-\lambda_3(1-e^{\delta t \lambda_2})}{\lambda_2-\lambda_3} & A_b(3,2) & \frac{\lambda_2 e^{\delta t \lambda_3}-\lambda_3 e^{\delta t \lambda_2}}{\lambda_2-\lambda_3} & \frac{e^{\delta t \lambda_2}-e^{\delta t \lambda_3}}{\lambda_2-\lambda_3} \\ \frac{\lambda_2 \lambda_3(e^{\delta t \lambda_2}-e^{\delta t \lambda_3})}{\lambda_2-\lambda_3} & A_b(4,2) & -\frac{\lambda_2 \lambda_3(e^{\delta t \lambda_2}-e^{\delta t \lambda_3})}{\lambda_2-\lambda_3} & \frac{\lambda_2 e^{\delta t \lambda_2}-\lambda_3 e^{\delta t \lambda_3}}{\lambda_2-\lambda_3} \end{pmatrix} \tag{A.8}$$

where,

$$A_b(3,2) = -\frac{k_1(e^{\delta t \lambda_2}-e^{\delta t \lambda_3}-\delta t \lambda_2+\delta t \lambda_3)+k_2\lambda_2(1-e^{\delta t \lambda_3})-k_2\lambda_3(1-e^{\delta t \lambda_2})}{k_1(\lambda_2-\lambda_3)}$$

$$A_b(4,2) = \frac{k_1(\lambda_2-\lambda_3-\lambda_2 e^{\delta t \lambda_2}+\lambda_3 e^{\delta t \lambda_3})-k_2\lambda_2\lambda_3(e^{\delta t \lambda_2}-e^{\delta t \lambda_3})}{k_1(\lambda_2-\lambda_3)}$$

A

A.2 Proof of the analytic description of the update step (Equations (5.11) and (5.12))

According to the definition of BB

$$\alpha^I_{k|k} = \int_{s_k} min(p(s_k|Z_k), p(\pi s_k|Z_k))ds_k \tag{A.9}$$

$$p^I(s_k|Z_k) = \frac{min(p(s_k|Z_k), p(\pi s_k|Z_k))}{\alpha^I_{k|k}} \tag{A.10}$$

$$p^V(s_k|Z_k) = \frac{p(s_k|Z_k) - \alpha^I_{k|k} p^I(s_k|Z_k)}{1 - \alpha^I_{k|k}} \tag{A.11}$$

Substituting $p(s_k|Z_k) = \frac{p(z_k|s_k)p(s_k|Z_{k-1})}{p(z_k|Z_{k-1})}$ and exploiting $p(z_k|s_k) = p(z_k|\pi s_k)$ leads to

$$\alpha^I_{k|k} = \frac{\int_{s_k} p(z_k|s_k) min(p(s_k|Z_{k-1}), p(\pi s_k|Z_{k-1}))ds_k}{p(z_k|Z_{k-1})} \tag{A.12}$$

$$p^I(s_k|Z_k) = \frac{p(z_k|s_k)}{p(z_k|Z_{k-1})\alpha^I_{k|k}} min(p(s_k|Z_{k-1}), p(\pi s_k|Z_{k-1})) \tag{A.13}$$

$$p^V(s_k|Z_k) = \frac{p(z_k|s_k)}{p(z_k|Z_{k-1})\alpha^V_{k|k}} (p(s_k|Z_{k-1}) - min(p(s_k|Z_{k-1}), p(\pi s_k|Z_{k-1}))) \tag{A.14}$$

Then recognizing that the above expressions can be written in terms of the components of the UD of the predictive density $p(s_k|Z_{k-1})$

$$min(p(s_k|Z_{k-1}), p(\pi s_k|Z_{k-1})) = \alpha^I_{k|k-1} p^I(s_k|Z_{k-1}) \tag{A.15}$$

$$p(s_k|Z_{k-1}) - min(p(s_k|Z_{k-1}), p(\pi s_k|Z_{k-1})) = \alpha^V_{k|k-1} p^V(s_k|Z_{k-1}) \tag{A.16}$$

and

$$\begin{aligned} p(z_k|Z_{k-1}) &= \int p(z_k|s_k)p(s_k|Z_{k-1})ds_k \\ &= \alpha^I_{k|k-1} \int p(z_k|s_k)p^I(s_k|Z_{k-1})ds_k + \alpha^V_{k|k-1} \int p(z_k|s_k)p^V(s_k|Z_{k-1})ds_k \\ &= \alpha^I_{k|k-1} p^I(z_k|Z_{k-1}) + \alpha^V_{k|k-1} p^V(z_k|Z_{k-1}) \end{aligned} \tag{A.17}$$

This then leads to the result

$$\begin{aligned} \alpha^X_{k|k} &= \frac{\alpha^X_{k|k-1} \int_{s_k} p(z_k|s_k) p^X(s_k|Z_{k-1}))ds_k}{p(z_k|Z_{k-1})} \\ &= \frac{p^X(z_k|Z_{k-1})\alpha^X_{k|k-1}}{p(z_k|Z_{k-1})} \end{aligned} \tag{A.18}$$

$$p^X(s_k|Z_k) = \frac{p(z_k|s_k)p^X(s_k|Z_{k-1})}{p^X(z_k|Z_{k-1})} \tag{A.19}$$

A.3 Naive generalization of o_k

A naive extension of the definition of "cross" from $2-1D$ to $2-2D$ settings will be presented in this appendix. This is not only to illustrate the complexity of the problem but also to familiarize the reader with some consistency checks that the correct extension of "cross" should comply with.

The naive attempt presented in this appendix considers that Inequation (6.27) is the "cross detector" for the $2-2D$ objects case. After all, a point can be evaluated by the $l2-norm$ function disregarding the dimensionality of the point. Only two formal modifications need to be accounted for when extending Inequation (6.27) from $2-1D$ to $2-2D$ settings. First, the $l2-norm$ calculation for the $2-2D$ objects case becomes:

$$norm(s'_k - s'_{k-1}) = \sqrt{(x^r_k - x^r_{k-1})^2 + (x^b_k - x^b_{k-1})^2 + (y^r_k - y^r_{k-1})^2 + (y^b_k - y^b_{k-1})^2} \tag{A.20}$$

where now $s'^{p}_k = [x^{p,b}_k \; y^{p,b}_k \; x^{p,r}_k \; y^{p,r}_k]^T$. Second, the permutation matrix Π for the $2-2D$ objects case becomes:

$$\Pi = \begin{pmatrix} 0 & 0 & 1 & 0 \\ 0 & 0 & 0 & 1 \\ 1 & 0 & 0 & 0 \\ 0 & 1 & 0 & 0 \end{pmatrix} \tag{A.21}$$

Given these modifications, the results provided by the CMT for the $2-2D$ objects case are shown in Figure A.1.

A.3.1 Discussion of results

The results reveal degraded estimation performance of the CMT both in the computation of LPEs and labeling probabilities. In fact, LPEs result in high OSPA errors (specially after objects separation) due to the well known "track coalescence" effect. This undesired effect is expected if MMSE point estimates are extracted from multimodal densities when labeling uncertainty characterization is not appropriately accounted for.

One can conclude that this attempt to generalize the definition of "cross" is naive. In fact, the use of Inequation (6.27) as the "cross detector" does not remove particle mixing inside each cluster after objects separation. This is illustrated at the bottom part of Figure A.1, where the particle mixing-ratio after CMT clustering does not drop to zero after target separation.

A

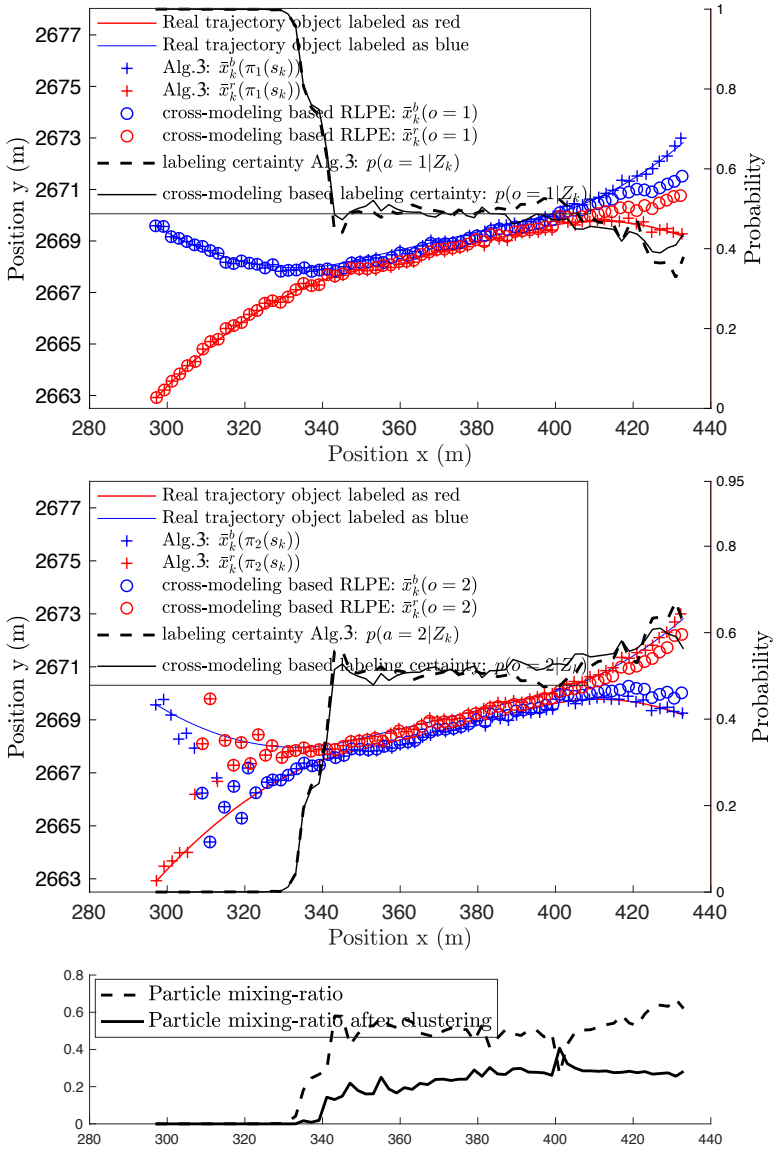

Figure A.1: Evaluation of estimation performance of the CM method using a naive $2-2D$ "cross" detector. Alg. 2 generates the optimal references.

Bibliography

References

[1] Y. Boers, E. Sviestins, and J. N. Driessen. Mixed labelling in multitarget particle filtering. *IEEE Transactions on Aerospace and Electronic Systems*, 46(2):792–802, 2010.

[2] M. Hadzagic, H. Michalska, and E. Lefebvre. Track-before detect methods in tracking low-observable targets: A survey. *Sensor Trans. Mag.*, 54:374–380, 09 2005.

[3] R. Mahler. "statistics 103" for multitarget tracking. *Sensors (Basel)*, 35(6):8–19, 2019.

[4] Y. Boers, J. N. Driessen, F. Verschure, W. P. M. H. Heemels, and A. Juloski. A multi target track before detect application. In *2003 Conference on Computer Vision and Pattern Recognition Workshop*, volume 9, pages 104–104, 2003.

[5] A. Lepoutre, O. Rabaste, and F. Le Gland. Exploiting amplitude spatial coherence for multi-target particle filter in track-before-detect. In *Proceedings of the 16th International Conference on Information Fusion*, pages 319–326, 2013.

[6] A. Cuillery and F. Le Gland. Track-before-detect on radar image observation with an adaptive auxiliary particle filter. In *2019 22th International Conference on Information Fusion (FUSION)*, pages 1–8, 2019.

[7] N. Ito and S. Godsill. A multi-target track-before-detect particle filter using super-positional data in non-gaussian noise. *IEEE Signal Processing Letters*, 27:1075–1079, 2020.

[8] Y. Zhang, A. Carballo, H. Yang, and K Takeda. Perception and sensing for autonomous vehicles under adverse weather conditions: A survey. In *2023 ISPRS J. Photogramm. Remote Sens.*, volume 196, page 146–177, 2023.

[9] A. N. Ramesh, C. Moreno-Leon, J. Centenera-Zafra, S. Brüggenwirth, and M. A. González-Huici. Landmark-based radar slam for autonomous driving. In *2021 21st International Radar Symposium (IRS)*, pages 1–10, 2021.

[10] A. Abosekeen, T. Karamat, A. Noureldin, and M. Korenberg. Adaptive cruise control radar-based positioning in gnss challenging environment. *IET Radar, Sonar Navigation*, 13, 10 2019.

[11] D. Reid. An algorithm for tracking multiple targets. *IEEE Transactions on Automatic Control*, 24(6):843–854, 1979.

[12] A. F. García Fernández. Detection and tracking of multiple targets using wireless sensor networks - detección y seguimiento de múltiples blancos en redes inalámbricas de sensores. 2011.

[13] A. Charlish, F. Hoffmann, C. Degen, and I. Schlangen. The development from adaptive to cognitive radar resource management. *IEEE Aerospace and Electronic Systems Magazine*, 35(6):8–19, 2020.

[14] P. W. Moo and Z. Ding. *Adaptive Radar Resource Management.* Academic Press, London, 1st ed., 2015.

[15] A. O. Hero and D. Cochran. Sensor management: Past, present, and future. *IEEE Sensors Journal*, 11(12):3064–3075, 2011.

[16] M.I Schope. *Approximately Optimal Resource Management for Multi-Function Radar Algorithmic Solutions Using a Generic Framework.* Phd thesis, TU Delft, Delft, The Netherlands, 2021.

[17] H. Griffiths R. Klemm and W. Koch. *Novel Radar Techniques and Applications, Volume 2 - Waveform Diversity and Cognitive Radar, and Target Tracking and Data Fusion.* Scitech Publishing, 2017.

[18] S. Ghosh, R. Rajkumar, J. Hansen, and J. Lehoczky. Integrated qos-aware resource management and scheduling with multi-resource constraints. *Rea-Time Syst*, 33:7–46, 07 2006.

[19] S. Durst and S. Brüggenwirth. Quality of service based radar resource management using deep reinforcement learning. In *2021 IEEE Radar Conference (RadarConf21)*, pages 1–6, 2021.

[20] F. Katsilieris. *Sensor management for surveillance and tracking: An operational perspective.* Phd thesis, TU Delft, Delft, The Netherlands, 2015.

[21] A. De Freitas, R. W. Focke, C. Beyers, and P. De Villiers. Global optimization for resource allocation in a networked-surveillance radar. In *2019 22th International Conference on Information Fusion (FUSION)*, pages 1–8, 2019.

[22] C. Moreno-Leon and H. Driessen. Evaluation of labeling uncertainty in multiple target tracking with track-before-detect radars. In *2019 22th International Conference on Information Fusion (FUSION)*, pages 1–8, 2019.

[23] Y. Bar-Shalom, X. Li, and T. Kirubarajan. Estimation with applications to tracking and navigation: Theory, algorithms and software. 2001.

[24] C. Moreno-Leon, H. Driessen, and P. K. Mandal. Efficient characterization of labeling uncertainty in closely-spaced targets tracking. In *2016 19th International Conference on Information Fusion (FUSION)*, pages 449–456, 2016.

[25] H. A.P. Blom and Edwin A. Bloem. Permutation invariance in bayesian estimation of two targets that maneuver in and out formation flight. In *2009 12th International Conference on Information Fusion*, pages 1296–1303, 2009.

[26] C. Moreno-Leon, L. S. Mihaylova, and H. Driessen. Tracking of interacting targets. In *2017 20th International Conference on Information Fusion (Fusion)*, pages 1–8, 2017.

[27] C. Moreno-Leon, H. Driessen, and A. Yarovoy. Data-association-free characterization of labeling uncertainty: the cross modeling tracker. 2021.

[28] B. Ristic, S. Arulampalam, and N. J. Gordon. Beyond the kalman filter: Particle filters for tracking applications. 2004.

[29] H. A.P. Blom, E. A. Bloem, Y. Boers, and H. Driessen. Tracking closely spaced targets: Bayes outperformed by an approximation? In *2008 11th International Conference on Information Fusion*, pages 1–8, 2008.

[30] M. R. Morelande and A. Zhang. Uniform sampling for multiple target tracking. In *14th International Conference on Information Fusion*, pages 1–7, 2011.

[31] T. Li, S. Sun, T. Sattar, and J. Corchado-Rodríguez. Fight sample degeneracy and impoverishment in particle filters: A review of intelligent approaches. *Expert Systems with Applications*, 41:3944–3954, 06 2014.

[32] X. Wang, T. Li, S. Sun, and J. M. Corchado. A survey of recent advances in particle filters and remaining challenges for multitarget tracking. *Sensors*, 17(12), 2017.

[33] A. F. García-Fernández, M. R. Morelande, and J. Grajal. Particle filter for extracting target label information when targets move in close proximity. In *14th International Conference on Information Fusion*, pages 1–8, 2011.

[34] H.A.P. Blom and E.A. Bloem. Probabilistic data association avoiding track coalescence. *IEEE Transactions on Automatic Control*, 45(2):247–259, 2000.

[35] T. Fortmann, Y. Bar-Shalom, and M. Scheffe. Sonar tracking of multiple targets using joint probabilistic data association. *IEEE Journal of Oceanic Engineering*, 8(3):173–184, 1983.

[36] R. Mahler. Multitarget bayes filtering via first-order multitarget moments. *IEEE Transactions on Aerospace and Electronic Systems*, 39(4):1152–1178, 2003.

[37] L. Svensson and M. Morelande. Target tracking based on estimation of sets of trajectories. In *17th International Conference on Information Fusion (FUSION)*, pages 1–8, 2014.

[38] A. F. García-Fernández, L. Svensson, and M. R. Morelande. Multiple target tracking based on sets of trajectories. *IEEE Transactions on Aerospace and Electronic Systems*, 56(3):1685–1707, 2020.

[39] A. F. García-Fernández. Track-before-detect labeled multi-bernoulli particle filter with label switching. *IEEE Transactions on Aerospace and Electronic Systems*, 52(5):2123–2138, 2016.

[40] Y. Xia, L. Svensson, A. F. García-Fernández, K. Granström, and J. L. Williams. Backward simulation for sets of trajectories. In *2020 IEEE 23rd International Conference on Information Fusion (FUSION)*, pages 1–8, 2020.

[41] E. H. Aoki, P. K. Mandal, L. Svensson, Y. Boers, and A. Bagchi. Labeling uncertainty in multitarget tracking. *IEEE Transactions on Aerospace and Electronic Systems*, 52(3):1006–1020, 2016.

[42] Y. Boers, E. Sviestins, and H. Driessen. Mixed labelling in multitarget particle filtering. *IEEE Transactions on Aerospace and Electronic Systems*, 46(2):792–802, 2010.

[43] D. F. Crouse, P. Willett, and Y. Bar-Shalom. Generalizations of blom and bloem's pdf decomposition for permutation-invariant estimation. In *2011 IEEE International Conference on Acoustics, Speech and Signal Processing (ICASSP)*, pages 3840–3843, 2011.

[44] D. F. Crouse, Peter Willett, and Y. Bar-Shalom. Developing a real-time track display that operators do not hate. *IEEE Transactions on Signal Processing*, 59(7):3441–3447, 2011.

[45] D. F. Crouse, P. Willett, L. Svensson, D. Svensson, and M. Guerriero. The set mht. In *14th International Conference on Information Fusion*, pages 1–8, 2011.

[46] *Manual On Remotely Piloted Aircaft Systems (RPAS).* ICAO, vol. DOC10019, 2015.

[47] A. Gning, L. Mihaylova, S. Maskell, S. K. Pang, and S. Godsill. Group object structure and state estimation with evolving networks and monte carlo methods. *IEEE Transactions on Signal Processing*, 59(4):1383–1396, 2011.

[48] D. Helbing and P. Molnar. Social force model for pedestrian dynamics. *Physical Review E*, 51, 05 1998.

[49] M. Luber, J. A. Stork, G. D. Tipaldi, and K. O. Arras. People tracking with human motion predictions from social forces. In *2010 IEEE International Conference on Robotics and Automation*, pages 464–469, 2010.

[50] A. Ur-Rehman, S. M. Naqvi, L. Mihaylova, and J. A. Chambers. Multi-target tracking and occlusion handling with learned variational bayesian clusters and a social force model. *IEEE Transactions on Signal Processing*, 64(5):1320–1335, 2016.

[51] R. Mazzon and A. Cavallaro. Multi-camera tracking using a multi-goal social force model. *Neurocomputing*, 100:41–50, 2013. Special issue: Behaviours in video.

[52] Y. Boers and J.N. Driessen. Multitarget particle filter track before detect application. *Radar, Sonar and Navigation, IEE Proceedings* -, 151:351 – 357, 01 2005.

[53] M.I. Skolnik. *Introduction to Radar Systems.* Electrical engineering series. McGraw-Hill, 2001.

[54] L. Svensson, D. Svensson, M. Guerriero, and P. Willett. Set jpda filter for multitarget tracking. *IEEE Transactions on Signal Processing*, 59(10):4677–4691, 2011.

[55] D. F. Crouse, P. Willett, M. Guerriero, and L. Svensson. An approximate minimum mospa estimator. In *2011 IEEE International Conference on Acoustics, Speech and Signal Processing (ICASSP)*, pages 3644–3647, 2011.

[56] H. A. P. Blom and E. A. Bloem. Decomposed particle filtering and track swap estimation in tracking two closely spaced targets. In *14th International Conference on Information Fusion*, pages 1–8, 2011.

[57] H. A.P. Blom and E. A. Bloem. Optimal decomposed particle filtering of two closely spaced gaussian targets. In *2011 50th IEEE Conference on Decision and Control and European Control Conference*, pages 7895–7901, 2011.

[58] A. F. García-Fernández. *Detection and tracking of multiple targets using wireless sensor network.* Universidad Politécnica de Madrid Available: http://oa.upm.es/9823/, Madrid, Spain, 2011.

[59] M. Guerriero, L. Svensson, D. Svensson, and P. Willett. Shooting two birds with two bullets: How to find minimum mean ospa estimates. In *2010 13th International Conference on Information Fusion*, pages 1–8, 2010.

[60] T. L. Corwin K. L. Bell L. D. Stone, R. L. Streit. *Bayesian Multiple Target Tracking.* Artech House, Norwood, MA, 2014.

[61] Y. Boers and H. Driessen. The mixed labeling problem in multi target particle filtering. In *2007 10th International Conference on Information Fusion*, pages 1–7, 2007.

[62] C. Moreno-Leon, H. Driessen, and Yarovoy A. Implementation of the unique pdf decomposition for tracking closely-spaced objects with track-before-detect radar systems, submitted for review. *Transactions on Aerospace and Electronic Systems*, 2023.

[63] S. M Sherman and D. K Barton. *Monopulse principles and techniques.* Artech House, 2011.

[64] W. Blair. Monopulse processing for track unresolved targets. *Dahlgren Division Naval Surface Warfare Center, Dahlgren, VA, USA*, pages 1–4, 1997.

Bio

Carlos Moreno León received his MSc in Telecommunications Engineering in 2013 from the University of Alcalá (UAH). From 2012 to 2014, he was employed by the Polytechnic University of Madrid (UPM), in the department of Signals, Systems and Radiocommunications, doing research on distributed signal processing. From 2014 to 2017, Carlos worked at Thales Nederland BV in the area of naval surveillance radar, while holding a European Commission Marie Curie research fellowship, with focal point on radar Multiple Target Tracking algorithm design. From 2017 to 2022, Carlos was with the Cognitive Radar department in the German Fraunhofer Institute for High Frequency Physics and Radar Techniques (FHR), where he worked in monostatic and multistatic radar-based solutions applied in automotive, aerospace and defence contexts. Since 2022, he is with the Systems Engineering department at Weibel Scientific A/S in Denmark. Since November 2017, and aside from his work at Fraunhofer FHR and Weibel Scientific, Carlos has been pursuing his PhD in the Microwave Sensing, Signals and Systems (MS3) group at TU-Delft. Carlos' professional interests lie in the area of Model Based Radar Systems Engineering to tackle challenges such as optimal estimation in centralized and distributed systems, system cognitive control and automated testing. His scientific interests lie in the area of Information Fusion, with special attention to Bayesian non-linear filtering applied in radar systems and Wireless Sensor Networks.

List of Publications

Included in this thesis.

1. **C. Moreno-León**, H. Driessen and A. Yarovoy. Data-association-free Characterization of Labeling Uncertainty: the Cross Modeling Tracker, in *Journal of Advances in Information Fusion*, December 2021

2. **C. Moreno-León**, H. Driessen and P. K. Mandal. Efficient characterization of labeling uncertainty in closely-spaced targets tracking, in *proceedings of the 19th International Conference on Information Fusion (FUSION)*, Heidelberg, Germany, 2016, pp. 449-456.

3. **C. Moreno-León** and H. Driessen. Evaluation of Labeling Uncertainty in Multiple Target Tracking with Track-before-detect Radars, in *22th International Conference on Information Fusion (FUSION)*, Ottawa, ON, Canada, 2019, pp. 1-8, doi: 10.23919/FUSION43075.2019.9011416.

4. **C. Moreno-León**, L. S. Mihaylova and H. Driessen. Tracking of Interacting Targets, in *20th International Conference on Information Fusion (FUSION)*, Xi'an, China, 2017, pp. 1-8, doi: 10.23919/ICIF.2017.8009855.

5. **C. Moreno-León**, H. Driessen and A. Yarovoy. Implementation of the Unique PDF Decomposition for tracking closely-spaced objects with Track-Before-Detect radar systems, submitted for publication to *IEEE Transactions on Aerospace and Electronic Systems*, November 2023

6. **C. Moreno-León**, H. Driessen and A. Yarovoy. Optimization of the Cross Modeling Tracker for tracking closely-spaced targets, under preparation, for submission to *Journal of Advances in Information Fusion*, December 2021, December 2023

Not included in this thesis.

7. **C. Moreno-León**, M. A. González-Huici and T. Dallmann. Data-driven Generation of Road Scenarios for Radar Target Simulation in Automotive Context, in *IEEE MTT-S International Conference on Microwaves for Intelligent Mobility (ICMIM)*, Detroit, MI, USA, 2019, pp. 1-5, doi: 10.1109/ICMIM.2019.8726648.

8. S. Valcarcel-Macua, **C. Moreno-León** et al. How to Implement Doubly-Stochastic Matrices for Consensus-Based Distributed Algorithms, in *IEEE 8th Sensor Array and Multichannel Signal Processing Workshop (SAM)*, A Coruna, Spain, 2014, pp. 333-336, doi: 10.1109/SAM.2014.6882409.

9. A. N. Ramesh, **C. Moreno-León**, J. C. Zafra, S. Brüggenwirth and M. A. González-Huici. Landmark-based Radar SLAM for Autonomous Driving, in *International Radar Symposium (IRS)*, Berlin, Germany, 2021, pp. 1-10, doi: 10.23919/IRS51887.2021.9466220.

10. S. Wald, T. Mathy, S. Nair, **C. Moreno-León** and T. Dallmann. ATRIUM: Test Environment for Automotive Radars, in *IEEE MTT-S International Conference on Microwaves for Intelligent Mobility (ICMIM)*, Linz, Austria, 2020, pp. 1-4, doi: 10.1109/ICMIM48759.2020.9298995.